National Library of Canada
Bibliothèque nationale du Canada

Canadian Theses Service
Service des thèses canadiennes

Ottawa, Canada
K1A 0N4

NOTICE

The quality of this microform is heavily dependent upon the quality of the original thesis submitted for microfilming. Every effort has been made to ensure the highest quality of reproduction possible.

If pages are missing, contact the university which granted the degree.

Some pages may have indistinct print especially if the original pages were typed with a poor typewriter ribbon or if the university sent us an inferior photocopy.

Reproduction in full or in part of this microform is governed by the Canadian Copyright Act, R.S.C. 1970, c. C-30, and subsequent amendments.

AVIS

La qualité de cette microforme dépend grandement de la qualité de la thèse soumise au microfilmage. Nous avons tout fait pour assurer une qualité supérieure de reproduction.

S'il manque des pages, veuillez communiquer avec l'université qui a conféré le grade.

La qualité d'impression de certaines pages peut laisser à désirer, surtout si les pages originales ont été dactylographiées à l'aide d'un ruban usé ou si l'université nous a fait parvenir une photocopie de qualité inférieure.

La reproduction, même partielle, de cette microforme est soumise à la Loi canadienne sur le droit d'auteur, SRC 1970, c. C-30, et ses amendements subséquents.

NL-339 (r. 88/04) c

Canada

THE UNIVERSITY OF ALBERTA

Heat Flow Density Estimation for the Jeanne d'Arc Sub-basin

by

Antonio Correia

(C)

A THESIS

SUBMITTED TO THE FACULTY OF GRADUATE STUDIES AND RESEARCH

IN PARTIAL FULFILMENT OF THE REQUIREMENTS FOR THE DEGREE

OF Master of Science

IN

Geophysics

Department of Physics

EDMONTON, ALBERTA

SPRING 1989

National Library of Canada
Bibliothèque nationale du Canada

Canadian Theses Service
Service des thèses canadiennes

Ottawa, Canada
K1A 0N4

The author has granted an irrevocable non-exclusive licence allowing the National Library of Canada to reproduce, loan, distribute or sell copies of his/her thesis by any means and in any form or format, making this thesis available to interested persons.

The author retains ownership of the copyright in his/her thesis. Neither the thesis nor substantial extracts from it may be printed or otherwise reproduced without his/her permission.

L'auteur a accordé une licence irrévocable et non exclusive permettant à la Bibliothèque nationale du Canada de reproduire, prêter, distribuer ou vendre des copies de sa thèse de quelque manière et sous quelque forme que ce soit pour mettre des exemplaires de cette thèse à la disposition des personnes intéressées.

L'auteur conserve la propriété du droit d'auteur qui protège sa thèse. Ni la thèse ni des extraits substantiels de celle-ci ne doivent être imprimés ou autrement reproduits sans son autorisation.

ISBN 0-315-52811-7

Canada

THE UNIVERSITY OF ALBERTA

RELEASE FORM

NAME OF AUTHOR Antonio Correia

TITLE OF THESIS Heat Flow Density Estimation for the Jeanne d'Arc Sub-basin

DEGREE FOR WHICH THESIS WAS PRESENTED Master of Science

YEAR THIS DEGREE GRANTED SPRING 1989

Permission is hereby granted to THE UNIVERSITY OF ALBERTA LIBRARY to reproduce single copies of this thesis and to lend or sell such copies for private, scholarly or scientific research purposes only.

The author reserves other publication rights, and neither the thesis nor extensive extracts from it may be printed or otherwise reproduced without the author's written permission.

(SIGNED) António Correia

PERMANENT ADDRESS:

Departamento de Fisica

Universidade de Evora

7000 EVORA, Portugal

DATED April 24 1989

THE UNIVERSITY OF ALBERTA

FACULTY OF GRADUATE STUDIES AND RESEARCH

The undersigned certify that they have read, and recommend to the Faculty of Graduate Studies and Research, for acceptance, a thesis entitled Heat Flow Density Estimation for the Jeanne d'Arc Sub-basin submitted by Antonio Correia in partial fulfilment of the requirements for the degree of Master of Science in Geophysics.

.....

Supervisor

.....

.....

.....

Date.. April 24, 1989.....

Abstract

Corrected bottom-hole temperatures from 35 wells together with measured and assumed rock thermal conductivities are used to estimate heat flow density in the Jeanne d'Arc Sub-basin. The results indicate that heat flow density is slightly higher in the deeper northern part of the basin than in the southern part. This suggests that heat flow density is not controlled by heat generation or topography of the basement. From the data so far available, it appears that the heat flow density distribution is strongly affected by fluid motion through the sedimentary layers of the basin. Hot fluids flow from the deeper northern part of the basin to the shallower sediments in the southern part through the gently rising layers. Dehydration is suggested as the mechanism that produces the fluid flow pattern that influences the heat flow distribution in the basin, and a simple model of fluid flow in the Jeanne d'Arc Sub-basin is presented.

Acknowledgements

This work would not be possible without the cooperation and participation of several individuals and institutions.

First of all I would like to thank Professor F. W. Jones for all the support, encouragement, and fruitful discussions and comments during the preparation of this dissertation.

Dr. Aubrey Fricker and Dr. Mel Best of the Atlantic Geoscience Center, and Mr. Roy Nishisaki of the Canadian Stratigraphic Service, Ltd. are thanked for their very helpful and unforgettable cooperation during the data collection stage of this dissertation.

I owe many thanks to Dr. J. Majorowicz for fruitful discussions we had during several stages of the work, to Mrs. I. Vinokurov who has measured the thermal conductivities of all the sample rocks from the Jeanne d'Arc Sub-basin, and to Mr. M. Ertman and Mr. J-M. Maillol for their help in programming matters.

I also owe my gratitude to the Dean, the Scientific Council, and the Director of the Physics Department of the University of Evora for their institutional and personal support.

The Natural Sciences and Engineering Research Council of Canada, and Imperial Oil Co. of Canada, Ltd. are

acknowledged for their financial support during various stages of the work.

The work was also supported by the University of Evora, Portugal, by the Junta Nacional de Investigacao Cientifica e Tecnologica, Portugal, and the University of Alberta, through a teacher assistantship. Their support is gratefully acknowledged.

Table of Contents

Chapter		Page
1.	INTRODUCTION	1
	1.1 Scope and Motivation of this Study	1
	1.2 Physical Basis of Heat Transfer in the Earth	5
	1.3 Regional Setting	9
2.	DESCRIPTION AND ANALYSIS OF THE DATA SET	14
	2.1 The Temperature Data Set	14
	2.2 Thermal Conductivity Data Set	25
	2.3 Heat Flow Estimates	35
	2.4 Error Analysis	42
3.	DISCUSSION AND CONCLUSIONS	46
	3.1 Heat Flow Trends	46
	3.2 Tentative Interpretation of the Heat Flow Density in the Jeanne d'Arc Sub-basin	52
	3.3 Future Work and Conclusions	60
REFERENCES		67
APPENDIX I		72
APPENDIX II		89

List of Tables

Table		Page
2.1	Well name, location, and uncorrected and corrected thermal gradients for the wells in the Jeanne d'Arc Sub-basin.	19
2.2	Summary of the thermal conductivity measurements.	28
2.3	Assumed values for the thermal conductivities of some rocks encountered in the Jeanne d'Arc Sub-basin (after Beach, 1985).	31
2.4	Assumed thermal conductivity values of the rocks encountered in the Jeanne d'Arc Sub-basin after Beach (1985) and Blackwell (1988).	32
2.5	Effective thermal conductivity for each well in the Jeanne d'Arc Sub-basin using measured and assumed (Beach, 1985) thermal conductivity values, and only assumed values (Beach, 1985; Blackwell, 1988).	34
2.6	Heat flow density (HFD) values calculated using measured and assumed thermal conductivity values (Set 1 of Table 2.5), and using only assumed thermal conductivity values (Set 2 of Table 2.5).	36

List of Figures

Figure		Page
1.1	Location of the Jeanne d'Arc Sub-basin and major tectonic elements in offshore Newfoundland; also shown is the 3 km basement depth contour (From Arthur et al., 1982; after Canadian Geological Survey, 1977).	2
1.2	Diagrammatic structure and sediment thickness map of the Jeanne d'Arc Sub-basin (From Grant et al., 1986; after Jackson, 1985).	11
1.3	Schematic section of the Jeanne d'Arc Sub-basin along profile BB' of Figure 1.2 (after Grant et al., 1986).	12
2.1	Histogram of the circulation times. The mean value of the circulation times is 2.56 hours.	17
2.2	Average thermal gradient in the well North Ben Nevis P-93 before application of the Horner plot correction technique. Depths are referred to the bottom of the sea.	20
2.3	Average thermal gradient in the well North Ben Nevis P-93 after application of the Horner plot correction technique. Depths are referred to the bottom of the sea.	21
2.4	Plot of all the corrected BHTs and average thermal gradients for the Jeanne d'Arc Sub-basin.	23
2.5	Map of the geothermal gradients in the Jeanne d'Arc Sub-basin (values in degrees Celsius per kilometer).	24
2.6	Map of the distribution of effective thermal conductivity calculated using measured and assumed thermal conductivity values (Set 1 of Table 2.5).	37
2.7	Map of the distribution of effective thermal conductivity calculated using only assumed thermal conductivity values (Set 2 of Table 2.5).	38
2.8	Heat flow density in the Jeanne d'Arc Sub-basin using the first set of values listed in Table 2.6.	40

Figure Page

2.9 Heat flow density in the Jeanne d'Arc Sub-basin using the second set of values listed in Table 2.6. 41

2.10 Example of graphical estimation of the error in the thermal gradient (see text for explanation). 43

3.1 HFD cross-sections I-I' and J-J' depicted in Figure 2.8. The arrow indicates the position of the line of separation of Region I from Region II. 48

3.2 HFD cross-sections K-K' and L-L' depicted in Figure 2.9. The arrow indicates the position of the line of separation of Region I from Region II. 49

3.3 Correlation between HFD values and depth of the deepest BHT measured in each well of the Jeanne d'Arc Sub-basin. HFD values are calculated using measured and assumed thermal conductivity values. 56

3.4 Correlation between HFD values and depth of the deepest BHT measured in the wells north of the line AA' of Figure 2.8 (Region I). HFD values are calculated using measured and assumed thermal conductivity values. 57

3.5 Correlation between HFD values and depth of the deepest BHT measured in each well south of the line AA' of Figure 2.8 (Region II). HFD values are calculated using only assumed thermal conductivity values. 58

3.6 Schematic of the proposed general fluid flow pattern in the Jeanne d'Arc Sub-basin. Arrows indicate the flow directions. Dashed arrows indicate flow resulting from dehydration of deep sediments. 61

3.7 Correlation between HFD values and depth of the deepest BHT measured in each well of the Jeanne d'Arc Sub-basin (Figure 2.9). HFD values are calculated using only assumed thermal conductivity values. 62

Figure Page

3.8 Correlation between HFD values and depth of the deepest BHT measured in the wells north of line AA' of Figure 2.9 (Region I). HFD values are calculated using only assumed thermal conductivity values. 63

3.9 Correlation between HFD values and depth of the deepest BHT measured in each well south of the line AA' of Figure 2.9 (Region II). HFD values are calculated using only assumed thermal conductivity values. 64

1. INTRODUCTION

1.1 Scope and Motivation of this Study

Geothermal studies in sedimentary basins have received a great deal of attention in recent years both for scientific and economic reasons. Hydrocarbons occur in sedimentary basins, and the genesis and evolution of the basins are related to their thermal histories. Therefore, knowledge of the thermal regimes in sedimentary basins help to more clearly understand the processes of generation, maturation, and migration of oil and gas (van Hinte and Deighton, 1987) as well as provide information needed to model the geodynamic behaviour associated with basin evolution (McKenzie, 1978). Furthermore, heat flow density (HFD) determinations provide necessary boundary conditions to calculate the distribution of temperature in the crust and upper mantle (MacDonald, 1965; Kappelmeyer and Haenel, 1974; Buntebarth, 1984).

This work is concerned with the determination of heat flow density in the Jeanne d'Arc Sub-basin in offshore eastern Canada (see Figure 1.1). Although some previous geothermal studies have been carried out for other offshore eastern Canada areas, and some thermal gradients and isolated heat flow density values have been calculated for

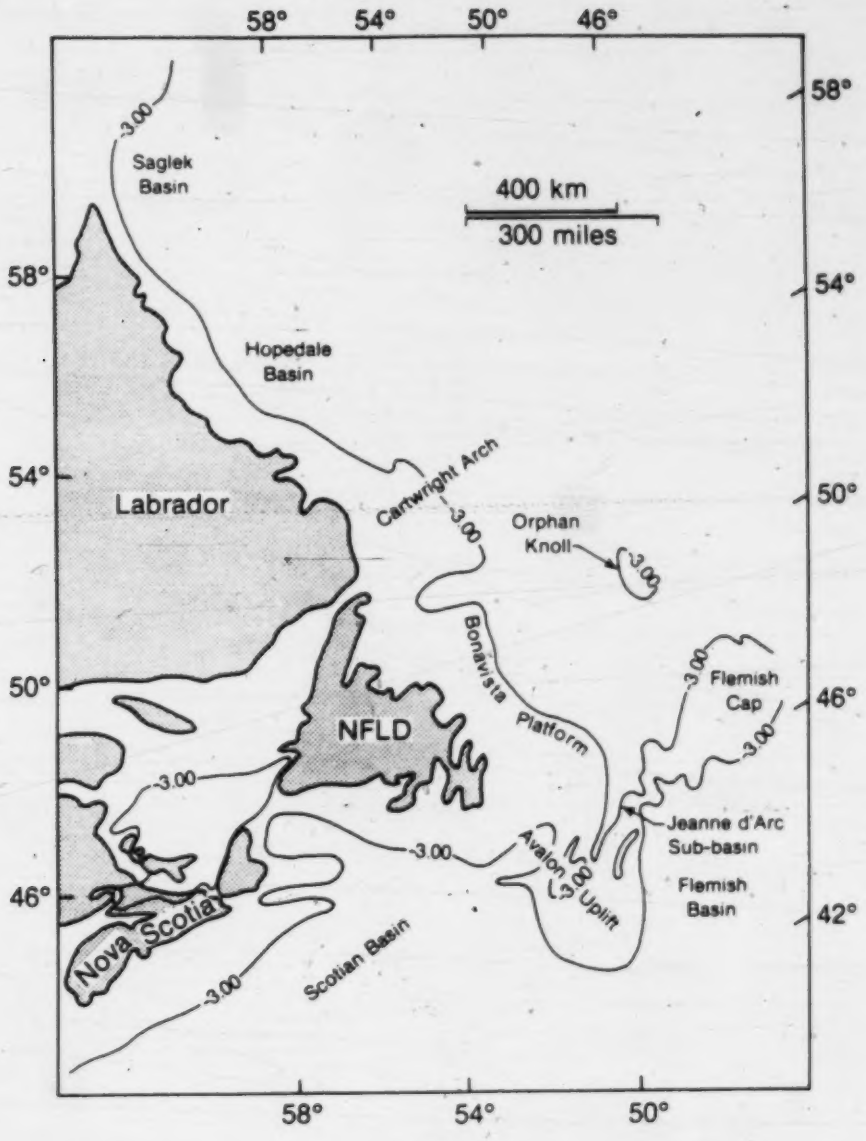

Figure 1.1 Location of the Jeanne d'Arc Sub-basin and major tectonic elements in offshore Newfoundland; also shown is the 3 km basement depth contour (From Arthur et al., 1982; after Canadian Geological Survey, 1977). modified.

the Jeanne d'Arc Sub-basin, no previous heat flow density study has been made for that particular area. In early work, Lewis and Hyndman (1976) calculated the heat flow density across the Nova Scotia continental rise and slope and the southern Grand Banks. Later, Hyndman et al. (1979) and Wright et al. (1980) calculated the heat flow densities in several wells in the Maritime Provinces. In more recent work, Issler (1984) used thermal gradients obtained from bottom-hole temperatures (BHT) measured in offshore oil wells to calculate organic maturation levels, and Reiter and Jessop (1985), Issler and Beaumont (1986) and Reiter and Jessop (1986) discussed the heat flow density pattern on the Canadian Atlantic Shelf.

In the context of offshore Atlantic Canada basins, the Jeanne d'Arc Sub-basin assumes an important role because of the relatively new discovery of the giant Hibernia oil field (Arthur et al., 1982). In the work of this thesis, heat flow densities in the Jeanne d'Arc Sub-basin are calculated by using all the available thermal information from oil wells drilled in the area. This information consists of bottom-hole temperatures obtained during logging operations in the wells and thermal conductivities measured on core samples collected from some of them.

It is well known that bottom-hole temperatures obtained from oil exploration wells are not particularly good data with which to study the thermal regime in the upper layers of the crust. In fact, acquisition of accurate temperatures

in oil wells is, generally, of secondary importance to the oil industry and errors associated with the use of uncalibrated thermometers and the depth determinations of the temperature measurements are common. Furthermore, all bottom-hole temperatures are obtained in wells where the temperatures of the geologic formations have been perturbed by the drilling process. In spite of these shortcomings, the great number of BHT data that is gathered in sedimentary basins contains some statistically significant information (Lam and Jones, 1984b; Speece et al., 1985). The problem, then, is to separate the significant information from the noise, and this is accomplished, at least in part, through the application of some corrections that will be described later. Therefore, the use of BHT sets combined with thermal conductivity measurements is a useful way to study the thermal state of sedimentary basins. This statement is confirmed by studies performed by Evans and Coleman (1974) and Andrews-Speed et al. (1984) of the North Sea oil fields, Carvalho and Vacquier (1977) of the Reconcavo Basin in Brazil, Reiter and Tovar (1982) of northern Chihuahua in Mexico, Chapman et al. (1984) of the Uinta Basin in the U.S., Speece et al. (1985) of the Michigan Basin in the U.S., Majorowicz and Jessop (1981) and Majorowicz et al. (1984) of the Western Canadian Basin, and Majorowicz et al. (1988) of the Yukon and Northwest Territories in Canada. However, it must be stressed, that BHT data sets are not substitutes for accurate determinations of temperatures in

wells. Nevertheless, these latter measurements are generally not performed in sedimentary basins and, therefore, nearly all the thermal information from such areas is obtained from bottom-hole temperatures.

1.2 Physical Basis of Heat Transfer in the Earth

The distribution of temperature inside the Earth is one of the most important parameters needed to understand its origin and evolution. In spite of this, the study of thermal processes within the Earth is one of the most speculative branches of geophysics. The physical basis to study the geothermal processes is well established, but problems arise when it is applied to the real Earth. This is because assumptions and simplifications must be made and as a result the problem is reduced to a simple model that is used to infer the internal thermal state of the Earth.

Energy can be transferred through radiation, convection and conduction. It is assumed here that heat flows only by conduction. Although heat transfer by radiation takes place within the Earth at great depths where temperatures are high, in the upper crust where temperatures are relatively low, heat transfer by radiation is negligible. Heat convection occurs in the upper crust by means of water circulation through the geologic formations. Its effect on the redistribution of heat and consequently on the temperature distribution inside the Earth can be

significant. However, construction of a convection model is difficult and will not further the work described here for two reasons; first, because little hydrogeologic information is available for the Jeanne d'Arc Sub-basin at the present time; and second, because any departure from a conduction model, as is used here as a first approximation, can be interpreted as a perturbation due to convection or heat generation. Nevertheless, it is important to obtain first estimates of the temperature distribution with depth and heat flow densities within the basin, and this can be done by neglecting modes of heat transport other than conduction.

The general equation for heat flow calculations in any medium is (Kappelmeyer and Haenel, 1974):

$$\vec{q} = -\overline{\overline{K}} \cdot \text{grad } T \qquad (1.1)$$

where $\vec{q}$ is the heat flow density vector, $\overline{\overline{K}}$ is the thermal conductivity tensor, and gradT is the temperature gradient. The above equation is normally simplified by assuming that the heat conduction occurs in an isotropic medium. In this case, the thermal conductivity is a scalar and so is easier to determine. Thermal conductivity is considered to be a scalar in almost all geothermal studies, because the Earth can be approximated by a series of horizotal isotropic layers. If it is further assumed that the heat conduction in

the Earth is vertical, which is generally true if horizontal thermal conductivity contrasts are not too great, then Equation 1.1 takes the form:

$$q = K \frac{dT}{dz} \qquad (1.2)$$

where q is now the heat flow density in the vertical direction, K is the thermal conductivity of the isotropic layer being considered, and dT/dz is the vertical temperature gradient; in this equation, and from now on, the heat flow density is assumed positive in the upward direction.

In sedimentary basin heat flow studies it is convenient to use a further simplified form of Equation 1.1, which is:

$$q = K_{eff} \left[\frac{dT}{dz}\right] \qquad (1.3)$$

In this equation, q is the scalar heat flow density as before, [dT/dz] is the average thermal gradient over a geologic section, and K_{eff} is the effective thermal conductivity of the same geologic section. The effective thermal conductivity of an interval of several layers can be calculated by using the following expression:

$$K_{eff} = \frac{\sum_{i=1}^{n} \Delta z_i}{\sum_{i=1}^{n} \frac{\Delta z_i}{K_i}} \qquad (1.4)$$

where i represents the different layers that compose the interval, and ΔZ_i and K_i are respectively the thicknesses and conductivities of those layers.

One of the most important aspects of heat flow studies is that they provide heat flow density values that can be used to determine the temperature distribution deep in the crust. If the thermal conductivity and heat generation with depth are known, the temperature at depth is given by:

$$T(z) = T_0 + \frac{q z}{K} - \frac{A z^2}{2K} \qquad (1.5)$$

In this equation, which results from the integration of the differential equation of heat conduction with heat generation, T(z) is the temperature at a depth z, T_o is the temperature at the surface of the Earth, A is the heat generation per unit of volume, and the other variables are as in Equation 1.2.

For geologic situations where the rock units are horizontal and form discrete and distinct layers, the thermal resistance method proposed by Bullard (1939) is

suitable for calculating the heat flow density. In this method the relation between heat flow density, q, and the temperature with depth, T(z), is given by:

$$T(z) = T_0 + q \sum_{i=1}^{n} \frac{\Delta z_i}{K_i} \qquad (1.6)$$

where K_i is the thermal conductivity of layer i with thickness Δz_i, n is the number of layers, and the other variables have the same meanings as in Equations 1.2 and 1.5. The heat flow density is determined by the slope of the best-fit straight line obtained by plotting the distribution of temperature with depth as a function of the sum $\Sigma(\Delta z_i/K_i)$. The ratio $\Delta z_i/K_i$ is generally called the thermal resistance. It is seen that Equation 1.6 is a simplified version of Equation 1.5.

1.3 Regional Setting

The brief geologic and tectonic descriptions of the East Newfoundland Basin and Jeanne d'Arc Sub-basin that follow are based on the work by Arthur et al. (1982). From Figure 1.1, it is seen that the offshore east coast of Canada is divided into a series of basins and sub-basins that are separated by major uplifts. The East Newfoundland Basin is the largest basin and covers an area of 155,400

square kilometers. It is bounded by the Bonavista Platform on the west, the Flemish Cap and Orphan Knoll on the east, the Cartwright Arc to the north, and the Avalon Uplift to the south. The Jeanne d'Arc Sub-basin, which can be considered as a southwestern extension of the larger East Newfoundland Basin, is approximately 100 km wide in the north and narrows to approximately 42 km width in the south (Figure 1.2). It lies between the Bonavista Platform, composed mainly of metamorphosed Precambrian and Paleozoic rocks, and the Outer Ridge Complex which contains highly faulted Mesozoic sediments.

The Jeanne d'Arc Sub-basin, which developed as a consequence of Mesozoic extensional rift tectonics, contains Mesozoic and Cenozoic sediments that attain a thickness of 20 km in the deep northern areas (Enachescu, 1987; Keen et al., 1987) (Figure 1.3). The sedimentary history of the East Newfoundland Basin and the Jeanne d'Arc Sub-basin can be described in terms of plate tectonics as a result of the separation of the European Plate from the North American Plate. During this separation, the North Atlantic developed and a series of northeast-southwest trending rift valleys were formed during the Triassic. This process was followed by seafloor spreading which took place in the Scotian Shelf area during the Mid-Jurassic. The East Newfoundland Basin area was not involved in active plate motion until Late-Jurassic or possibly Early-Cretaceous. However, during subsequent motion, the active spreading center was located

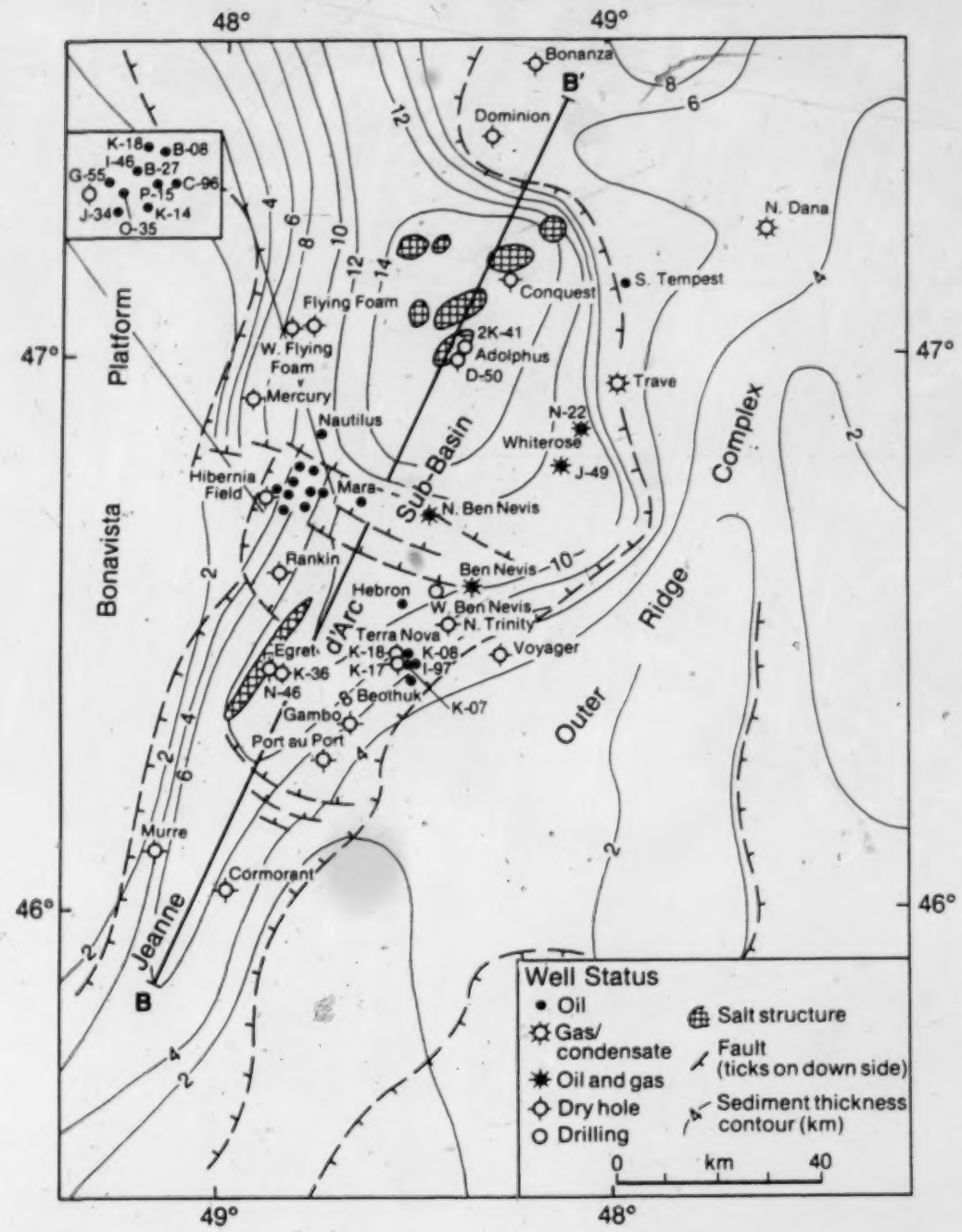

Figure 1.2 Diagrammatic structure and sediment thickness map of the Jeanne d'Arc Sub-basin (From Grant et al., 1986; after Jackson, 1985). modified.

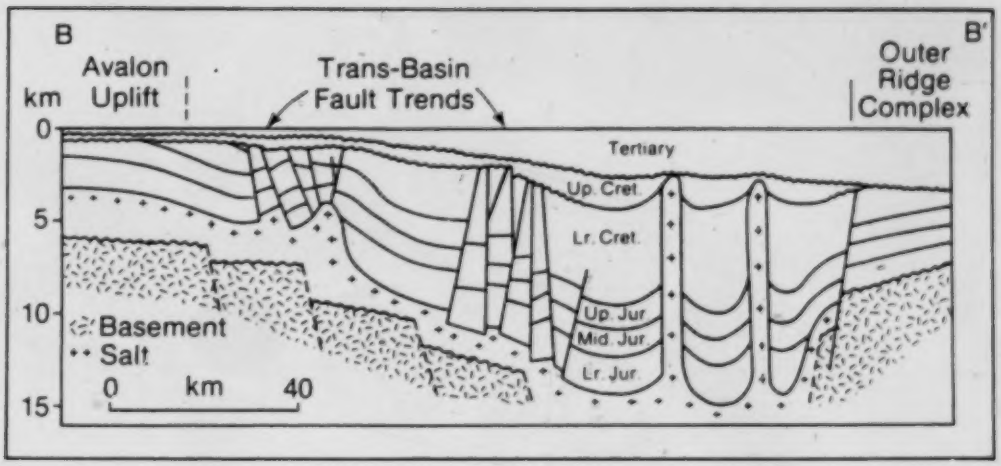

Figure 1.3 Schematic section of the Jeanne d'Arc Sub-basin along profile BB' of Figure 1.2 (after Grant et al., 1986). modified.

east of the basin. By this time the Avalon Uplift had developed and caused erosion in the Lower Cretaceous and Jurassic sediments.

The deposition of Mesozoic and Cenozoic sediments began when Jurassic seas transgressed areas of earlier salt and red-bed depositions. The resulting deposits were predominantly shallow water carbonates, shales, and sandstones. The Lower Cretaceous sedimentation was dominated by major progradational deltaic pulses and the sediment origin was the craton in the west and the Avalon Uplift in the south. The Upper Cretaceous was essentially a period of marine transgression and the resulting stratigraphic sequence is primarily composed of calcareous shales. Finally, during the Tertiary, interfingered marine shales and sandstones were deposited during several regressive and transgressive episodes.

The resulting complex tectonic structure of the Jeanne d'Arc Sub-basin, as seen in Figures 1.2 and 1.3, strongly influences the thermal regime within it.

2. DESCRIPTION AND ANALYSIS OF THE DATA SET

2.1 The Temperature Data Set

The temperature data set consists of 614 bottom-hole temperatures (BHT) measured in 44 wells drilled in the Jeanne d'Arc Sub-basin. The locations of the wells are shown in Figure 1.2; and in Table 2.1 the names of the wells and their geographic coordinates are listed.

Bottom-hole temperatures differ from the true formation temperatures because of the drilling process and the cooling effect of the mud circulation. Those BHT values are generally lower than the undisturbed formation temperatures and a correction must be applied in order to obtain estimates of the true formation temperatures. There are several correction methods (Cao et al., 1988), and the Horner plot technique (Lachenbruch and Brewer, 1959; Dowdle and Cobb, 1975; Fertl and Wichmann, 1977) is used here. To apply this method, two or more BHT values must be known at the same depth for different times after the mud circulation has ceased. The ideal situation would be to have for each well several BHT values for several depths measured at different times. Such data are not generally available, and it was necessary to reject the data from two wells because of an insufficient number ot BHT values. These two wells are

not listed in Table 2.1.

The Horner plot technique consists of plotting, for the same depth, the bottom-hole temperatures as a function of the logarithm of $[(t_c+t_e)/t_e]$, where t_c is the mud circulation time and t_e is the time elapsed between the end of circulation and the time of temperature measurement. This procedure is represented analytically by the following equation:

$$T(t) = T\,(inf) + A \cdot \log\left(\frac{t_e + t_c}{t_e}\right) \qquad (2.1)$$

where T(t) represents the BHT values, T(inf) is the true formation temperature, and A is the slope of the best-fit straight line drawn through the data points. Equation 2.1 shows that to obtain T(inf), t_e must approach infinity, and so the well temperature at a long time after the mud circulation has ceased is represented.

The Horner plot technique is one of the most used methods to correct oil well BHT values. However, it must be emphasized that the BHT measurements often suffer from unknown uncertainties and, therefore, even the corrected temperatures can differ by several degrees from the true formation temperatures. In consideration of this three wells were rejected because of unreasonably high scatter in the corrected BHT values; these three wells are Hibernia P-15,

Hibernia J-34, and Terra Nova K-08.

To correct BHT values, it is necessary to know the t_e and t_c values. For the data here, t_e is known for every BHT. However, the t_c values are not known for every case. Therefore, in order not to drastically reduce the data set by rejecting values for which t_c is not known, a study of the influence of the circulation time on the average thermal gradients of some wells was performed so that a reasonable value for t_c could be assumed for those cases. First, all the wells for which both values of t_e and t_c are available were selected, and a histogram of the circulation times was drawn to determine the mean circulation time. This histogram is given in Figure 2.1 and the mean value is 2.56 hours; to draw this histogram 177 circulation times were used. Using this mean value, the average thermal gradient for one well for which both t_e and t_c are known (North Ben Nevis P-93) and that for a second well for which only t_e values are known (South Tempest G-88) were determined. In addition, the average gradients for these two wells were calculated using circulation times ranging from 0.5 to 8.5 hours and the results are given Appendix I. The main conclusion is that the influence of the circulation time on the average thermal gradients in the wells is small and less than the uncertainties in the average gradients themselves. Therefore, for all the wells for which the circulation time is not known, the mean circulation time of 2.56 hours was used for the Horner plot corrections. Figure 2.2 and Figure

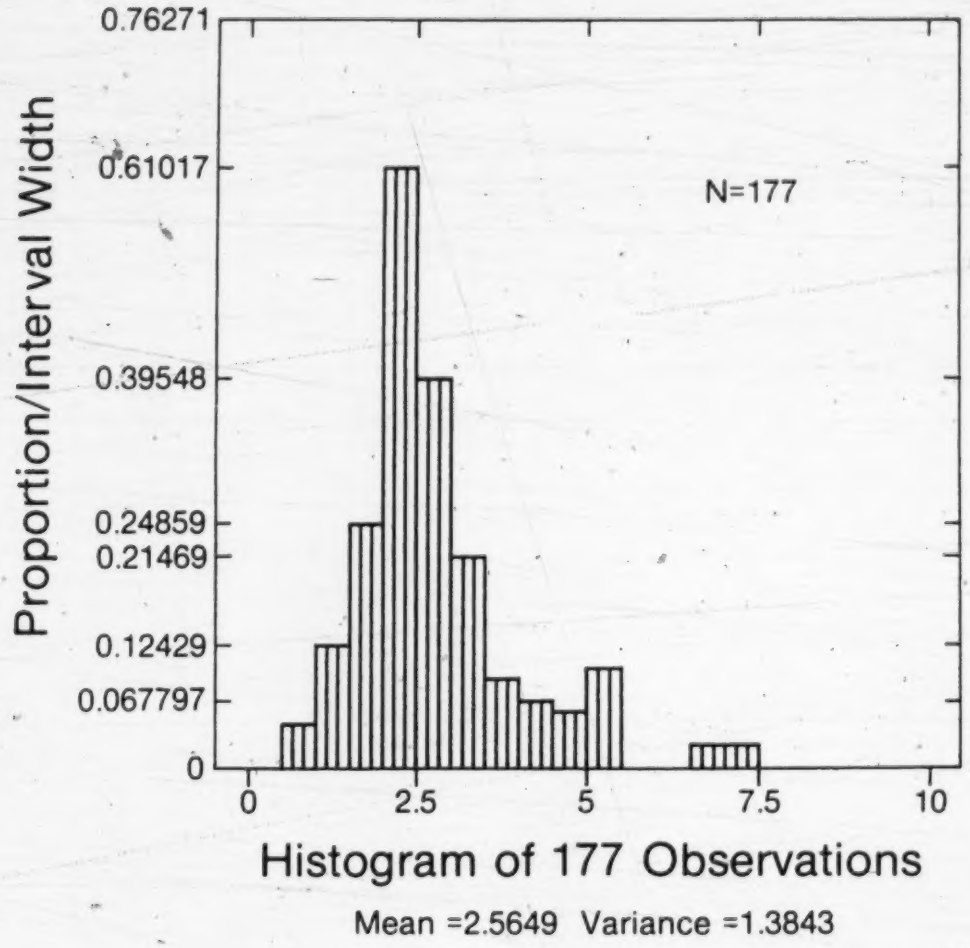

Figure 2.1 Histogram of the circulation times. The mean value of the circulation times is 2.56 hours.

2.3 show examples of the average thermal gradient calculations for one of the wells before and after the Horner plot correction respectively. In these figures, the slope of the solid straight line gives the most probable average thermal gradient, while the dashed lines define the 95% confidence limits that are $1.96*S_e$ above and below the best-fit regression line, where S_e is the standard error of the estimate and is calculated from the equation:

$$S_e = \left[\frac{\sum_{i=1}^{n} (y_i - y_i')^2}{n-2} \right]^{1/2} \qquad (2.2)$$

where n is the number of data points and y_i' are the points on the regression line of y on x (Lam et al., 1985).

The plots of the average thermal gradients calculated from corrected BHT values for all the wells are presented in Appendix II. In Table 2.1 the uncorrected and corrected average gradients are listed, as well as the geographic coordinates of the wells.

The average thermal gradients calculated from the corrected BHT values are higher (4 ^{o}C on average) than those calculated using the uncorrected values. This difference is consistent with the magnitudes of similar corrections elsewhere (Jones et al.,1984; Jones et al.,1985; Majorowicz et al., 1985; Majorowicz et al., 1986).

Table 2.1 - Well name, location, and uncorrected and corrected thermal gradients for the wells in the Jeanne d'Arc Sub-basin.

Well name	Geographic Coordinates (Lat.)	(Lon.)	Uncorr. Grad. (°C/km)	Corr. Grad. (°C/km)
Adolphus D-50	46°59'05"	48°22'29"	25.6 ± 6.9	30.8 ± 1.0
Adolphus 2K-41	47°00'37"	48°22'00"	28.7 ± 8.5	33.3 ± 6.2
Ben Nevis I-45	46°36'36"	48°21'15"	23.8 ± 6.0	25.4 ± 4.8
Beothuk M-05	46°24'49"	48°31'14"	22.2 ± 3.1	24.9 ± 3.7
Bonanza M-71	47°30'47"	48°11'55"	27.4 ± 6.6	32.3 ± 1.0
Conquest K-09	47°08'34"	48°15'44"	30.7 ± 8.9	33.4 ± 2.2
Cormorant N-83	46°02'42"	48°58'05"	24.0 ± 3.1	25.3 ± 4.0
Dominion O-23	47°22'49"	48°18'28"	24.1 ± 5.3	26.4 ± 1.8
Egret K-36	46°25'38"	48°50'22"	21.2 ± 3.7	23.7 ± 1.6
Egret N-46	46°25'57"	48°51'48"	23.4 ± 6.8	26.9 ± 0.0
Flying Foam I-13	47°02'39"	48°46'32"	24.9 ± 3.7	26.7 ± 0.0
Gambo N-70	46°19'53"	48°39'55"	21.6 ± 2.8	25.7 ± 2.9
Hebron I-13	46°32'34"	48°31'46"	21.8 ± 3.7	24.0 ± 3.4
Hibernia B-08	46°47'05"	48°45'26"	23.3 ± 3.3	26.2 ± 3.2
Hibernia B-27	46°46'16"	48°48'28"	23.1 ± 6.4	26.2 ± 5.1
Hibernia C-96	46°45'10"	48°44'36"	22.8 ± 1.9	25.1 ± 1.3
Hibernia G-55A	46°44'18"	48°53'11"	20.0 ± 3.8	23.4 ± 3.8
Hibernia I-46	46°45'41"	48°51'17"	21.0 ± 5.5	23.5 ± 5.5
Hibernia J-34	46°43'34"	48°50'13"	19.8 ± 4.2	(1)
Hibernia K-14	46°43'40"	48°47'36"	20.8 ± 1.9	22.8 ± 1.1
Hibernia K-18	46°47'35"	48°47'17"	23.8 ± 6.2	26.7 ± 2.1
Hibernia O-35	46°44'56"	48°49'51"	19.8 ± 10.7	23.7 ± 4.7
Hibernia P-15	46°44'59"	48°46'51"	24.8 ± 30.1	(1)
Mara M-54	46°43'49"	48°38'44"	22.0 ± 2.9	25.4 ± 0.2
Mercury K-76	46°55'35"	48°56'34"	20.4 ± 2.0	22.6 ± 0.3
Murre G-67	46°06'20"	49°09'38"	22.6 ± 11.0	25.7 ± 0.6
Nautilus C-92	46°51'04"	48°44'21"	25.2 ± 7.3	28.9 ± 3.3
N Ben Nevis P-93	46°42'49"	48°28'34"	24.6 ± 5.4	28.5 ± 2.0
N Dana I-43	47°12'44"	47°36'13"	26.7 ± 8.3	30.4 ± 6.1
N Trinity H-71	46°30'24"	48°26'04"	24.2 ± 8.2	27.0 ± 2.4
Port au Port J-97	46°16'38"	48°44'06"	24.0 ± 2.9	25.5 ± 0.0
Rankin M-36	46°35'47"	48°50'56"	19.3 ± 2.5	21.3 ± 1.8
S Tempest G-88	47°07'18"	47°57'32"	27.0 ± 8.9	31.6 ± 6.8
Terra Nova I-97	46°26'43"	48°28'49"	20.2 ± 7.3	22.0 ± 0.0
Terra Nova K-07	46°26'44"	48°30'58"	20.6 ± 8.9	24.2 ± 7.8
Terra Nova K-08	46°27'30"	48°30'59"	22.9 ± 4.0	(1)
Terra Nova K-17	46°26'42"	48°32'28"	21.1 ± 7.2	21.4 ± 6.3
Terra Nova K-18	46°27'44"	48°32'32"	22.8 ± 1.3	25.7 ± 1.2
Trave E-87	46°56'18"	47°58'08"	27.6 ± 7.4	30.4 ± 8.3
Voyager J-18	46°27'30"	48°17'02"	23.9 ± 5.4	28.7 ± 0.1
W Ben Nevis B-75	46°34'01"	48°26'04"	24.7 ± 4.6	26.8 ± 3.2
W Flying Foam L-23	47°02'44"	48°49'17"	24.4 ± 4.0	29.8 ± 7.9
Whiterose J-49	46°48'31"	48°06'28"	25.9 ± 4.4	31.9 ± 1.5
Whiterose N-22	46°51'48"	48°03'57"	27.5 ± 4.4	31.8 ± 2.0

(1) Well with too high scatter in the BHT values.

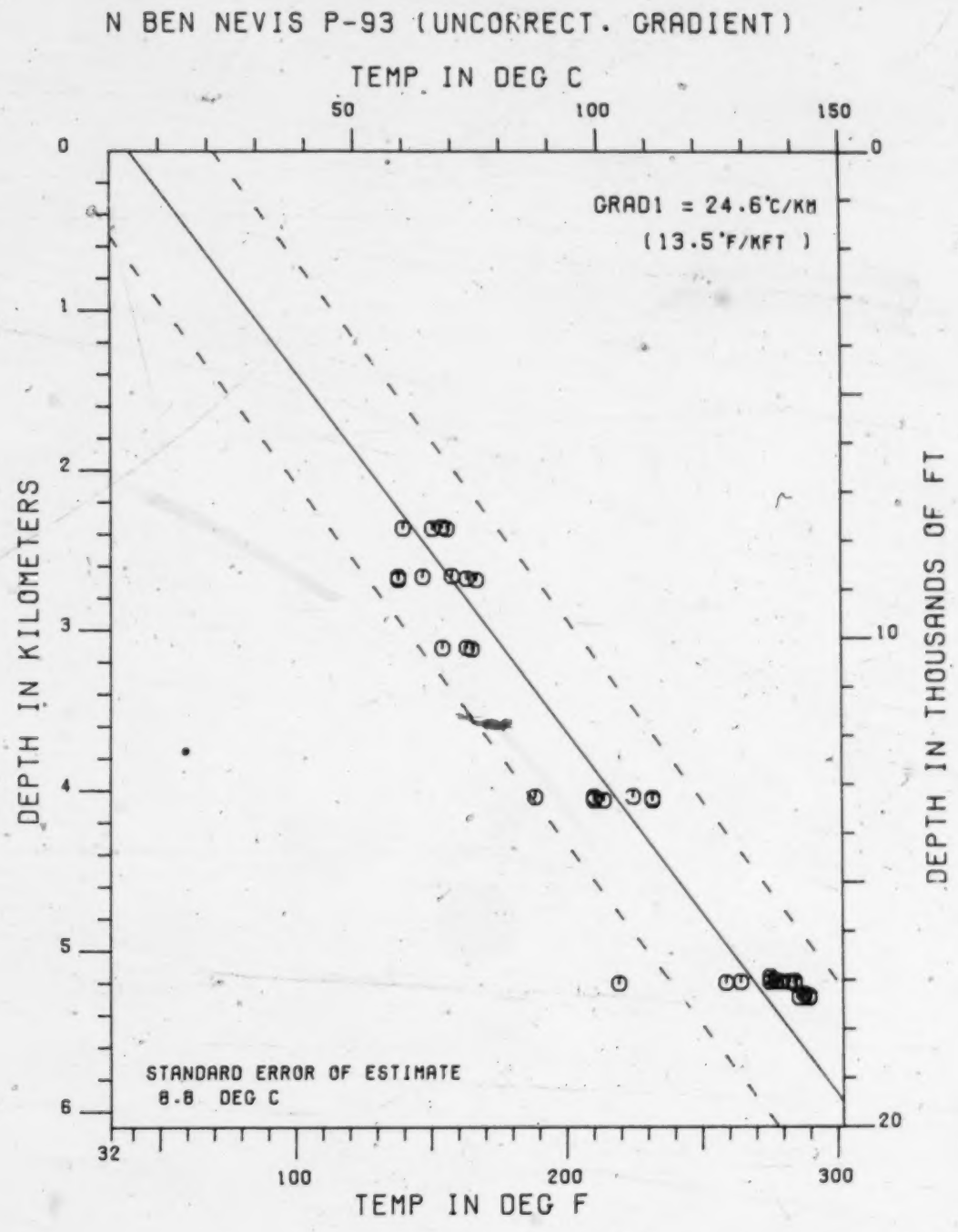

Figure 2.2 Average thermal gradient in the well North Ben Nevis P-93 before application of the Horner plot correction technique. Depths are referred to the bottom of the sea.

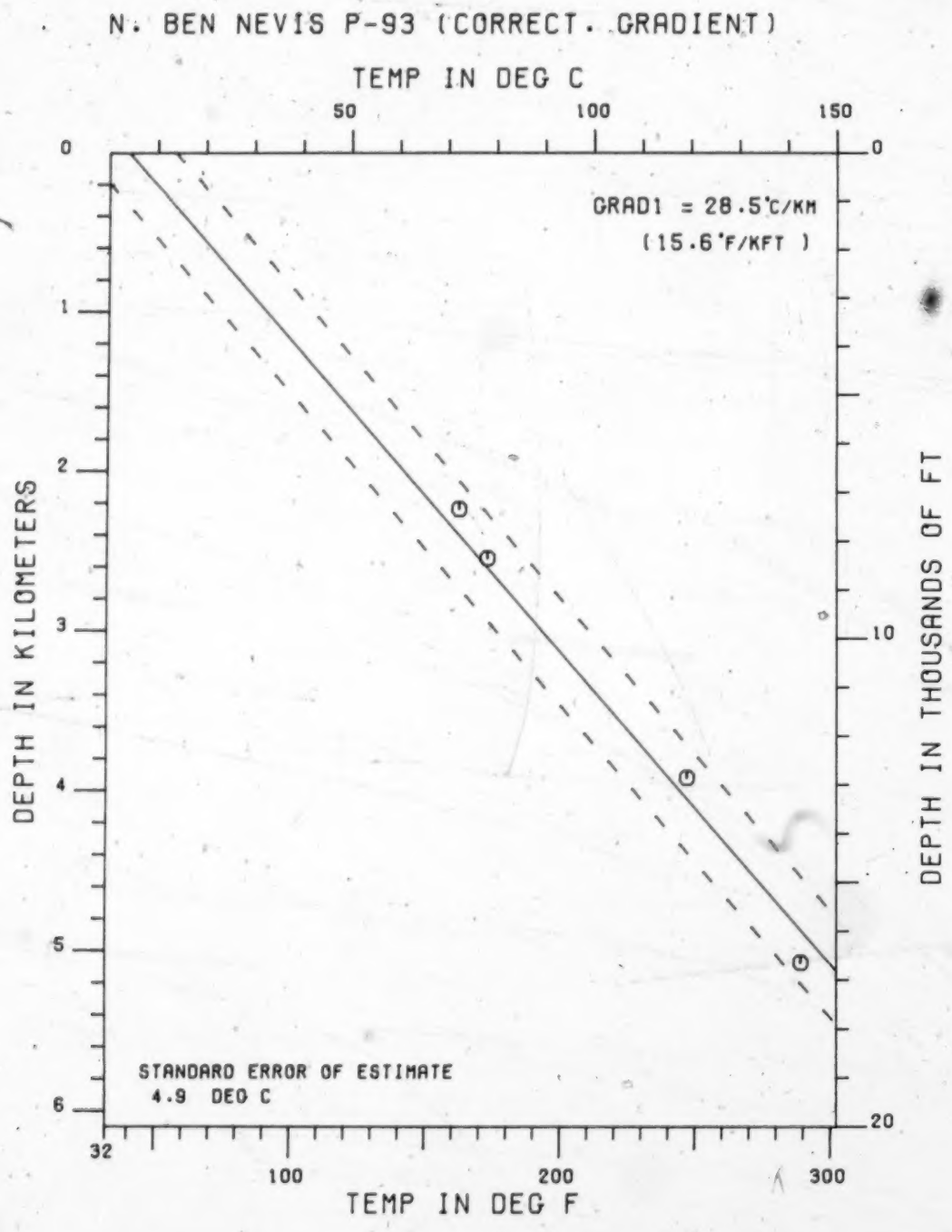

Figure 2.3 Average thermal gradient in the well North Ben Nevis P-93 after application of the Horner plot correction technique. Depths are referred to the bottom of the sea.

It should be noted that, to determine the average thermal gradient in each well, the sea bottom temperature was assumed to be 4 degrees Celsius. This value agrees with values reported by Evans and Coleman (1975), Hyndman et al. (1979), and Moir (1988). Furthermore, no permafrost occurs in the basin, and so its effect need not to be considered.

Figure 2.4 shows the average thermal gradient for all the Jeanne d'Arc Sub-basin using only the corrected BHT values.

With respect to error in the thermal gradient calculations, it should be noted that the uncertainties in individual BHT measurements are generally not known, and therefore it is difficult to estimate the errors in the geothermal gradient; nevertheless, later in this work, a method to calculate the error in it will be described. It should be stressed, however, that the spread of the corrected BHTs over a certain area may have some geophysical or geological meaning. For example, large values of the standard error of the estimate can reflect vertical as well as horizontal variations of thermal properties, the existence of faults (Lam and Jones, 1984a; Lam and Jones, 1984b), or changes in geological facies (Chapman et al., 1988).

Figure 2.5 is a map of the average thermal gradients for the wells in the Jeanne d'Arc Sub-basin.

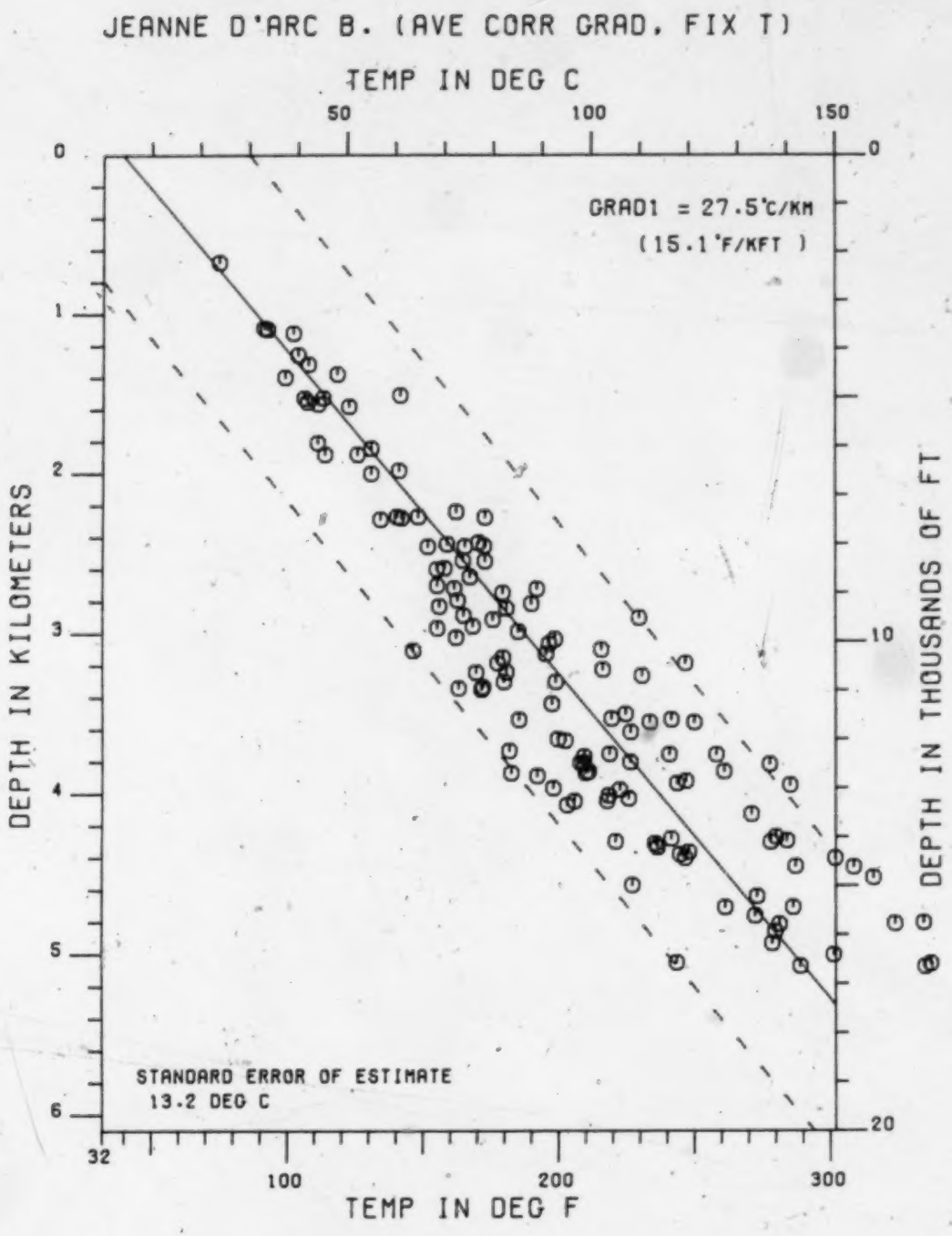

Figure 2.4 Plot of all the corrected BHTs and average thermal gradient for the Jeanne d'Arc Sub-basin.

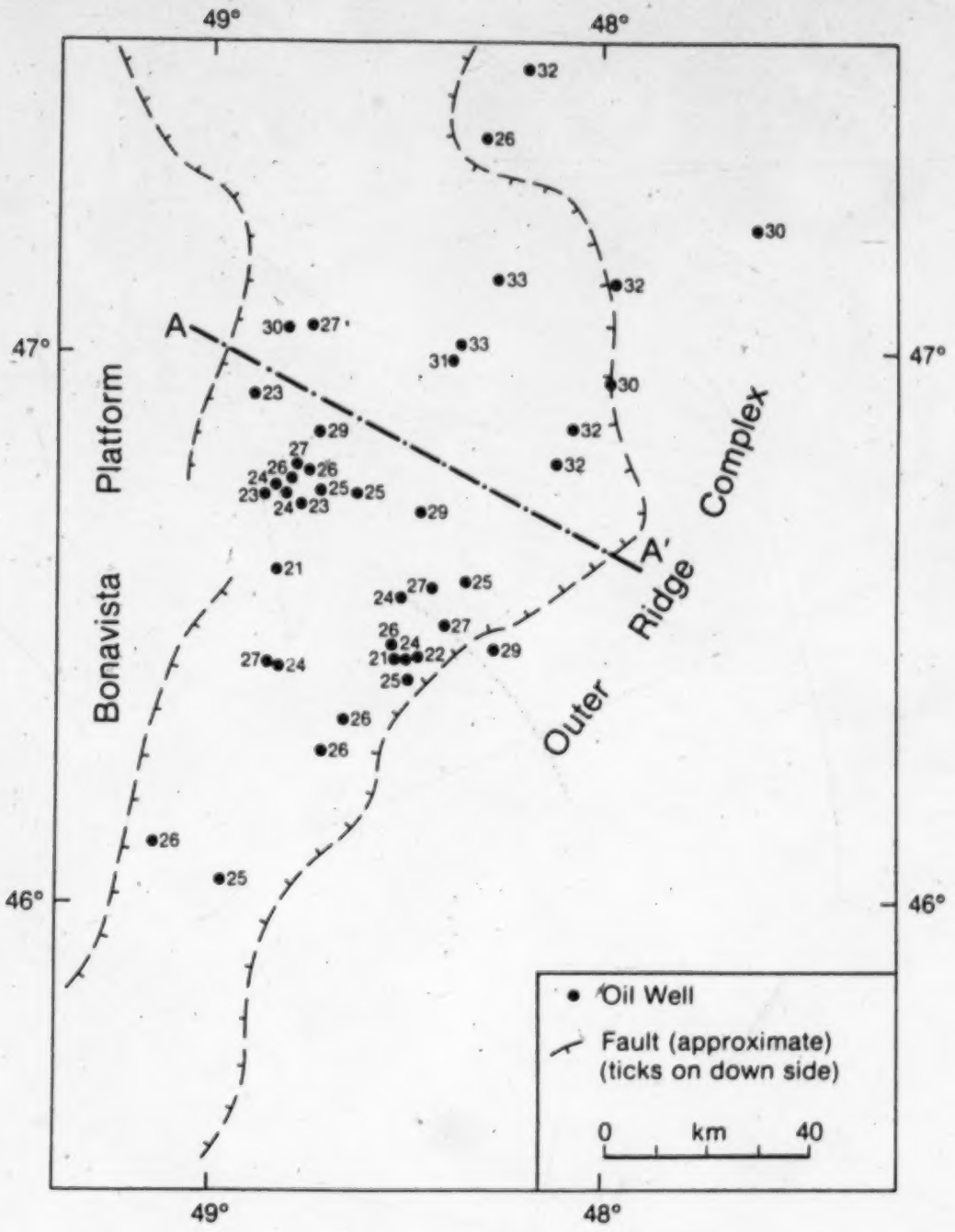

Figure 2.5 Map of the geothermal gradients in the Jeanne d'Arc Sub-basin (values in degrees Celsius per kilometer).

2.2 Thermal Conductivity Data Set

One of the most important parameters in geothermal gradient and heat flow density studies is the thermal conductivity, K; despite this, it remains one of the least well known quantities, and furthermore, is difficult to evaluate. If, however, mean thermal conductivities are not accurately determined for geological formations in sedimentary basins, construction of models to represent their thermal histories and organic maturation levels will not be possible.

Rock thermal conductivities depend on several factors. The most important are rock type, composition, temperature, porosity, fluid content, and pressure. Generally speaking, the thermal conductivities of rocks decrease with increasing temperature and increasing porosity but increase with increasing confining pressure. Furthermore, for the same porosity, thermal conductivity is higher in rocks with oil as the pore fluid than in rocks where water or gas fills the pores (Buntebarth, 1984).

Measured thermal conductivity values can be corrected for some of the above factors. The wells drilled in the Jeanne d'Arc Sub-basin are deeper than 1000 meters and so correction of thermal conductivities for increasing temperature with depth was carried out in this work (Kappelmeyer and Haenel, 1974; Beach, 1985; Beach et al., 1987). To perform this correction it was assumed that the mean geothermal gradient in the area is 30 ^{o}C/km and that

the thermal conductivity varies with temperature in accordance with the equation (Beach, 1985):

$$K(T) = [K(22)] \left(\frac{295}{T+273}\right) \qquad (2.3)$$

where K(22) is the thermal conductivity measured at 22 ^{o}C, and T is the temperature in degrees Celsius. Corrections for porosity, which is difficult to determine, and pressure, which would be insignificant (Kappelmeyer and Haenel, 1974), are not performed in this thesis.

To study the thermal conductivity distribution in the Jeanne d'Arc Sub-basin, 34 discs of 38 mm diameter and thicknesses between 5 and 10 mm, were cut from cores from four wells in the basin. These discs were provided by the Geological Survey of Canada and came from the following wells: Hibernia I-46, Hebron I-13, Cormorant N-83, and South Tempest G-88 (see Figure 1.2 for locations). The cores from which the discs were cut were from depths ranging from 1830 to 4400 meters. The discs were cut perpendicularly to the core lengths and, therefore, their axes were perpendicular to the wells. Thermal conductivities measured in the horizontal direction in sediments are generally different from those measured in the vertical direction, and so the measured thermal conductivities were corrected for anisotropy by means of the following equation;

$$A = \frac{K_{par}}{K_{per}} \qquad (2.4)$$

where $K_{(par)}$ is the thermal conductivity parallel to the bedding, $K_{(per)}$ is the thermal conductivity perpendicular to the bedding, and A is the coefficient of anisotropy. The coefficients of anisotropy used in this work are presented in Table 2.2 and are based on Table 6.6 of Kappelmeyer and Haenel (1974) and Table 2.1 of Beach (1985). The correction for anisotropy was only performed for the rocks listed in Table 2.2.

From the initial set of 34 discs it was possible to obtain one or two more from some of them. However, the condition of the shales and claystones deteriorated so badly during the preparation of the discs for thermal conductivity measurements (polishing surfaces and water saturation) that measurements on them were not possible. Only 33 discs were of adequate quality for the measurements, and so values from these were used to estimate the thermal conductivities of some of the geological formations of the Jeanne d'Arc Sub-basin. The thermal conductivities of the discs that were destroyed were measured by the cell method as described by Sass et al. (1971).

It must be emphasized that 33 thermal conductivity values are not sufficient for a reliable determination of

Table 2.2 - Summary of the thermal conductivity measurements.

Rock type	Number of samples	K_{par} (W/m.K)	Coef. of anisotropy	K_{per} (W/m.K)
Limestone	8	3.21 ± 1.28	1.33	2.41 ± 0.96
Dolomite	3	3.10 ± 1.24	1.02	3.04 ± 1.22
Anhydrite	2	5.33 ± 2.13	1.02	5.23 ± 2.09
Shale	5	2.30 ± 0.92	(1)	2.30 ± 0.92
Sandstone	14	4.69 ± 1.88	1.12	4.19 ± 1.68
Siltstone	6	4.24 ± 1.70	1.00	4.24 ± 1.70
Claystone	1	3.11 ± 1.24	(1)	3.11 ± 1.24

(1) Thermal conductivity measurement using the cell method (Sass et al., 1971).

the heat flow density in the basin. Furthermore, as can be seen from Table 2.2, no thermal conductivity values were determined from disc samples of shales and claystones. Since cell measurements are generally not as good as those on discs, this means that the thermal conductivity control for the most abundant rocks in the basin is poor. When rocks are isotropic, the cell method described by Sass et al. (1971) can be use to determine thermal conductivities. However, shales and claystones, and many other rocks, are anisotropic; therefore, the measurement of their thermal conductivities by the cell method is not very reliable.

The thermal conductivities of the 33 water saturated discs and the cell samples were measured using the divided-bar apparatus of the geothermal laboratory of the Physics Department at the University of Alberta. The measurements were performed at room temperature (22 degrees Celsius) and the discs and cells were subjected to a moderate confining pressure in order to maintain good thermal contact between them and the heat source and heat sink of the device. Table 2.2 summarizes the results of the thermal conductivity measurements.

The rock type information for the sedimentary sequence in the Jeanne d'Arc Sub-basin was purchased from Canadian Stratigraphic Services, Calgary. These data provided the compositions of consecutive 1000 foot intervals for each well in terms of twelve sedimentary rock types, which are: limestone, dolomite, anhydrite, shale, sandstone, siltstone,

marlstone, chert, coal, conglomerate, salt, and claystone. In addition, the number of feet of skipped rocks in each 1000 foot interval is also given. The effective thermal conductivity, K_{eff}, for each well was then calculated using Equation 1.4 and, whenever possible, the measured thermal conductivities were integrated into the calculation. Assumed values were only used when no measured thermal conductivity for the particular rock from this basin was available. In Table 2.3 the assumed values for thermal conductivities of some of the rock types encountered in the Jeanne d'Arc Sub-basin are listed. This table is based on the values reported by Beach (1985).

As stated above, for shales and claystones it was not possible to make thermal conductivity measurements on the discs, and the values obtained using the cell method are high when compared to other reported values (Beach, 1985; Blackwell, 1988). Besides this, there are only six thermal conductivity measurements of siltstone, another rock that is abundant in the Jeanne d'Arc Sub-basin. Therefore, a statistical analysis of the measured thermal conductivities of the discs was not possible. However, a calculation of the effective thermal conductivity for each well was performed using only assumed values for the thermal conductivities of the rock types encountered in the basin. These assumed values are listed in Table 2.4. In this table the thermal conductivities of limestone, dolomite, anhydrite, shale, sandstone, and siltstone are the same as those reported by

Table 2.3 - Assumed values for the thermal conductivities of some rocks encountered in the Jeanne d'Arc Sub-basin (after Beach, 1985).

Rock type	Thermal conductivity (W/m.K)
Marlstone	3.0 ± 1.1
Chert	1.4 ± 0.5
Coal	0.2 ± 0.2
Conglomerate	3.2 ± 1.8
Salt	5.7 ± 1.0
Skipped interval	2.3 ± 2.0

Table 2.4 - Assumed thermal conductivity values of the rocks encountered in the Jeanne d'Arc Sub-basin after Beach (1985) and Blackwell (1988).

Rock type	Thermal conductivity (W/m.K)
Limestone	2.8 ± 1.1
Dolomite	5.03 ± 2.01
Anhydrite	5.35 ± 2.14
Shale	1.25 ± 0.50
Sandstone	3.35 ± 1.34
Siltstone	1.03 ± 0.41
Claystone	1.03 ± 0.41
Marlstone	3.0 ± 1.1
Chert	1.4 ± 0.5
Coal	0.2 ± 0.2
Conglomerate	3.2 ± 1.8
Salt	5.7 ± 1.0
Skipped interval	2.3 ± 2.0

Blackwell (1988); all the other values are equal to the values in Table 2.3.

It can be seen from Table 2.4 that the most abundant rocks in the Jeanne d'Arc Sub-basin, shale, siltstone, and claystone, have assumed thermal conductivity values that are lower than the measured values of Table 2.2.

In Table 2.5 the effective thermal conductivity for each well is presented. The values of the second column were obtained using the values of Table 2.2 and Table 2.3, and the values of the third column were obtained using the values of Table 2.4. As should be expected, the effective thermal conductivity values obtained using the data from Blackwell (1988) are lower than those obtained using the measured thermal conductivities. As the values reported by Blackwell seem to be the lowest ever reported for shales and siltstones, and those obtained in this study seem to be slightly high, the two sets of effective thermal conductivities listed in Table 2.5 can be considered as lower and upper bounds for that parameter in this particular basin. Close inspection of the samples used to measure thermal conductivity showed that some contained salt. This can explain, to a certain degree, the generally high thermal conductivity values measured in some of the rocks of the Jeanne d'Arc Sub-basin.

In Table 2.5 the wells Terra Nova I-97, Terra Nova K-17, Terra Nova K-18, North Ben Nevis P-93, Hibernia B-08, and Gambo N-70 are not listed because Canadian Stratigraphic

Table 2.5 - Effective thermal conductivity for each well in the Jeanne d'Arc Sub-basin using measured and assumed (Beach, 1985) thermal conductivity values (Set 1), and only assumed values (Beach, 1985; Blackwell, 1988) (Set 2).

Well name	K_{eff} (Set 1) (W/m.K)	K_{eff} (Set 2) (W/m.K)
Adolphus D-50	2.23 ± 0.64	1.19 ± 0.34
Adolphus 2K-41	2.40 ± 0.76	1.29 ± 0.40
Ben Nevis I-45	2.25 ± 0.73	1.14 ± 0.35
Beothuk M-05	2.60 ± 0.56	1.44 ± 0.31
Bonanza M-71	2.18 ± 0.76	0.95 ± 0.29
Conquest K-09	2.24 ± 0.65	1.02 ± 0.28
Cormorant N-83	2.68 ± 0.55	1.51 ± 0.35
Dominion O-23	2.28 ± 0.75	1.05 ± 0.31
Egret K-36	2.63 ± 0.55	1.64 ± 0.34
Egret N-46	2.74 ± 0.58	1.61 ± 0.35
Flying Foam I-13	2.40 ± 0.64	1.17 ± 0.32
Hebron I-13	2.41 ± 0.58	1.17 ± 0.28
Hibernia B-27	2.70 ± 0.62	1.08 ± 0.28
Hibernia C-96	2.55 ± 0.65	1.06 ± 0.27
Hibernia G-55A	2.99 ± 0.65	1.38 ± 0.32
Hibernia I-46	2.91 ± 0.69	1.25 ± 0.34
Hibernia K-14	2.21 ± 0.70	1.08 ± 0.32
Hibernia K-18	2.15 ± 0.74	1.11 ± 0.37
Hibernia O-35	3.00 ± 0.76	1.03 ± 0.33
Mara M-54	2.43 ± 0.63	1.10 ± 0.29
Mercury K-76	2.59 ± 0.65	1.23 ± 0.30
Murre G-67	2.37 ± 0.63	1.38 ± 0.38
Nautilus C-92	2.11 ± 0.70	1.06 ± 0.32
N Dana I-43	2.50 ± 0.65	0.98 ± 0.27
N Trinity H-71	2.41 ± 0.60	1.16 ± 0.30
Port au Port J-97	2.56 ± 0.55	1.54 ± 0.36
Rankin M-36	2.30 ± 0.52	1.26 ± 0.30
S Tempest G-88	2.23 ± 0.69	1.07 ± 0.31
Terra Nova K-07	2.58 ± 0.60	1.29 ± 0.30
Trave E-87	2.36 ± 0.71	1.04 ± 0.29
Voyager J-18	2.53 ± 0.54	1.34 ± 0.29
W Ben Nevis B-75	2.32 ± 0.74	1.15 ± 0.34
W Flying Foam L-23	2.36 ± 0.71	1.02 ± 0.28
Whiterose J-49	2.34 ± 0.74	1.08 ± 0.32
Whiterose N-22	2.27 ± 0.72	1.00 ± 0.29

Service does not yet have rock analyses for them.

Figures 2.6 and 2.7 are maps of the effective thermal conductivity distributions for the two data sets listed in Table 2.5.

2.3 Heat Flow Estimates

Using Equation 1.3, the corrected thermal gradients of Table 2.1, and the effective thermal conductivities listed in Table 2.5, heat flow density estimates have been made for the Jeanne d'Arc Sub-basin.

Table 2.6 presents the heat flow density values for wells for which thermal gradients and effective thermal conductivities were calculated using measured and assumed (Column 3) as well as only assumed (Column 4) thermal conductivitiy values; also shown are the depths of the deepest BHT measurements. As can be seen, the heat flow densities obtained using the thermal conductivities reported by Blackwell (1988) (Column 4) are less than those obtained using the measured thermal conductivities of some rocks of the basin. Therefore, as for the effective thermal conductivity values themselves, these heat flow density values may constitute upper and lower bounds for the heat flow density at these locations in the Jeanne d'Arc Sub-basin.

Maps of heat flow density for the two sets of data listed in Table 2.6 are shown in Figures 2.8 and 2.9. These

Table 2.6 - Heat flow density (HFD) values calculated using measured and assumed thermal conductivity values (Set 1 of Table 2.5), and using only assumed thermal conductivity values (Set 2 of Table 2.5).

Well name	Maximum depth (m)	HFD (Set 1) (mW/m^2)	HFD (Set 2) (mW/m^2)
Adolphus D-50	3537	69 ± 20	37 ± 11
Adolphus 2K-41	3502	80 ± 29	43 ± 16
Ben Nevis I-45	4707	57 ± 22	29 ± 11
Beothuk M-05	3659	65 ± 17	36 ± 9
Bonanza M-71	5077	71 ± 25	31 ± 10
Conquest K-09	4804	75 ± 22	34 ± 10
Cormorant N-83	2888	68 ± 18	38 ± 11
Dominion O-23	3803	60 ± 20	28 ± 8
Egret K-36	3241	62 ± 14	39 ± 9
Egret N-46	2646	74 ± 16	43 ± 9
Flying Foam I-13	1088	64 ± 17	31 ± 8
Hebron I-13	4569	58 ± 16	28 ± 8
Hibernia B-27	4279	71 ± 21	28 ± 9
Hibernia C-96	4309	64 ± 17	26 ± 7
Hibernia G-55A	3342	70 ± 19	32 ± 9
Hibernia I-46	3302	68 ± 23	29 ± 10
Hibernia K-14	3965	50 ± 16	25 ± 7
Hibernia K-18	4932	57 ± 20	30 ± 10
Hibernia O-35	4072	71 ± 23	26 ± 9
Mara M-54	4333	62 ± 16	28 ± 7
Mercury K-76	5051	58 ± 15	28 ± 7
Murre G-67	2913	61 ± 16	35 ± 10
Nautilus C-92	5003	61 ± 21	31 ± 10
N Dana I-43	5059	76 ± 25	30 ± 10
N Trinity H-71	4638	65 ± 17	31 ± 9
Port au Port J-97	2591	65 ± 14	39 ± 9
Rankin M-36	3871	49 ± 12	27 ± 7
S Tempest G-88	4456	70 ± 27	34 ± 12
Terra Nova K-07	3025	62 ± 25	31 ± 12
Trave E-87	3815	71 ± 29	32 ± 12
Voyager J-18	3615	73 ± 15	39 ± 8
W Ben Nevis B-75	4857	62 ± 21	31 ± 10
W Flying Foam L-23	3532	70 ± 28	30 ± 12
Whiterose J-49	4401	75 ± 24	34 ± 10
Whiterose N-22	3755	72 ± 23	32 ± 9

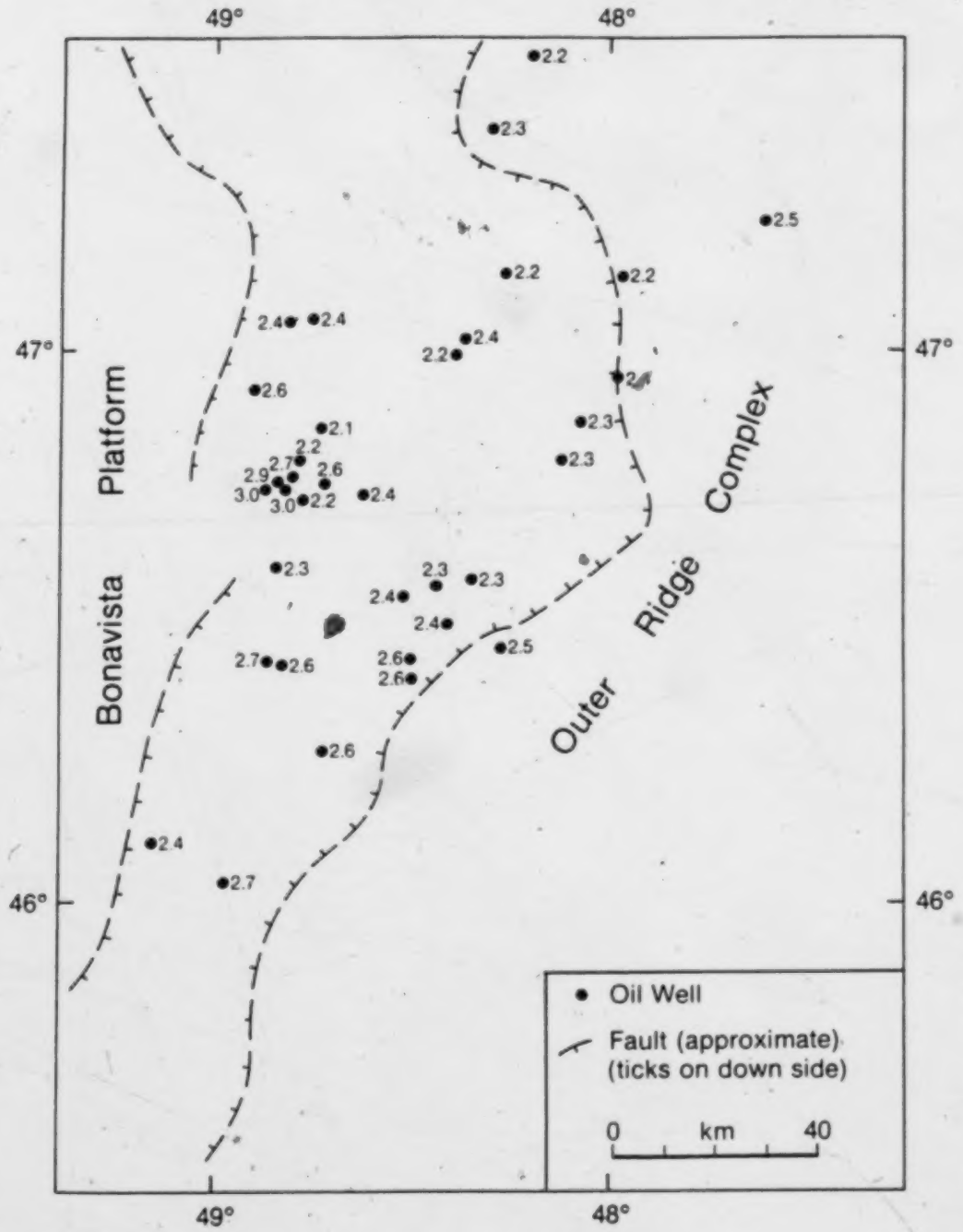

Figure 2.6 Map of the distribution of effective thermal conductivity calculated using measured and assumed thermal conductivity values (Set 1 of Table 2.5).

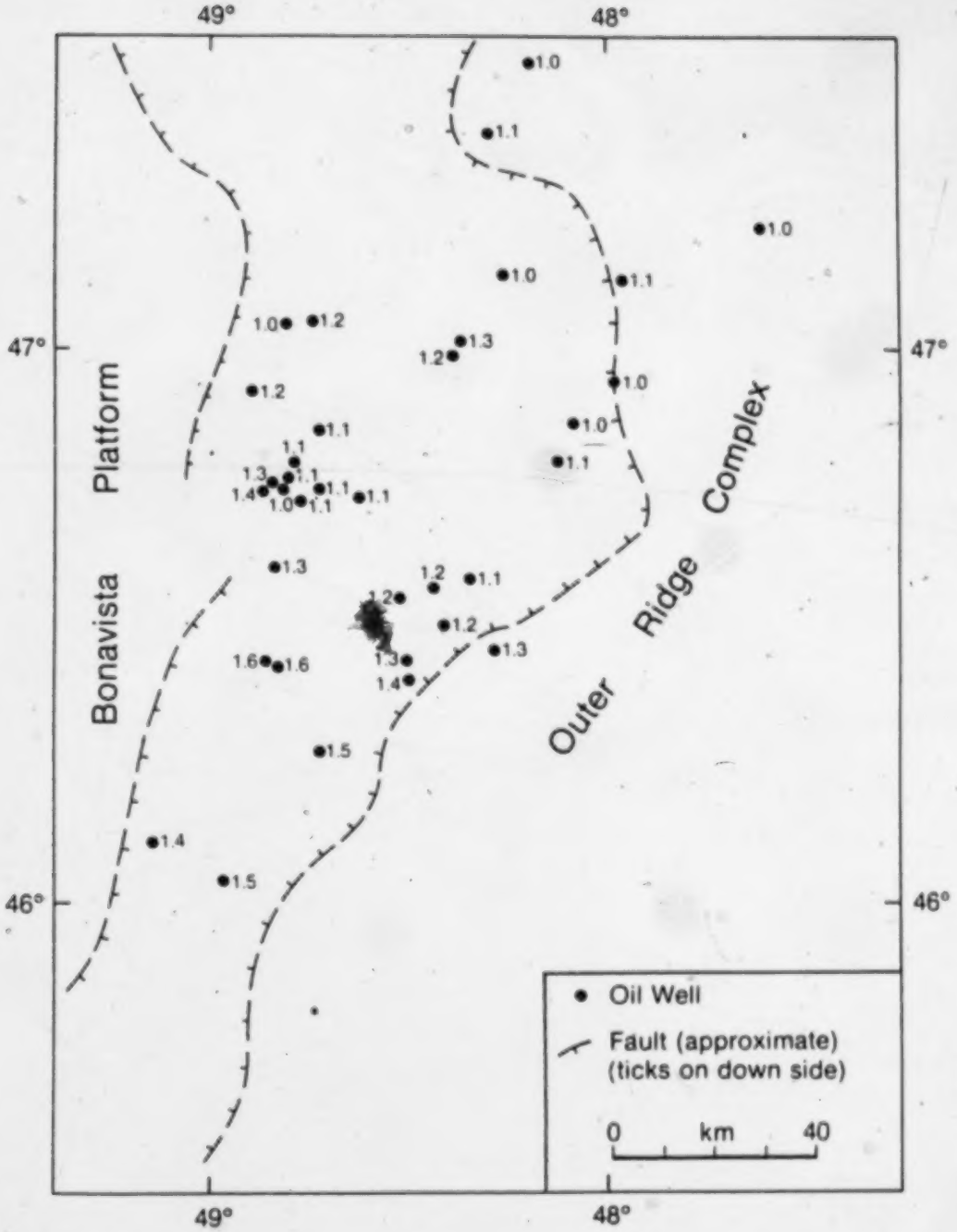

Figure 2.7 Map of the distribution of effective thermal conductivity calculated using only assumed thermal conductivity values (Set 2 of Table 2.5).

figures indicate that two main heat flow density regions occur in the basin, separated in the figures by profile AA'. Data Set 1 indicates that the mean heat flow density north of AA' is 71 mW/m^2 and to the south is 63 mW/m^2 compared with an average for the whole basin of 66 mW/m^2. Data Set 2 gives a mean heat flow density in the northern part of the area of 33 mW/m^2 and in the south of 32 mW/m^2 compared with an average value for the basin of 32 mW/m^2.

However, the errors in the heat flow density values are high, and therefore their distribution may have little meaning when the whole basin is considered. In spite of this, the general trend seems to indicate two regions with slightly different heat flow density values.

It is interesting to note that the region that appears to have higher heat flow density corresponds to the deeper part of the basin, while the shallower part corresponds to the area of lower heat flow density values. Generally, however, shallowest basement means higher surface heat flow density and so the above result may indicate that the heat flow density, and therefore the thermal regime in the Jeanne d'Arc Sub-basin, is not controlled by topography or heat generation in the basement.

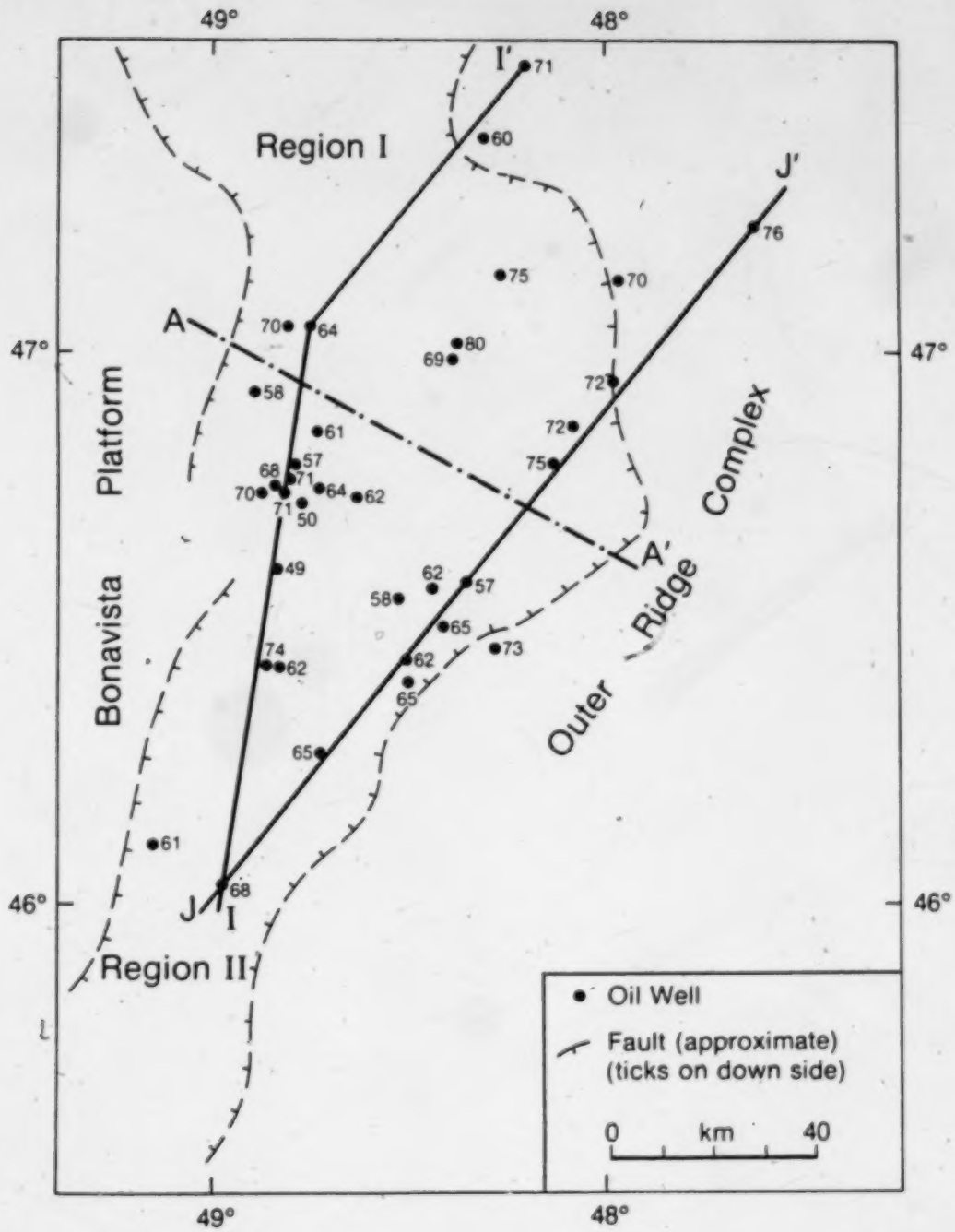

Figure 2.8 Heat flow density in the Jeanne d'Arc Sub-basin using the first set of values listed in Table 2.6.

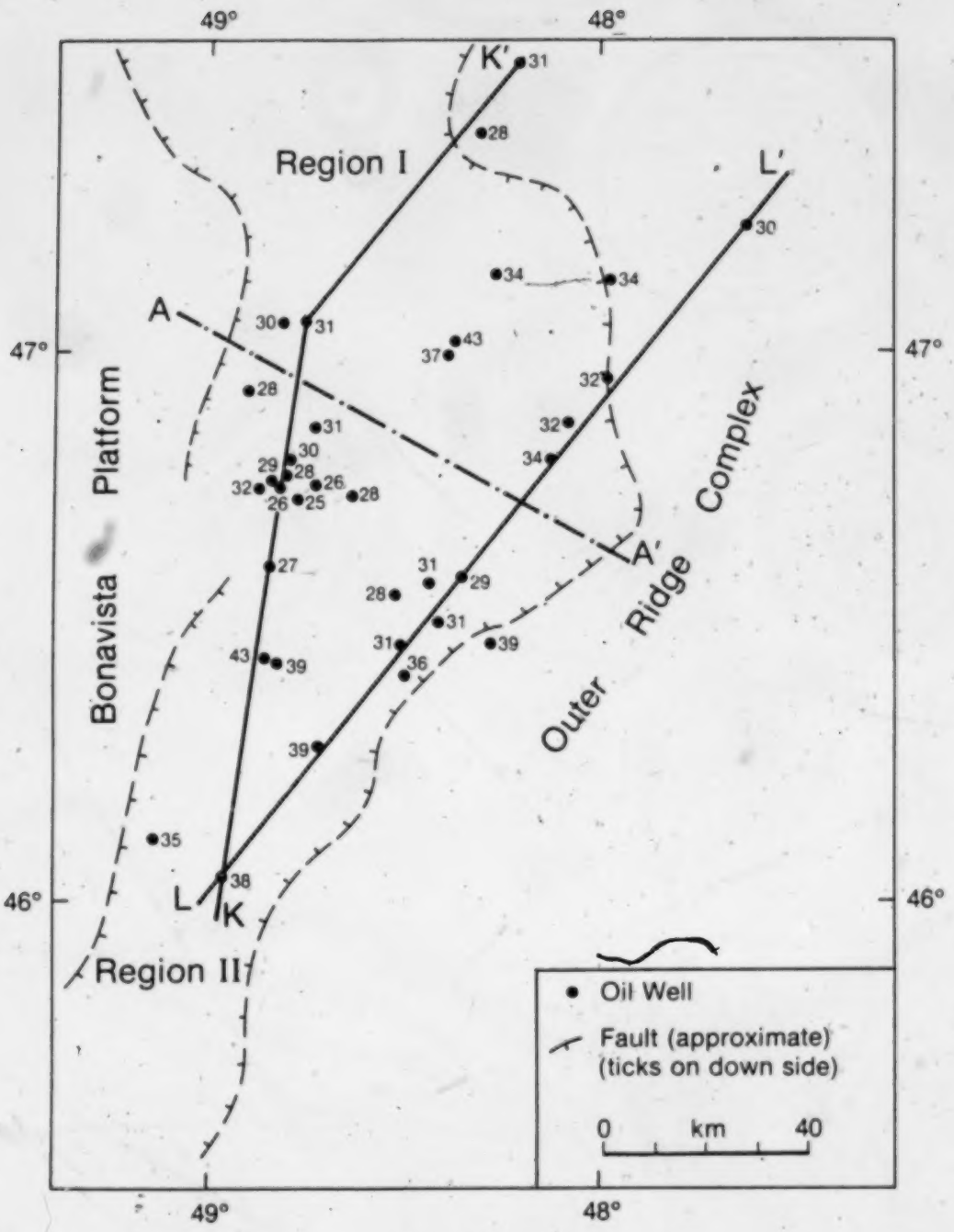

Figure 2.9 Heat flow density in the Jeanne d'Arc Sub-basin using the second set of values listed in Table 2.6.

2.4 Error Analysis

During the calculations of thermal gradients, effective thermal conductivities, and heat flow densities for each well of the Jeanne d'Arc Sub-basin, errors and error propagation were computed using the general rules of error analysis.

To estimate the error in the thermal gradient for each well, two lines with the same origin as the average thermal gradient and passing through the two BHT values that are most distant above and below it were drawn on the plots of corrected BHTs versus depth. These two lines represent the maximum and the minimum gradients that can be drawn in each particular plot. The differences in gradient between these maximum and minimum values and the average thermal gradient was calculated, and the larger value was taken to be the error in the average thermal gradient. A schematic representation of this procedure is given in Figure 2.10, where the solid line represents the average thermal gradient, and the dashed lines represent the maximum and minimum gradients for the well.

To estimate the error in the effective thermal conductivity the following formula is used (Beach, 1985):

$$\delta K_{eff} = \frac{\left(\sum_{i=1}^{n} \Delta z_i\right) \sqrt{\sum_{i=1}^{n} \left(\frac{\Delta z_i \delta K_i}{K_i^2}\right)^2}}{\left(\sum_{i=1}^{n} \frac{\Delta z_i}{K_i}\right)^2} \qquad (2.5)$$

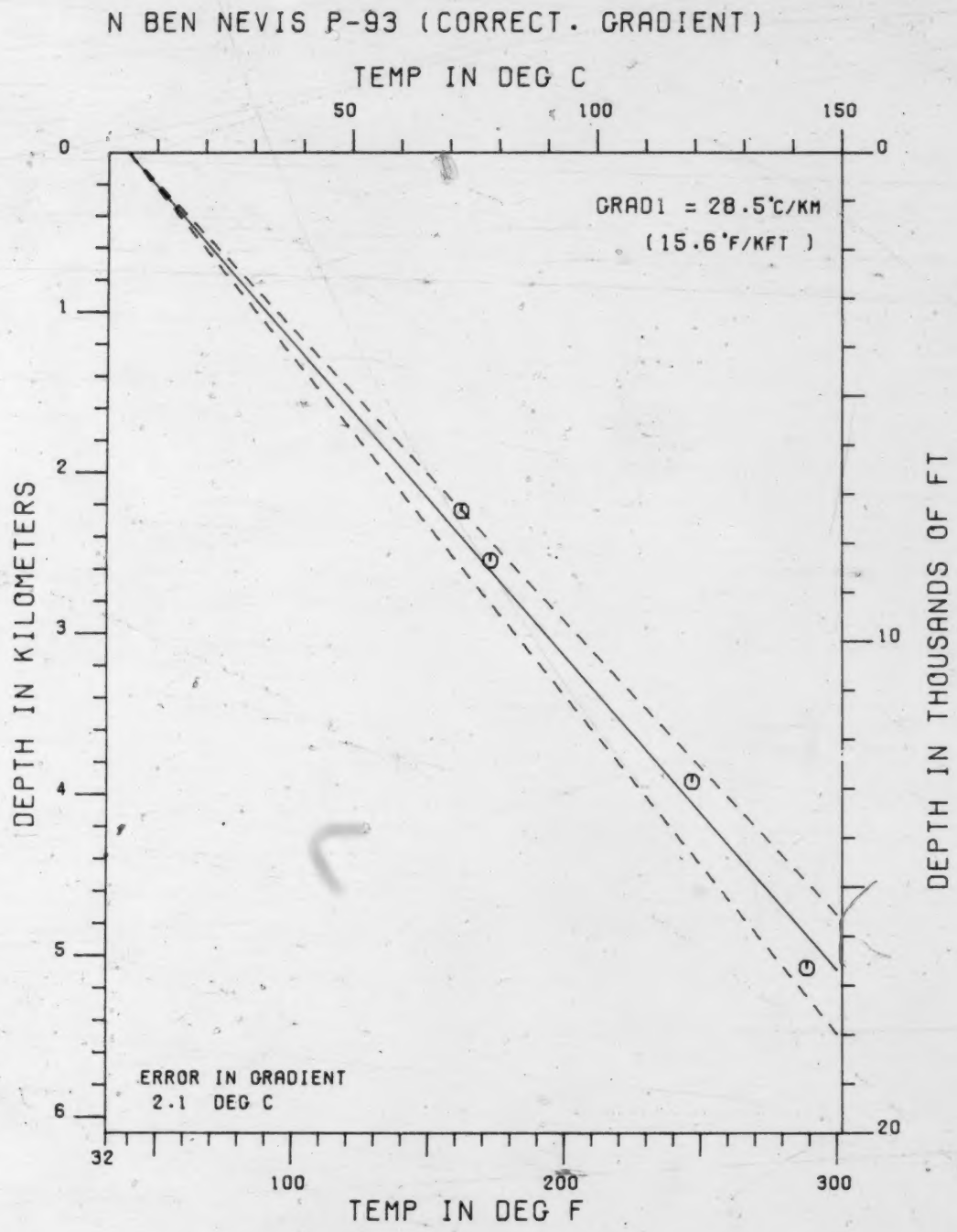

Figure 2.10 Example of graphical estimation of the error in the thermal gradient (see text for explanation).

where Δz_i is the total thickness of rock type i, K_i is the thermal conductivity of rock type i at 22 ^{o}C, and δK_i is the error in the thermal conductivity of rock type i.

To estimate the errors in the thermal conductivities of the rocks two approaches were followed. First, since it was not possible to estimate a statistical error in each individual thermal conductivity measurement because of an insufficient number of measurements for the same rock type, an error of 40% of the average thermal conductivity for each rock type was chosen (Table 2.3 and Table 2.4). The same criterion was applied to assumed values from the literature that did not have any error estimate associated with them (e. g., the values obtained from Blackwell (1988)). The value of 40% of the average thermal conductivity of each rock type was chosen because it is approximately equal to the maximum average error found in the literature for rocks of the type encountered in the Jeanne d'Arc Sub-basin. Second, for all assumed values that had errors associated with their average thermal conductivities in the literature, the errors assumed for the rocks found in the Jeanne d'Arc Sub-basin (Table 2.3) were taken equal to the published ones. These high errors in the thermal conductivity values contribute to the high errors in the calculated heat flow densities.

As the errors estimated for the thermal gradients and the effective thermal conductivities are uncorrelated, the following error formula, deduced from Equation 1.3, was

applied to calculate the errors in the heat flow densities:

$$\delta q = q\left[\left(\frac{\delta K_{eff}}{K_{eff}}\right)^2 + \left(\frac{\delta G}{G}\right)^2 \right]^{1/2} \qquad (2.6)$$

where the variables have the same meaning as in Equation 1.3 and G now represents the average thermal gradient over the geologic section, [dT/dz].

It is seen that the errors in the calculated heat flow densities are very high. However, the major contribution to those errors is due to the uncertainties in the thermal conductivity values used; i.e. the 40% as stated above. Therefore, additional measurements on discs and rock cuttings would make better thermal conductivity estimates possible, and so substantially reduce the errors in the heat flow density values.

3. DISCUSSION AND CONCLUSIONS

3.1 Heat Flow Trends

From Figure 2.8 and Figure 2.9 it is apparent that heat flow density is not uniform throughout the Jeanne d'Arc Sub-basin. For subsequent discussion, and in accordance with the heat flow density pattern, the maps shown in the two figures are divided into two regions that have different average heat flow densities by the line AA'. It should be noticed that the line AA' lies slightly north of the northern trans-basin fault trend of the basin (see Figure 1.2).

In Figure 2.8 the average heat flow density for the basin is 66 mW/m^2 and it is seen that the heat flow densities in the northern region (Region I) are generally higher (average 71 mW/m^2) than those in the southern region (Region II) (average 63 mW/m^2).

In Figure 2.9 the average heat flow density for the basin is 32 mW/m^2 and the heat flow density pattern is more complex than that of Figure 2.8. Careful inspection of Figure 2.9 indicates that in going from Region I to Region II, the heat flow density values seem to first decrease and then increase again as the southern part of the basin is approached. The central part of the basin has heat flow

density values that are slightly lower than the average for the basin, while the heat flow density values increase in the south to slightly higher values than the average value for the basin.

It is interesting to note the high heat flow density values calculated for the wells Adolphus D-50, Adolphus 2K-41, and Egret N-46. These high values are probably associated with salt diapirs identified in the basin (see Figure 1.2). The fact that four wells in the Hibernia oil field (see Fifure 2.8) have high heat flow density values is also very interesting. This is probably not only an indication of less shale content in the formations, but also the result of the high thermal conductivity that sediments generally have when their pores are filled with oil (Buntebarth, 1984). If this interpretation is correct, it means that heat flow density methods constitute another tool for the identification of liquid hydrocarbons.

Figures 3.1 and 3.2 present four heat flow density profiles across the Jeanne d'Arc Sub-basin for the lines II' and JJ' in Figure 2.8 and KK' and LL' in Figure 2.9. The values with S indicate that the wells are near a known diapir.

As stated in Chapter II, in spite of the fact that the errors in heat flow densities for the individual wells are high, it appears that, in a statistical sense, the differences between the two regions defined above convey information about the heat flow density pattern in the

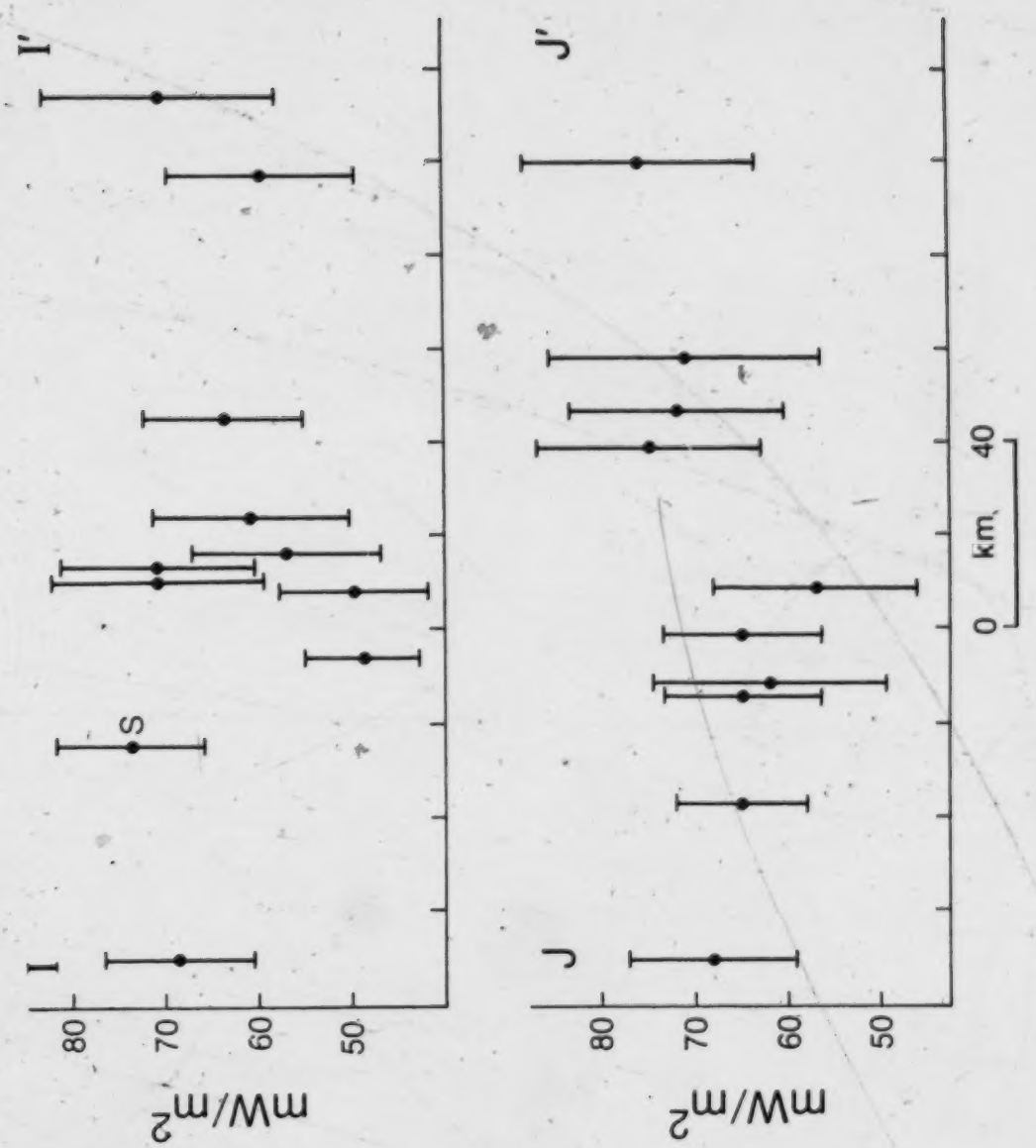

Figure 3.1 HFD cross-sections I-I' and J-J' depicted in Figure 2.8. The arrow indicates the position of the line of separation of Region I from Region II.

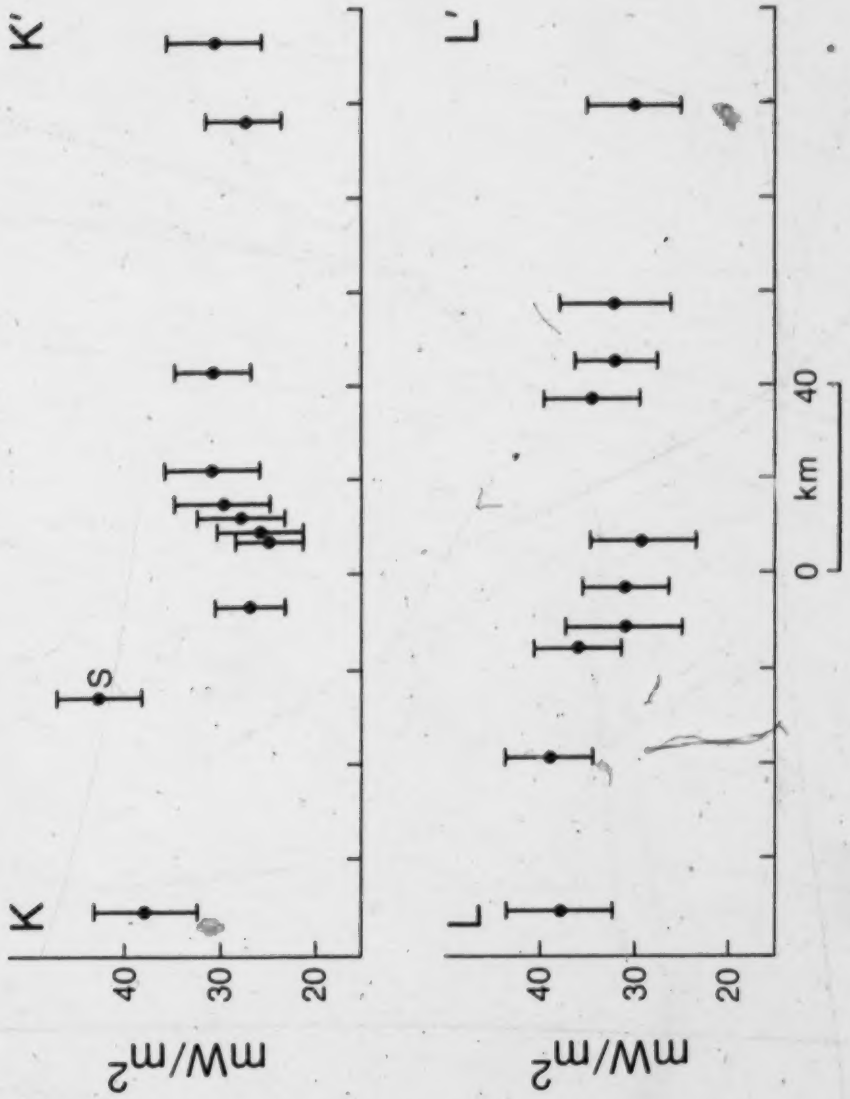

Figure 3.2 HFD cross-sections K-K' and L-L' depicted in Figure 2.9. The arrow indicates the position of the line of separation of Region I from Region II.

Jeanne d'Arc Sub-basin.

Since the heat flow density is the product of the average geothermal gradient and the effective thermal conductivity calculated for each well, it is of interest to consider the distribution patterns of these two parameters in the basin, as are shown in Figures 2.5, 2.6, and 2.7. From Figure 2.5 it is apparent that two geothermal gradient regions with different average values exist; the northern area, which coincides with Region I of Figures 2.8 and 2.9 with high geothermal gradient values, and the southern area, which coincides with Region II of Figures 2.8 and 2.9 with low values, compared with the average geothermal gradient.

For the effective thermal conductivity (see Figure 2.6 and Figure 2.7), however, distinctive zones with different average values cannot be identified. Nevertheless, it appears that in both figures the effective thermal conductivity gradually increases from north to south. If this increase is real, it means that the clay content of the sediments is higher in the northern part of the basin than in the southern part. This could explain the higher geothermal gradients calculated in the northern region of the basin. Furthermore, the fact that wells in the Hibernia oil field have high effective thermal conductivities is interesting. As already stated with reference to the heat flow density maps, this may be an indication that in that local area the sediments are less shaly than in other parts of the basin; this may help explain the occurrence of oil

accumulations there (Roberts, 1981).

Reiter and Jessop (1985) calculated heat flow densities in offshore eastern Canada from bottom-hole temperature data. They used all the available thermal information for the area and calculated the heat flow densities in some of the wells that are used in this study. Those wells are Adolphus D-50, Adolphus 2K-41, Cormorant N-83, Egret N-46, and Murre G-67. The heat flow density values presented by Reiter and Jessop (1985) as the most reliable ones for these wells are 102, 96, 71, 60, and 84 mW/m^2 respectively. When compared with the corresponding values of Table 2.6, these heat flow density values are higher than those calculated in the present work, except for the well Egret N-46. In their study, Reiter and Jessop (1985) used assumed values for the thermal conductivities of the rocks, whereas in this thesis measured as well as assumed thermal conductivity values have been used to calculate the heat flow densities. As explained earlier, the heat flow density values calculated with measured as well as assumed thermal conductivity values (Table 2.6, set 1) define upper limits for the heat flow densities for these wells in the Jeanne d'Arc Sub-basin. This conclusion, which was inferred from the analysis of the thermal conductivity measurements performed on discs from four wells of the basin, implies that the heat flow density values reported by Reiter and Jessop (1985) are possibly overestimated.

It is also interesting to note that heat flow density values determined by more precise techniques in the southern Grand Banks (six heat flow density values with an average of 44 mW/m^2, and ranging from 33 to 59 mW/m^2) (Lewis and Hyndman, 1976) fall within the upper and lower limits of the heat flow densities calculated here for the Jeanne d'Arc Sub-basin.

3.2 Tentative Interpretation of the Heat Flow Density in the Jeanne d'Arc Sub-basin

When trying to interpret heat flow density patterns in sedimentary basins or discussing their thermal regimes it must be borne in mind that a particular temperature distribution can be caused by several factors or even by errors in the calculations of the thermal quantities. Considering this latter problem, it is certain that errors are introduced in the calculations as a result of the method itself as well as inaccuracies in the fundamental data, i.e., bottom-hole temperature values. However, in spite of these problems, in most regions thermal gradients and heat flow density values seem to show coherent patterns, in a statistical sense. Therefore, as a first approximation, it can be said that the heat flow density patterns reported in this thesis are probably real.

There are a number of mechanisms that can explain vertical as well as horizontal heat flow density

heterogeneities in sedimentary basins. Among the most important ones are the refraction of heat by geological structures with thermal conductivity contrasts, radioactive heat generation in sediments, fluid motion within the basins, and geological events such as igneous activity and rapid sedimentation, erosion, uplift or subsidence. In what follows, each of these mechanisms will be considered to see if they can qualitatively explain the heat flow density pattern of the Jeanne d'Arc Sub-basin.

For the area studied in this thesis, there has been no known significant igneous activity, at least during periods that could affect the present heat flow density distribution at the surface.

Also it does not seem probable that refraction of heat occurs to a significant extent in the Jeanne d'Arc Sub-basin. In fact, this process is particularly important in faulted regions where geological formations with high thermal conductivity contrasts lie side by side. That is not the case in this basin. There is, however, a small scale heat refraction process that may occur in two particular areas of the basin that are located near the wells Adolphus D-50, Adolphus 2K-41, Egret K-36, and Egret N-46. These wells have a high calculated heat flow density value which results from the fact that they are near salt diapirs.

Subsidence cannot explain the heat flow density pattern in the Jeanne d'Arc Sub-basin. It is only important for rates approximately equal to or higher than 1 mm/year, and

when different parts of the basin have different rates of subsidence. For the Jeanne d'Arc Sub-basin the rate of subsidence lies between 0.1 and 0.03 mm/year (Enachescu, 1987), so the accumulated sediments remain close to thermal equilibrium.

Radioactive heat generated in sediments can greatly change the heat flow density pattern in a basin, particularly when its depth is greater than 5 km and the sediments have a high content of radioactive materials (Rybach, 1986). Values of sedimentary heat generation reported by Keen and Lewis (1982) show that for the Jeanne d'Arc Sub-basin its contribution to the surface heat flow density may lie between 5 and 10 mW/m^2. However, this is not consistent with the heat flow density patterns shown in Figures 2.8 and 2.9. In fact, the region corresponding to the shallower part of the basin has equal or higher heat flow values than the region corresponding to the deeper part (see Figure 2.8 and Figure 2.9), which contradicts the fact that thicker sediments should correspond to higher heat generation and, therefore, higher heat contribution to the surface heat flow density.

One of the most important ways to determine whether or not the thermal regime in a certain basin is influenced by heat convection is to determine if the heat flow density changes with depth; if it changes with depth, there is probably fluid motion taking place. This was investigated for the Jeanne d'Arc Sub-basin using both of the heat flow

density patterns depicted in Figure 2.8 and Figure 2.9. The average heat flow densities for the wells were plotted as a function of the depths to the deepest bottom-hole temperature determination in each well. This determination of variation of heat flow density with depth has a smoothing effect, since any possible change of heat flow density with depth along the lengths of the wells is not considered. This results from the approach followed in this thesis where only linear average thermal gradients and average effective thermal conductivities were calculated. Nevertheless, if the wells have different depths, and if the heat flow density changes with depth, this variation should be seen in the graphs of the heat flow density values as a function of the depths of the wells.

Let us first consider the heat flow density values shown in Figure 2.8. For these values three correlation graphs were plotted: one in which the heat flow density values for all the basin are plotted as a function of the depths of the wells (Figure 3.3); one in which the heat flow density values north of the line AA' are plotted as a function of the depths (Figure 3.4); and one in which the heat flow density values south of line AA' are plotted as a function of depths (Figure 3.5). The solid lines in the figures are the least squares best fit straight lines, and the dashed lines represent the 95% confidence limits. From Figure 3.3 it is seen that for the whole basin there is no apparent dependence of the heat flow density with depth.

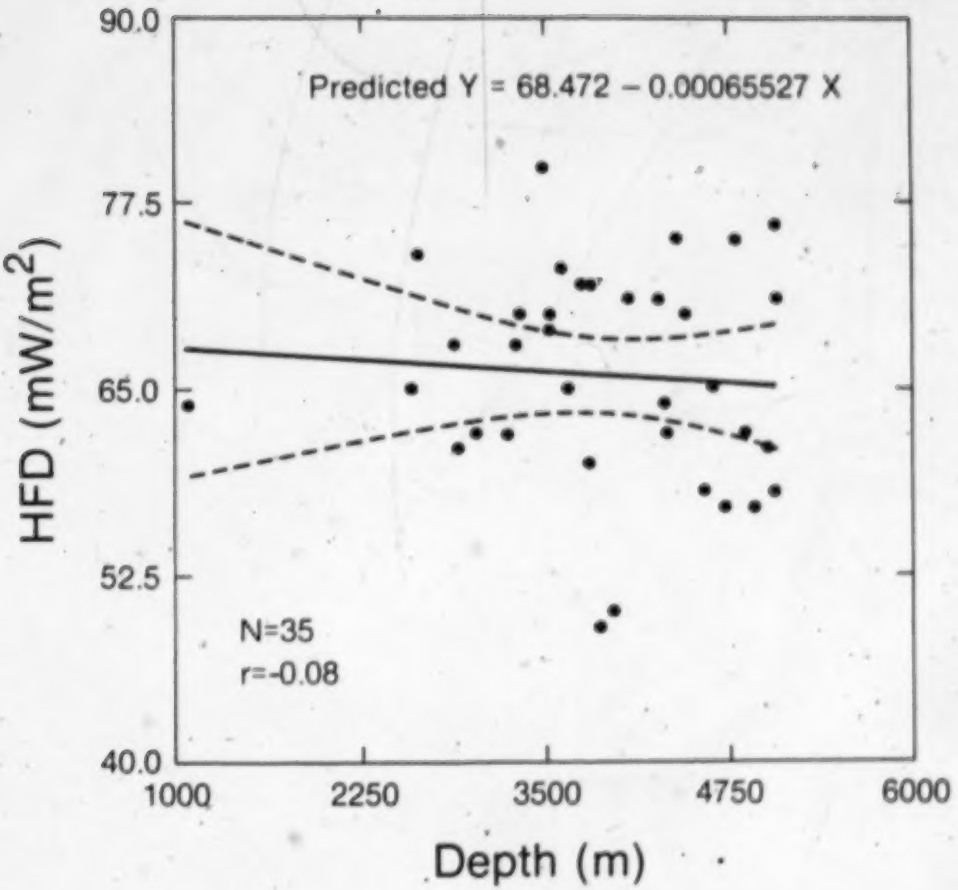

Figure 3.3 Correlation between HFD values and depth of the deepest BHT measured in each well of the Jeanne d'Arc Sub-basin. HFD values are calculated using measured and assumed thermal conductivity values.

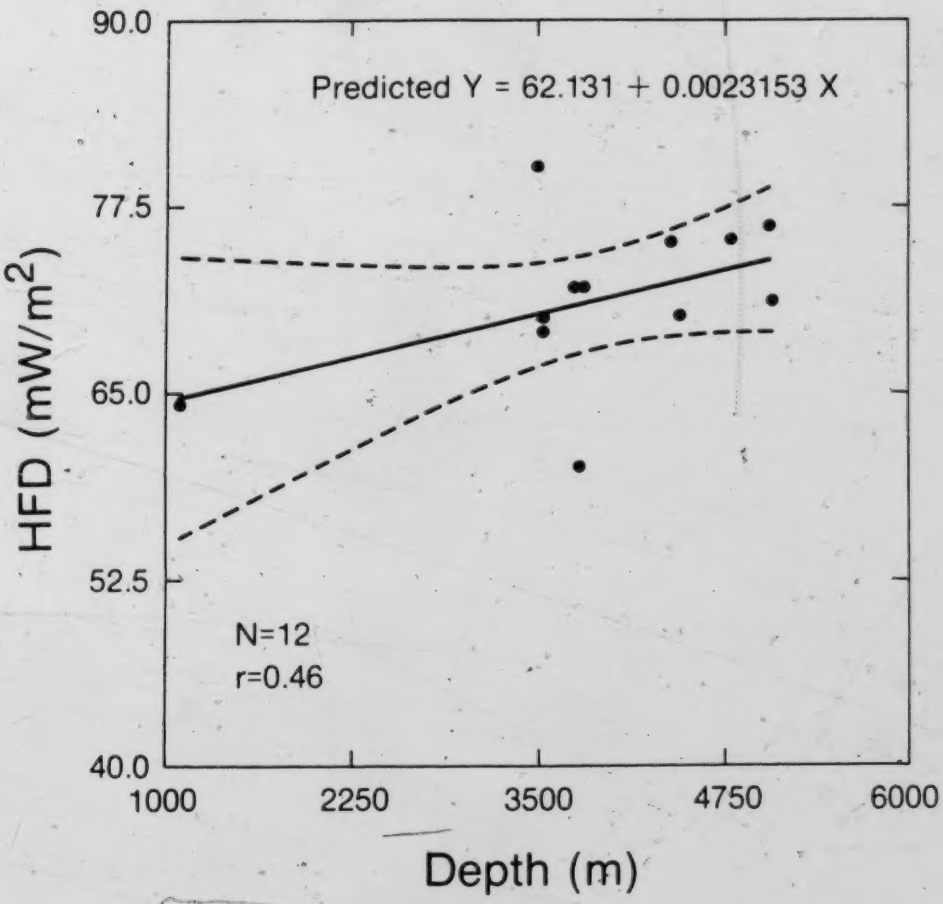

Figure 3.4 Correlation between HFD values and depth of the deepest BHT measured in the wells north of the line AA' of Figure 2.8 (Region I). HFD values are calculated using measured and assumed thermal conductivity values.

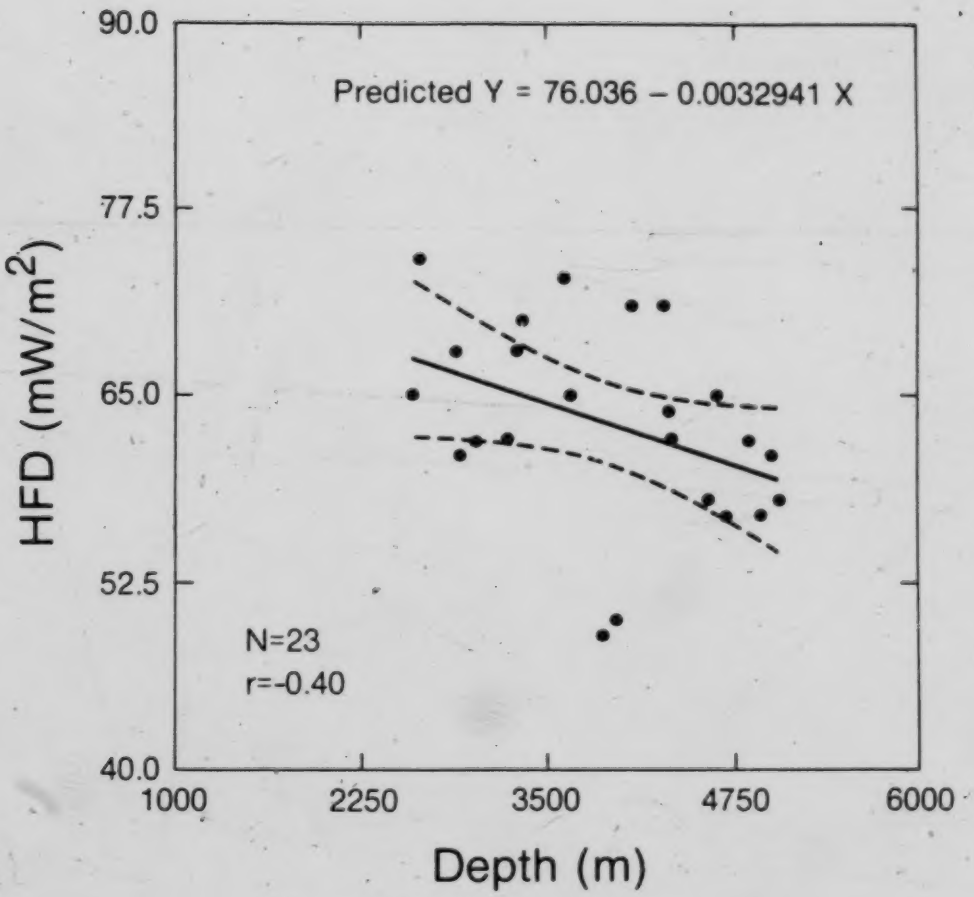

Figure 3.5 Correlation between HFD values and depth of the deepest BHT measured in each well south of the line AA' of Figure 2.8 (Region II). HFD values are calculated using measured and assumed thermal conductivity values.

However, this is not the case for Figures 3.4 and 3.5. In fact, the former indicates that heat flow density increases with depth while the second indicates the opposite. Of course, the correlation coefficients are poor and, therefore, the results are only qualitative; however, it should be remembered that the smoothing effect described above tends to decrease the dependence between the variables. Moreover, at this stage in the state of knowledge about the Jeanne d'Arc Sub-basin, a qualitative approach is appropriate.

If the pattern described above is true, it implies that the basin is not in thermal equilibrium and the cause of the non-equilibrium condition is heat transport by convection; i.e., fluid flow is occuring within the sediments. Figure 3.4 indicates that there is a downward component of fluid flow in the northern part of the basin, while Figure 3.5 shows an upward component of fluid flow in the south. Therefore, in the shallow sediments above the deeper part of the Jeanne d'Arc Sub-basin fluid is moving downward, while in the shallower part the fluids are rising. When the structural framework of the basin is considered (see Figure 1.2 and Figure 1.3), it can be inferred from this result that deep in the basin the main direction of the fluid flow must be from north to south through the gently rising layers. This model does not suggest any driving mechanism for the fluid flow in that direction. However, the northern part of the basin is extremely deep, and so dehydration may

be the driving force that maintains the fluid flow. Hot fluid may be forced from the deep part of the basin in the north to the shallow part in the south through the layers of sediments and transporting heat to increase the heat flow density there. This pattern would then imply descent of cold fluid from the upper sedimentary layers in the northern part of the basin. Figure 3.6 is a schematic diagram of the proposed general fluid flow pattern.

Similar correlation graphs were obtained for the heat flow density data of Figure 2.9 (see Figures 3.7, 3.8, and 3.9). In spite of the fact that these data indicate a more complex situation, upward fluid motion in the southern part of the basin appears to occur. However, there is little evidence from these data of downward fluid flow in the north.

It should be stressed that these results and conclusions are qualitative and the explanation of the heat flow density pattern in the Jeanne d'Arc Sub-basin and the suggested fluid flow model should still be considered as speculative. More data are necessary to confirm or discard the proposed model.

3.3 Future Work and Conclusions

The heat flow density pattern and the heat transport model described and discussed above are an attempt, perhaps the first one, to try to understand the thermal regime of

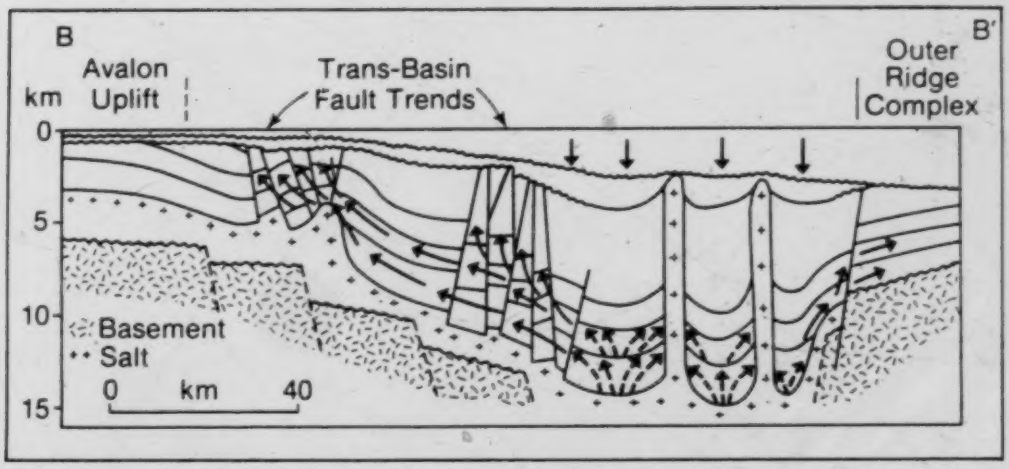

Figure 3.6 Schematic of the proposed general fluid flow pattern in the Jeanne d'Arc Sub-basin. Arrows indicate the flow directions. Dashed arrows indicate flow resulting from dehydration of deep sediments.

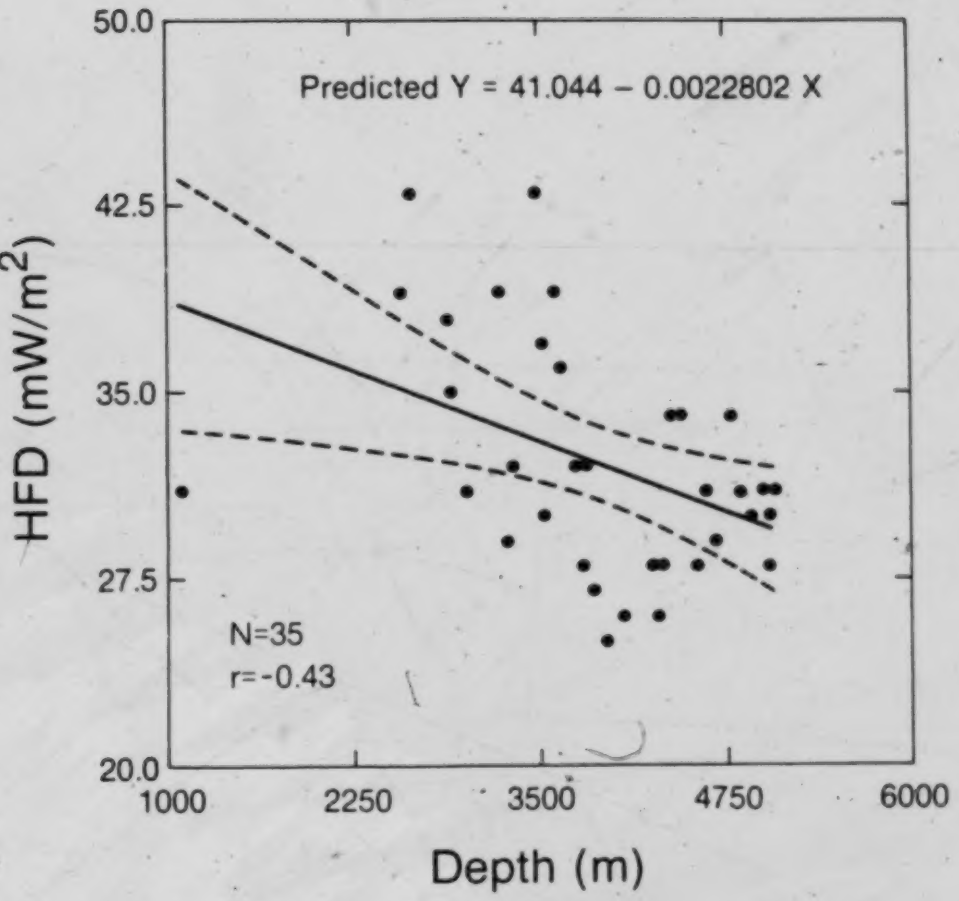

Figure 3.7 Correlation between HFD values and depth of the deepest BHT measured in each well of the Jeanne d'Arc Sub-basin (Figure 2.9). HFD values are calculated using only assumed thermal conductivity values.

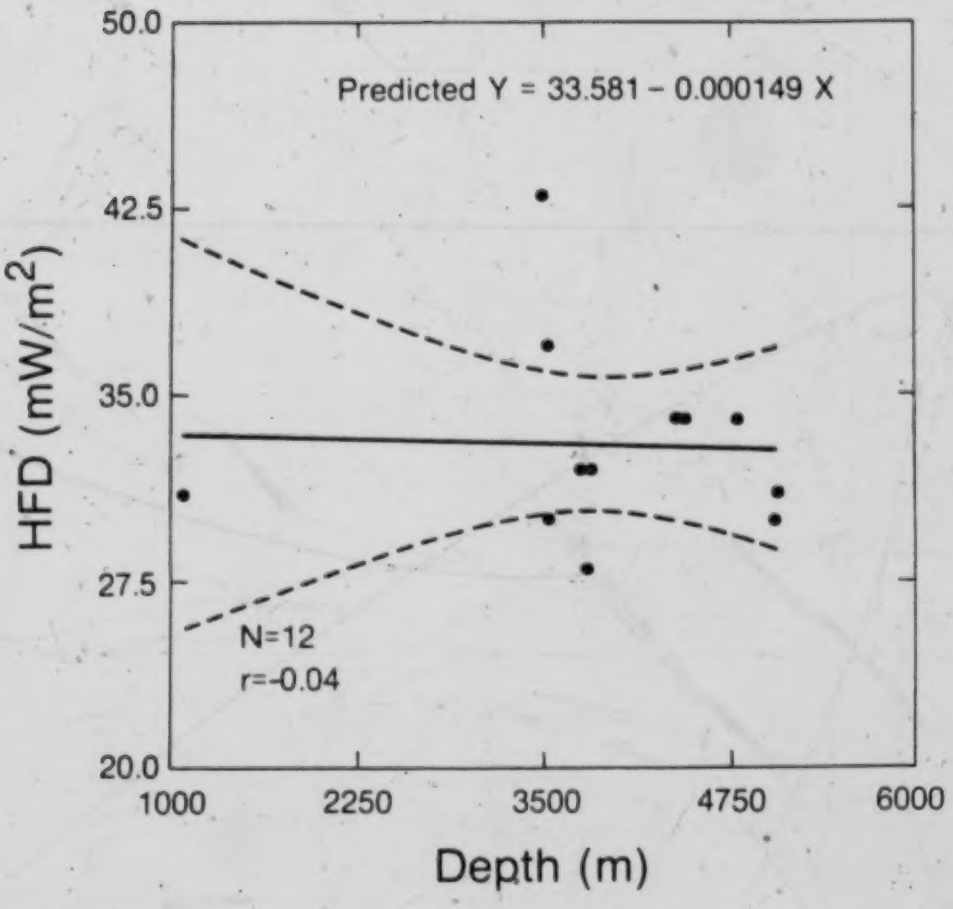

Figure 3.8 Correlation between HFD values and depth of the deepest BHT measured in the wells north of line AA' of Figure 2.9 (Region I). HFD values are calculated using only assumed thermal conductivity values.

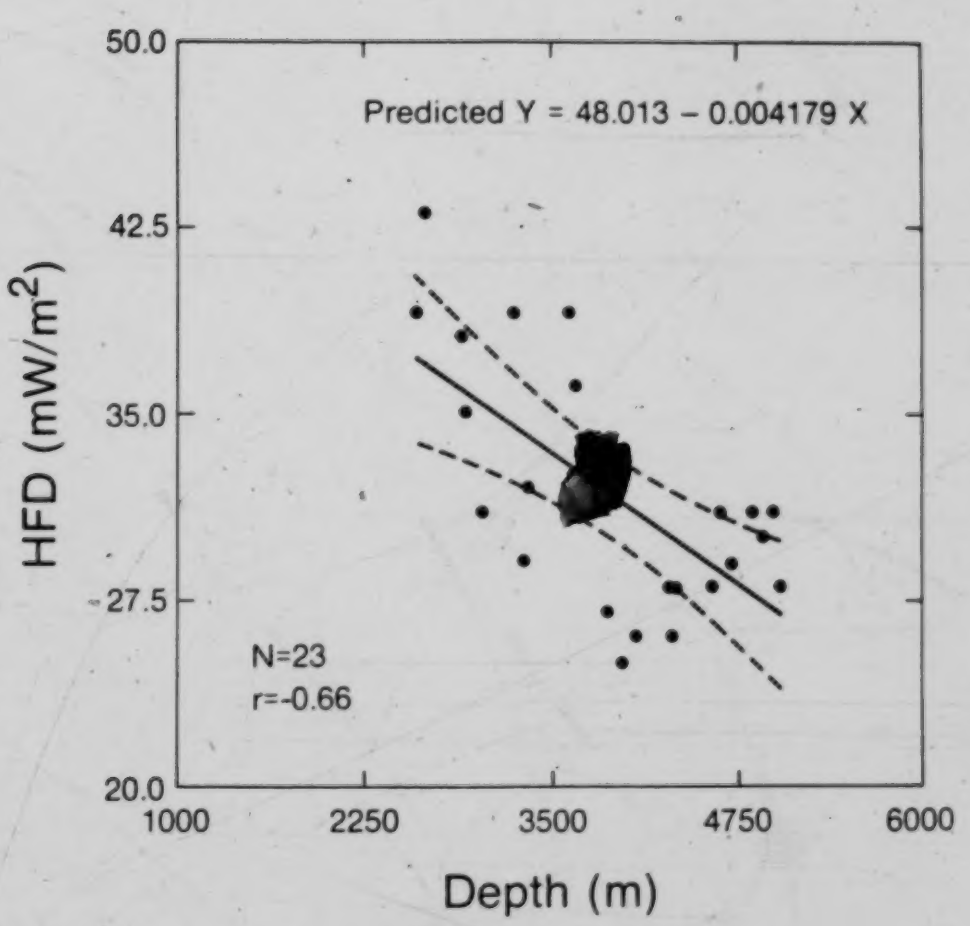

Figure 3.9 Correlation between HFD values and depth of the deepest BHT measured in each well south of the line AA' of Figure 2.9 (Region II). HFD values are calculated using only assumed thermal conductivity values.

the Jeanne d'Arc Sub-basin. The explanation and model are simple and only give clues about the mechanisms that create the present heat flow density pattern in the basin. Therefore, at this stage of knowledge, they can be considered speculative. The next natural step should be to try to quantitatively model the basin. In order to do that it is critically important to acquire more information about the thermal conductivity distribution and heat generation within the basin. This means that many more thermal conductivity measurements must be made on rock discs and cuttings as well as more determinations of the radiogenic element content of the rocks. This is particularly true for the basin claystones and shales, the most abundant rocks in the basin. Without new data it will be difficult to improve to any extent our knowledge of the thermal regime in the Jeanne d'Arc Sub-basin.

The average geothermal gradient in the Jeanne d'Arc Sub-basin is 27 ^{o}C/km. The average heat flow density is 66 mW/m^{2} if measured as well as assumed thermal conductivity values for the rocks in the basin are used for the calculation, and 32 mW/m^{2} if only assumed values obtained from the literature are used. Taking into account these averages, it can be inferred that the Jeanne d'Arc Sub-basin is an area of low to intermediate heat flow density (Reiter and Jessop, 1985) if additional measurements of thermal conductivity show the same trend as reported in this thesis. The value of 32 mW/m^{2} seems to be too low for the basin. In

fact, other studies in the Maritime Provinces of Canada suggest higher values of heat flow density (Lewis and Hyndman, 1976; Hyndman et al., 1979; Reiter and Jessop, 1985).

The results here indicate that the Jeanne d'Arc Sub-basin has two heat flow density zones: one in the north with relatively high heat flow density values, and one to the south with lower values. As expected, high heat flow density values were obtained for wells near salt diapirs.

The results suggest that the surface heat flow density in the Jeanne d'Arc Sub-basin is not controlled by the topography of the basement. Instead, fluid flow seems to play a fundamental role in the redistribution of heat throughout the basin. The thermal regime suggests that fluids flow from the deeper sediments of the northern region of the basin to the shallower sediments in the southern region. If this trend is true it can qualitatively explain the heat flow density pattern calculated for the basin and, at the same time, the accumulation of oil in the high thermal conductive and highly faulted Hibernia region (Roberts, 1981).

Because the Jeanne d'Arc Sub-basin is very deep and, at this stage, it is not possible to estimate the distribution of thermal conductivity of the sediments with depth or their heat generation, it is not possible to calculate the heat flow density from the basement or the temperature distribution there.

REFERENCES

Andrews-Speed, C. P., Oxburgh, E. R., and Cooper, B. A., 1984, Temperatures and depth-dependent heat flow in Western North Sea, Am. Assn. Petr. Geol. Bull., 68, 1764-1781.

Arthur, K. R., Cole, D. R., Henderson, G. G. L., and Kushnir, D. W., 1982, Geology of the Hibernia discovery, in: Halbouty, M. T., ed., The deliberate search for the subtle trap, American Association of Petroleum Geologists, Memoir 32, 181-196.

Beach, R. D. W., 1985, Sedimentary heat flow in Alberta, M.S. thesis, University of Alberta, Edmonton.

Beach, R. D. W., Jones, F. W., and Majorowicz, J. A., 1987, Heat flow and heat generation estimates for the Churchill basement of the Western Canadian Basin in Alberta, Canada, Geothermics, 16, 1-16.

Blackwell, D. D., and Steele, J. L., 1988, Thermal conductivity of sedimentary rocks: measurement and significance, in: Naeser E. Q., and McCulloh, T. H., eds., Thermal history of sedimentary basins, Springer-Verlag, 13-36.

Bullard, E. C., 1939, Heat flow in South Africa, Proc. R. Soc. London, Ser. A, 173, 474-502.

Buntebarth, G., 1984, Geothermics, an introduction, Springer-Verlag, Berlin Heidelberg, 144 pp.

Cao, S., Lerche, I., and Hermanrud, C., 1988, Formation temperature estimation by inversion of borehole measurements, Geophysics, 53, 979-988.

Carvalho, H. D. S., and Vacquier, V., 1977, Method for determining terrestrial heat flow in oil fields, Geophysics, 42, 584-593.

Chapman, D. S., Keho, T. H., Bauer, M. S., and Picard, M. D., 1984, Heat flow in the Uinta Basin determined from bottom hole temperature (BHT) data, Geophysics, 49, 453-466.

Chapman, D. S., Deming, and D., Willett, S., 1988, Analysis of temperature in sedimentary basins, in: Salle, C., Larson, R. M., and Sierding-Larsen, R., eds., Extensional basin modelling and paleotemperature reconstruction, International Union of Geodesy and

Geophysics, IUGS Monograph, in press.

Dowdle, W. L., and Cobb, W. M., 1975, Static formation temperature from well logs - an empirical approach, J. Pet. Technol., 27, 1326-1330.

Enachescu, M. E., 1987, Tectonic and structural framework of the Northeast Newfoundland continental margin, in: Beaumont, C., and Tankard, A. J., eds., Sedimentary basins and basin-forming mechanisms, Canadian Society of Petroleum Geologists, Memoir 12, 117-146.

Evans, T. R., and Coleman, N. C., 1974, North Sea geothermal gradients, Nature, 247, 28-30.

Fertl, W. H., and Wichmann, P. A., 1977, How to determine static BHT from well log data, World Oil, 184, 105-106.

Grant, A. C., McAlpine, and K. D., Wade, J. A., 1986, The continental margin of Eastern Canada: geological framework and petroleum potential, in: Halbouty, M. T., ed., Future petroleum provinces of the World, American Association of Petroleum Geologists, Memoir 40, 177-205.

Hyndman, R. D., Jessop, A. M., Judge, A. S., and Rankin, D. S., 1979, Heat flow in the Maritime Provinces of Canada, Can. J. Earth Sci., 16, 1154-1165.

Issler, D. R., 1984, Calculation of organic maturation levels for offshore eastern Canada - implications for general application of Lopatin's method, Can. J. Earth Sci., 21, 477-488.

Issler, D. R., and Beaumont, C., 1986, Estimates of terrestrial heat flow in offshore eastern Canada: discussion, Can. J. Earth Sci., 23, 2083-2085.

Jackson, A. E., 1985, Sediment thickness map, offshore eastern Canada: Geological Survey of Canada Open File Report.

Jones, F. W., Kushigbor, C., Lam, H. L., Majorowicz, J. A., and Rahman, M., 1984, Estimates of terrestrial thermal gradients and heat flow variations with depth in the Hinton-Edson area of the Alberta Basin derived from petroleum bottom-hole temperature data, Geophys. Prospect.,32, 1111-1130.

Jones, F. W., Majorowicz, J. A., and Lam, H. L., 1985, The variation of heat flow density with depth in the Prairies Basin of Western Canada, Tectonophysics, 121, 35-44.

Kappelmeyer, O., and Haenel, R., 1974, Geothermics with Special Reference to Application, Borntrager, Berlin-Stuttgart, 237 pp.

Keen, C. E., and Lewis, T., 1982, Measured radiogenic heat production in sediments from the continental margin of Eastern North America: implications for petroleum generation, Am. Assn. Petr. Geol. Bull., 66, 1402-1407.

Keen, C. E., Boutilier, R., De Voogd, B., Mudford, B., and Enachescu M. E., 1987, Crustral geometry and extensional models for the Grand Banks, Eastern Canada: constraints from deep seismic reflection data, in: Beaumont, C., and Tankard, A. J., Sedimentary basins and basin-forming mechanisms, Canadian Society of Petroleum Geologists, Memoir 12, 101-115.

Lachenbruch, A. H., and Brewer, M. C., 1959, Dissipation of the temperature effect of drilling a well in Arctic Alaska, U.S. Geol. Surv. Bull., 1083 C, 73-109.

Lam, H. L., and Jones, F. W., 1984a,Geothermal gradients of Alberta in Western Canada, Geothermics, 13, 181-192.

Lam, H. L., and Jones, F. W., 1984b, A statistical analysis of bottom-hole temperature data in the Hinton area of West-Central Alberta, Tectonophysics, 103, 273-281.

Lam, H. L., Jones, F. W., and Majorowicz, J. A., 1985, A statistical analysis of bottom-hole temperature data in southern Alberta, Geophysics, 50, 677-684.

Lewis, J. F., and Hyndman, R. D., 1976, Oceanic heat flow measurements over the continental margins of eastern Canada, Can. J. Earth Sci., 13, 1031-1038.

MacDonald, G. J. F., 1965, Geophysical deductions from observations of heat flow, in: Lee, W. H. K., ed., Terrestrial Heat Flow, American Geophysical Union, Geophysical Monograph Series, Number 8, 191-210.

Majorowicz, J. A., and Jessop, A. M., 1981, Regional heat flow patterns in the Western Canadian sedimentary basin, Tectonophysics, 74, 209-238.

Majorowicz, J. A., Jones, F. W., and Jessop, A. M., 1988, Preliminary geothermics of the sedimentary basins in the Yukon and Northwest Territories (60°N - 70°) - estimates from petroleum bottom-hole temperature data, Bull. Can. Petr. Geol., 36, 39-51.

Majorowicz, J. A., Jones, F. W., Lam, H. L., and Jessop, A. M., 1984, The variability of heat flow both regional and with depth in southern Alberta, Canada: effect of

groundwater flow?, Tectonophysics, 106, 1-29.

Majorowicz, J. A., Jones, F. W., Lam, H. L., and Jessop, A. M., 1985, Terrestrial heat flow and geothermal gradients in relation to hydrodynamics in the Alberta Basin, Canada, J. Geodynam., 4, 265-283.

Majorowicz, J. A., Jones, F. W., and Jessop, A. M., 1986, Geothermics of the Williston basin in Canada in relation to hydrodynamics and hydrocarbon occurrences, Geophysics, 51, 767-779.

McKenzie, D., 1978, Some remarks on the development of sedimentary basins, Earth Planet. Sci. Lett., 40, 25-32.

Moir, P. N., 1988, The geothermal regime of the Labrador Shelf, offshore eastern Canada from exploration well measurements, in press.

Reiter, M., and Tovar, J. C., 1982, Estimates of terrestrial heat flow in northern Chihuahua, Mexico, based upon petroleum bottom-hole temperatures, Geol. Soc. Am. Bull., 93, 613-624.

Reiter, M., and Jessop, A. M., 1985, Estimates of terrestrial heat flow in offshore eastern Canada, Can. J. Earth Sci., 22, 1503-1517.

Reiter, M., and Jessop, A. M., 1986, Estimates of terrestrial heat flow in offshore eastern Canada: reply, Can. J. Earth Sci., 23, 2085-2086.

Roberts, W. H., 1981, Some uses of temperature data in petroleum exploration, in: Gottlieb, B. M., ed., Unconventional methods in exploration for petroleum and natural gas, SMU Press, Dallas, 8-49.

Rybach, L., 1986, Amount and significance of radioactive heat sources in sediments, in: Burrus, J., ed., Thermal modelling in sedimentary basins, Editions Technip, Paris, 311-322.

Sass, J. H., Lachenbruch, A. H., and Munroe, R. J., 1971, Thermal conductivity of rocks from measurements on fragments and its application to heat flow determinations, J. Geophys. Res., 76, 3391-3401.

Speece, M. A., Bowen, T. D., Folcik, J. L., and Pollack, H. N., 1985, Analysis of temperatures in sedimentary basins: the Michigan Basin, Geophysics, 50, 1318-1334.

van Hinte, J. E., and Deighton, I. C., 1987, Burial and thermal geohistory modelling of sedimentary basins,

Notes for JAPEC course no. 57, Imperial College.

Wright, J. A., Jessop, A. M., Judge, A. S., and Lewis, T. J., 1980, Geothermal measurements in Newfoundland, Can. J. Earth Sci., 17, 1370-1376.

APPENDIX I

Corrected temperature versus depth plots and average corrected geothermal gradients for the wells North Ben Nevis P-93 and South Tempest G-88 using circulation times ranging from 0.5 to 8.5 hours.

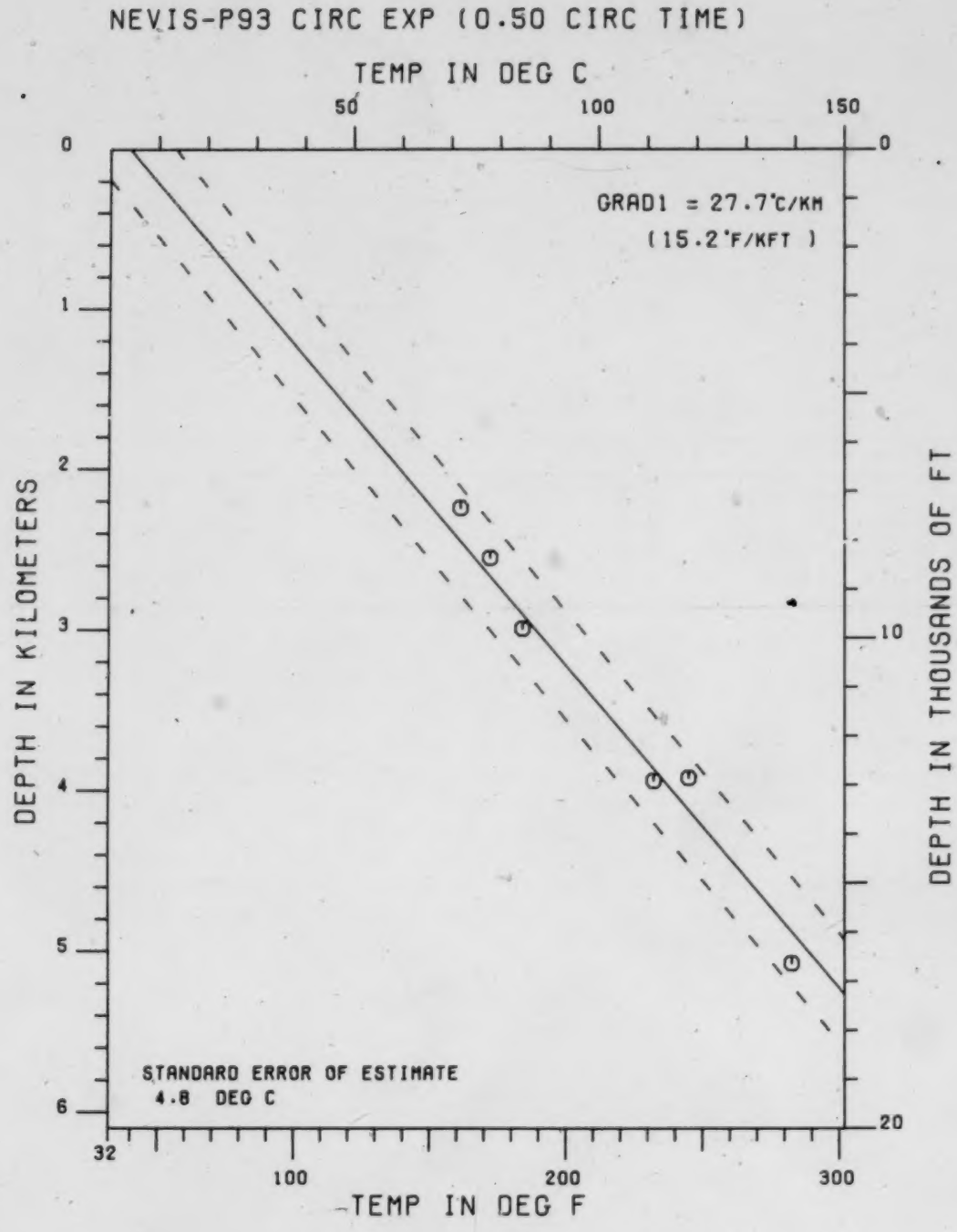
NEVIS-P93 CIRC EXP (0.50 CIRC TIME)
TEMP IN DEG C
50
100
150
0
GRAD1 = 27.7°C/KM
(15.2°F/KFT)
1
2
3
4
5
6
DEPTH IN KILOMETERS
DEPTH IN THOUSANDS OF FT
10
20
STANDARD ERROR OF ESTIMATE
4.8 DEG C
32
100
200
300
TEMP IN DEG F

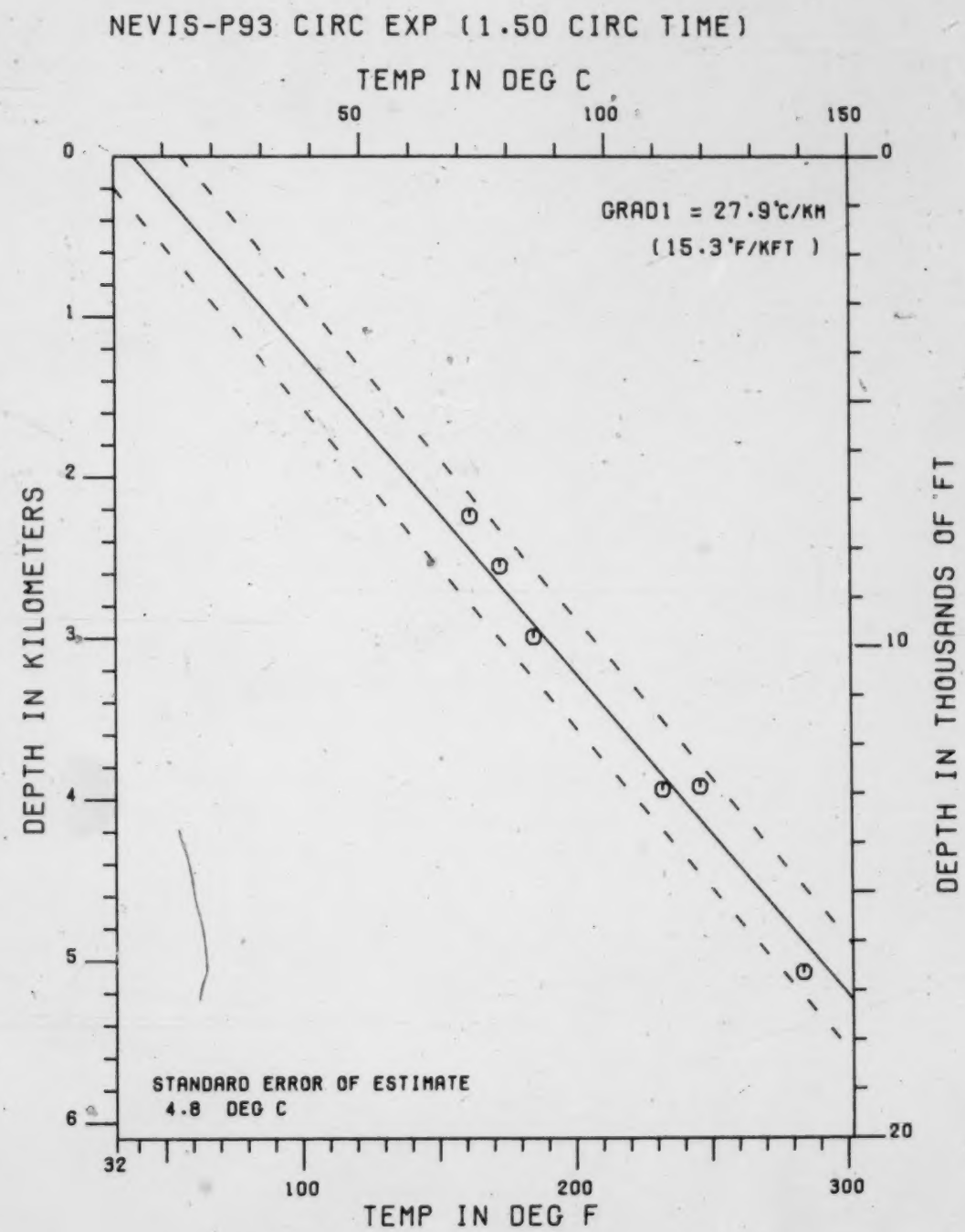
NEVIS-P93 CIRC EXP (1.50 CIRC TIME)
TEMP IN DEG C
50
100
150
0
GRAD1 = 27.9°C/KM
(15.3°F/KFT)
1
2
3
4
5
6
DEPTH IN KILOMETERS
DEPTH IN THOUSANDS OF FT
10
20
STANDARD ERROR OF ESTIMATE
4.8 DEG C
32
100
200
300
TEMP IN DEG F

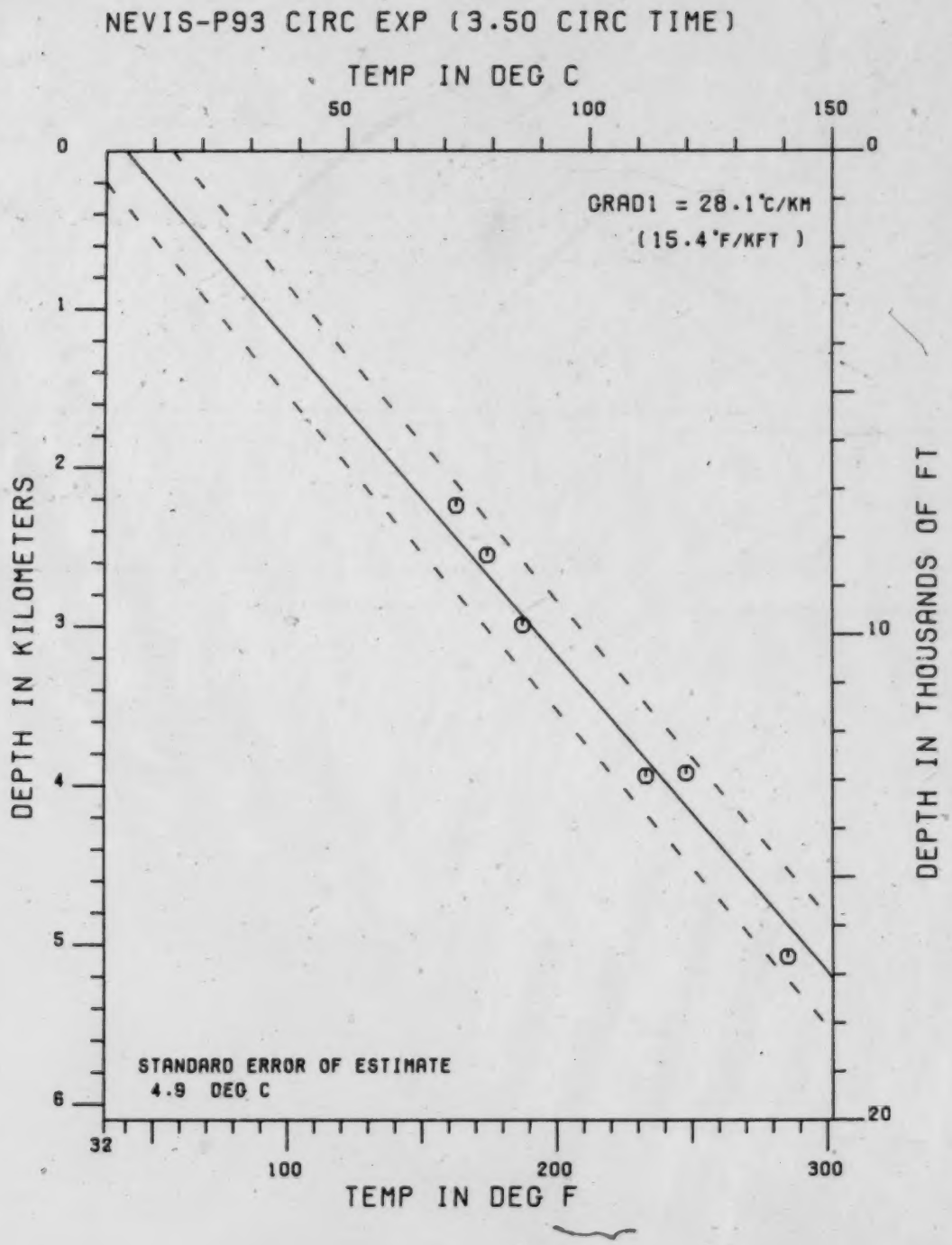
NEVIS-P93 CIRC EXP (3.50 CIRC TIME)
TEMP IN DEG C
50
100
150
0
GRAD1 = 28.1°C/KM
(15.4°F/KFT)
1
2
3
4
5
6
DEPTH IN KILOMETERS
DEPTH IN THOUSANDS OF FT
10
20
STANDARD ERROR OF ESTIMATE
4.9 DEG C
32
100
200
300
TEMP IN DEG F

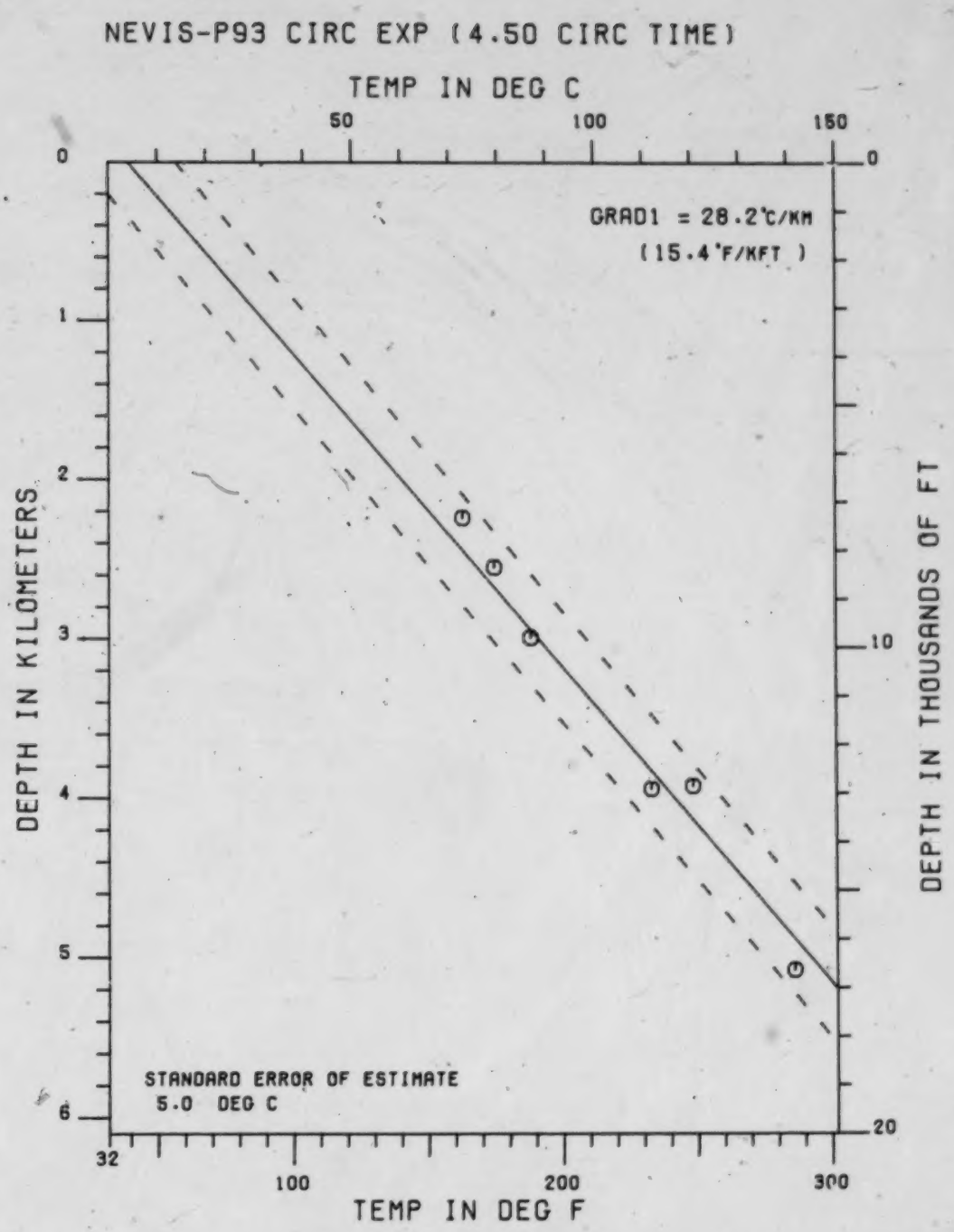
NEVIS-P93 CIRC EXP (4.50 CIRC TIME)
TEMP IN DEG C
50
100
150
0
GRAD1 = 28.2°C/KM
(15.4°F/KFT)
1
2
3
4
5
6
DEPTH IN KILOMETERS
DEPTH IN THOUSANDS OF FT
10
20
STANDARD ERROR OF ESTIMATE
5.0 DEG C
32
100
200
300
TEMP IN DEG F

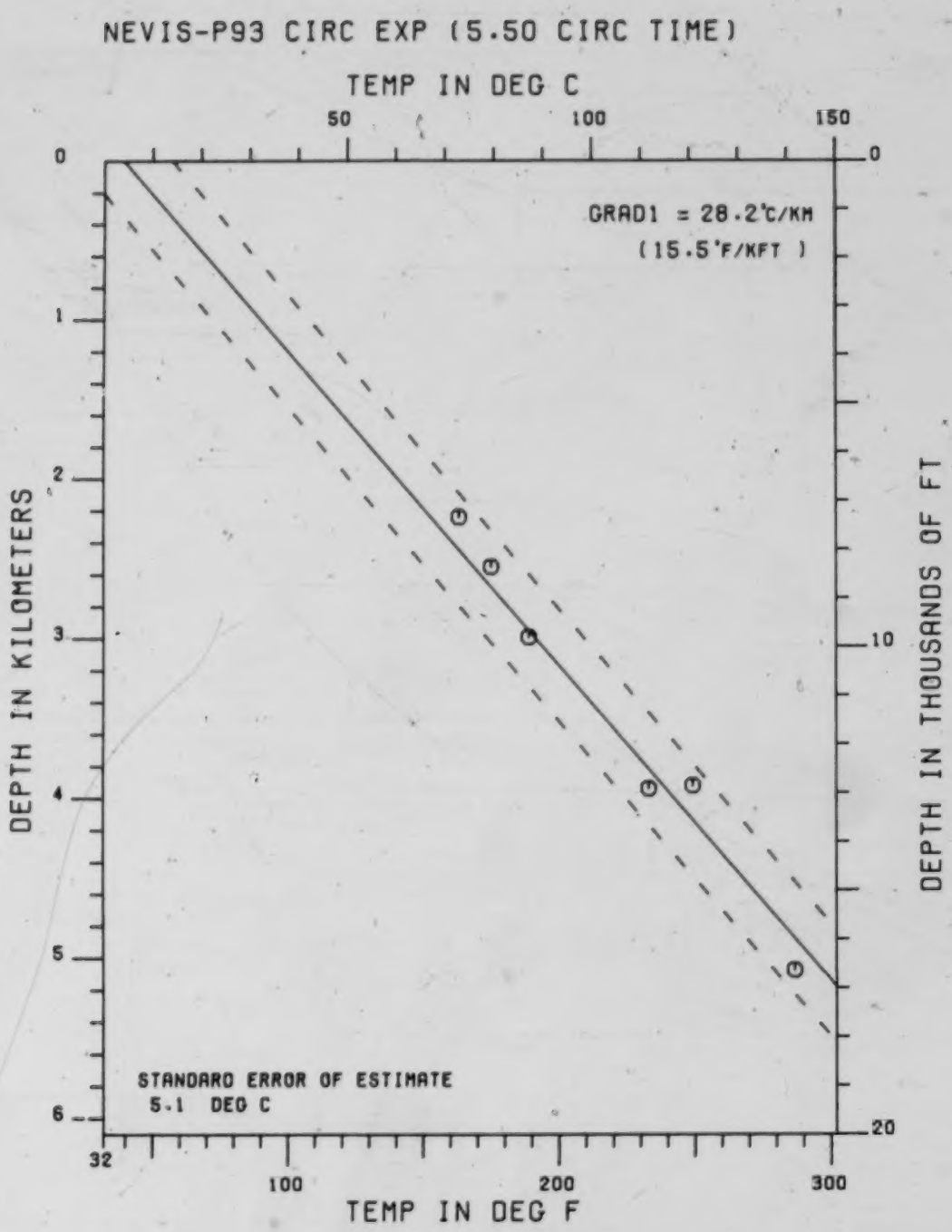
NEVIS-P93 CIRC EXP (5.50 CIRC TIME)
TEMP IN DEG C
50
100
150
0
GRAD1 = 28.2'C/KM
(15.5'F/KFT)
1
2
3
4
5
6
DEPTH IN KILOMETERS
DEPTH IN THOUSANDS OF FT
10
20
STANDARD ERROR OF ESTIMATE
5.1 DEG C
32
100
200
300
TEMP IN DEG F

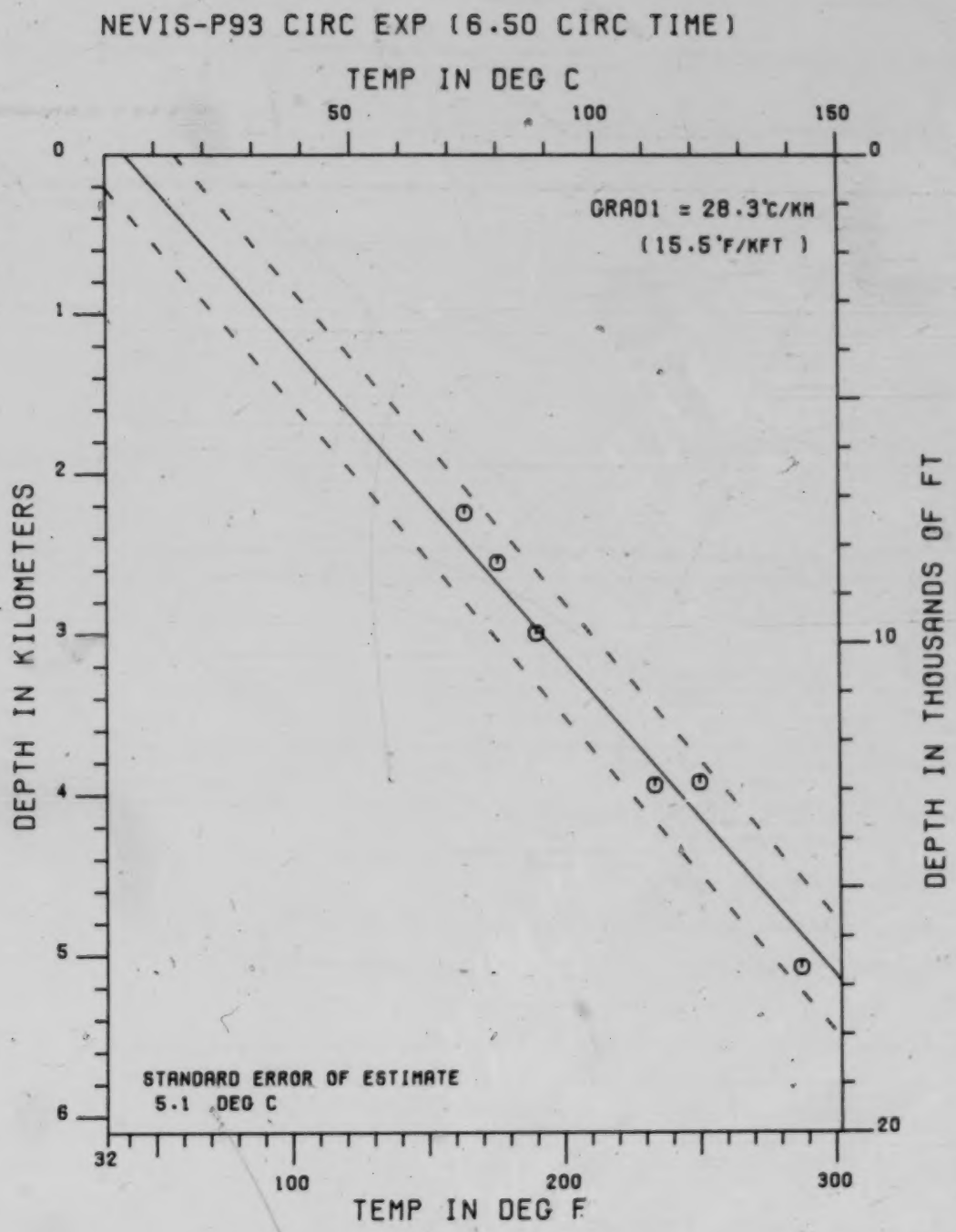
NEVIS-P93 CIRC EXP (6.50 CIRC TIME)
TEMP IN DEG C
50
100
150
0
GRAD1 = 28.3°C/KM
(15.5°F/KFT)
1
2
3
4
5
6
DEPTH IN KILOMETERS
10
20
DEPTH IN THOUSANDS OF FT
STANDARD ERROR OF ESTIMATE
5.1 DEG C
32
100
200
300
TEMP IN DEG F

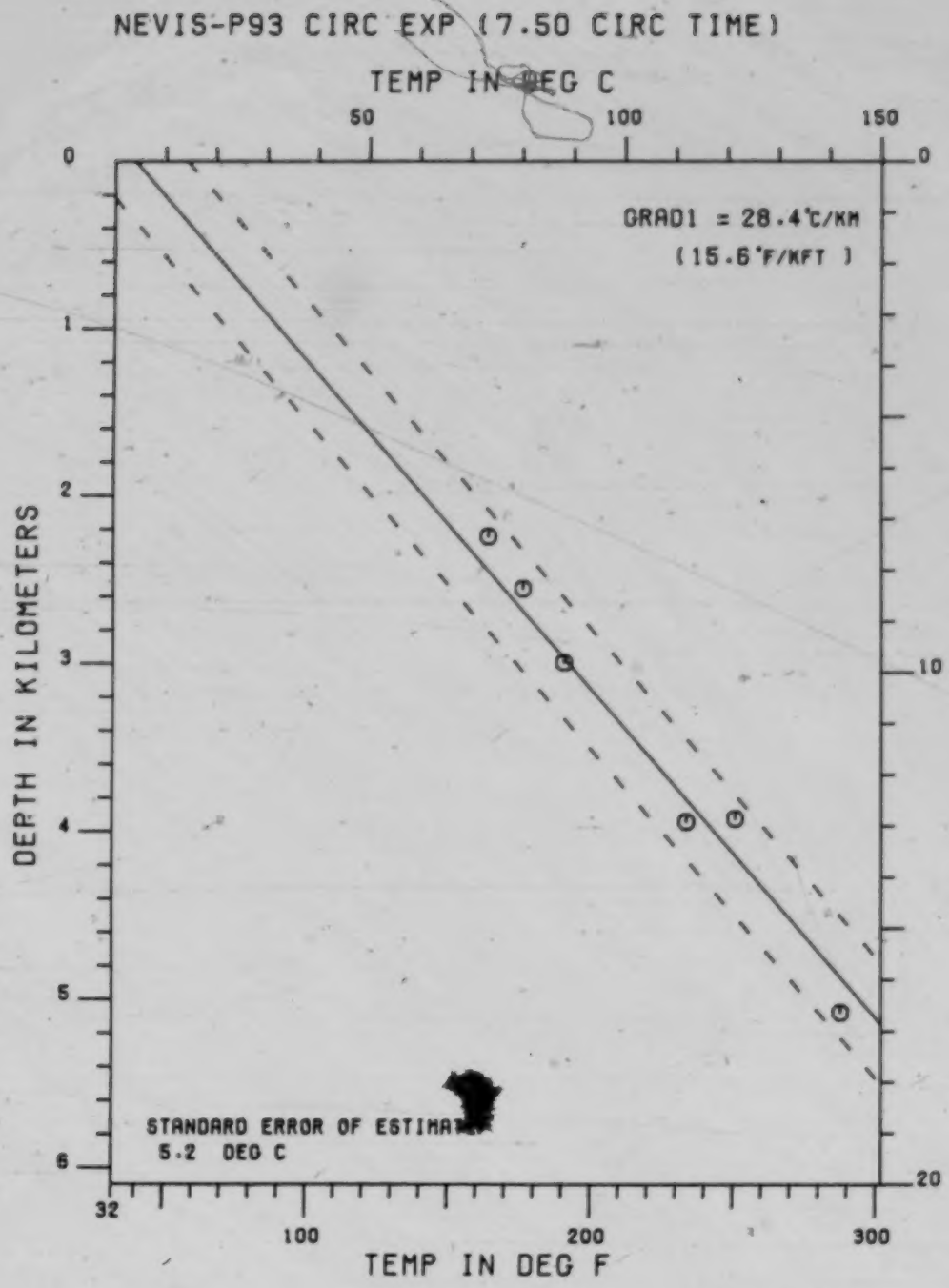
NEVIS-P93 CIRC EXP (7.50 CIRC TIME)
TEMP IN DEG C
50
100
150
0
GRAD1 = 28.4°C/KM
(15.6°F/KFT)
1
2
3
4
5
6
DEPTH IN KILOMETERS
DEPTH IN THOUSANDS OF FT
10
20
STANDARD ERROR OF ESTIMA
5.2 DEG C
32
100
200
300
TEMP IN DEG F

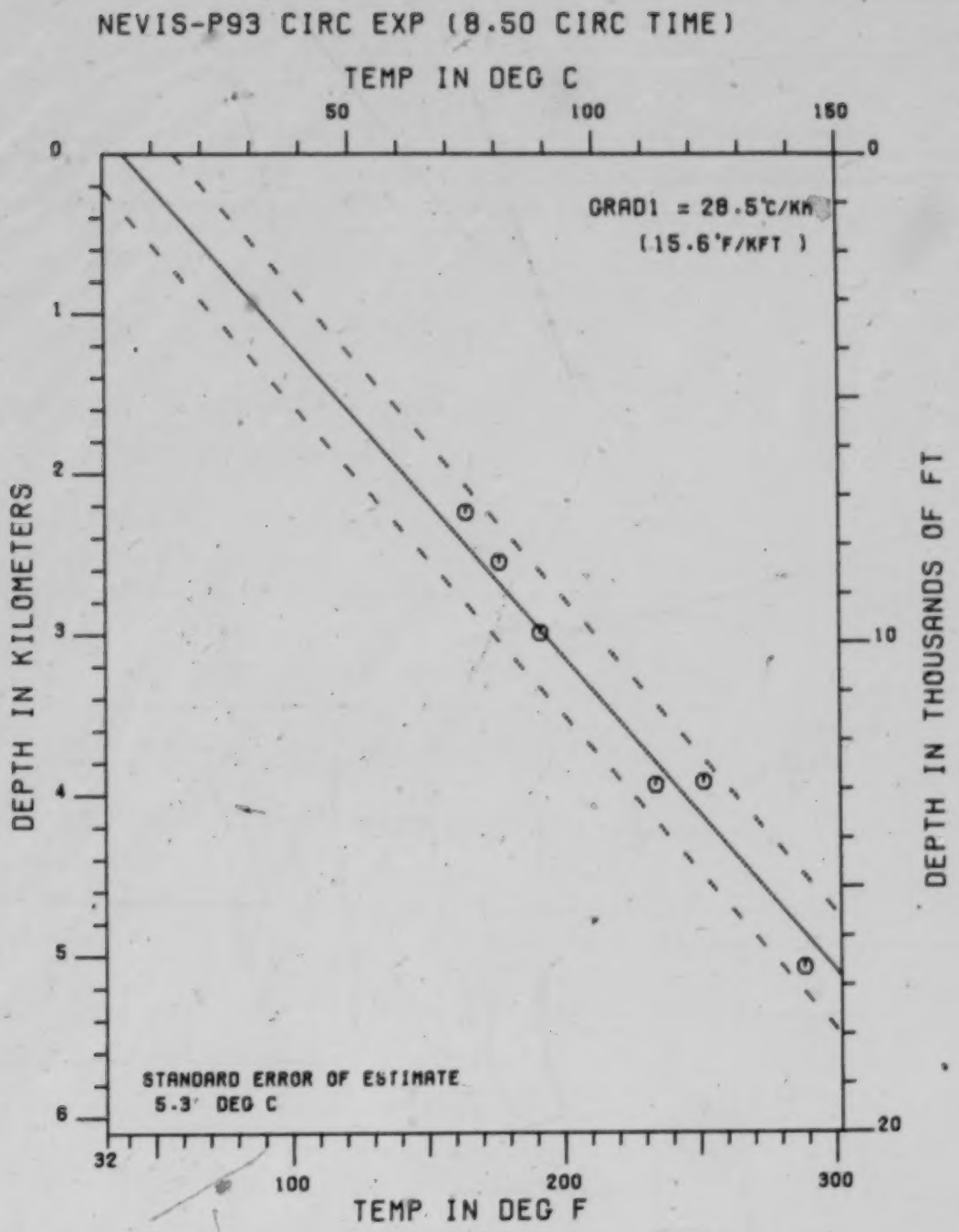
NEVIS-P93 CIRC EXP (8.50 CIRC TIME)
TEMP IN DEG C
50
100
150
0
GRAD1 = 28.5°C/KM
(15.6°F/KFT)
1
2
3
4
5
6
DEPTH IN KILOMETERS
10
20
DEPTH IN THOUSANDS OF FT
STANDARD ERROR OF ESTIMATE
5.3 DEG C
32
100
200
300
TEMP IN DEG F

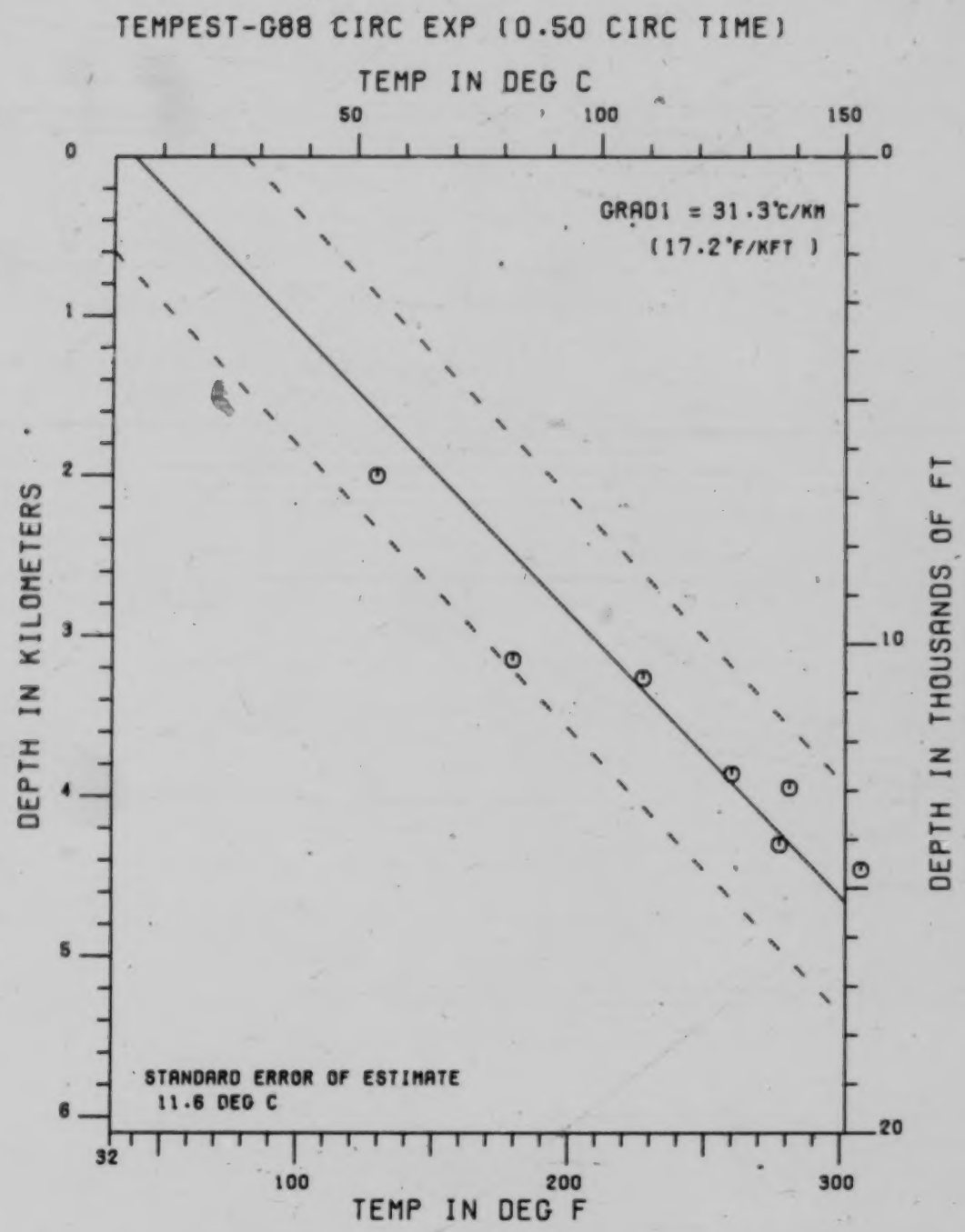
TEMPEST-G88 CIRC EXP (0.50 CIRC TIME)
TEMP IN DEG C
50
100
150
0
GRADI = 31.3°C/KM
(17.2°F/KFT)
1
2
3
4
5
6
DEPTH IN KILOMETERS
DEPTH IN THOUSANDS OF FT
10
20
STANDARD ERROR OF ESTIMATE
11.6 DEG C
32
100
200
300
TEMP IN DEG F

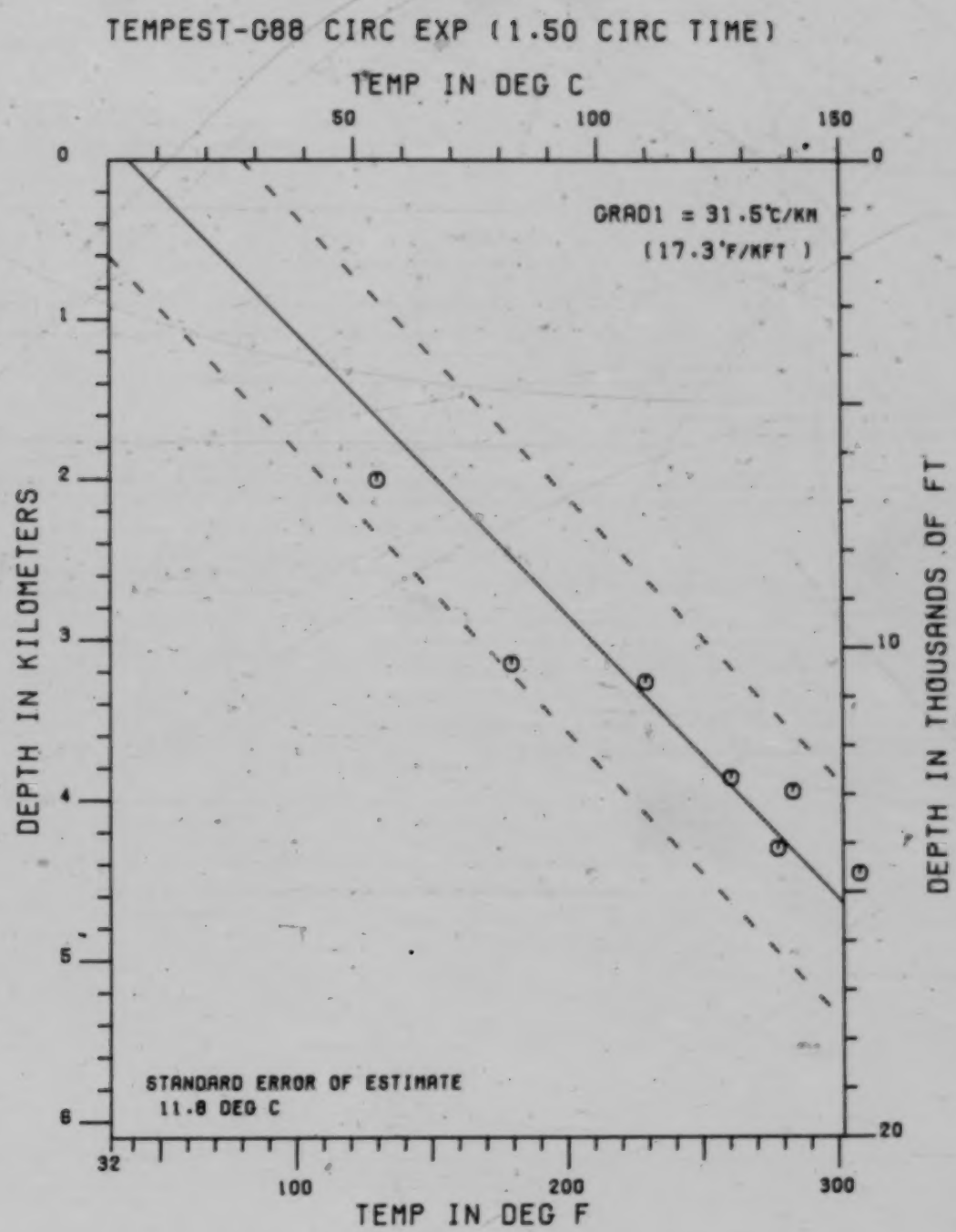
TEMPEST-G88 CIRC EXP (1.50 CIRC TIME)
TEMP IN DEG C
50
100
150
0
GRAD1 = 31.5°C/KM
(17.3°F/KFT)
1
2
3
4
5
6
DEPTH IN KILOMETERS
DEPTH IN THOUSANDS OF FT
10
20
STANDARD ERROR OF ESTIMATE
11.8 DEG C
32
100
200
300
TEMP IN DEG F

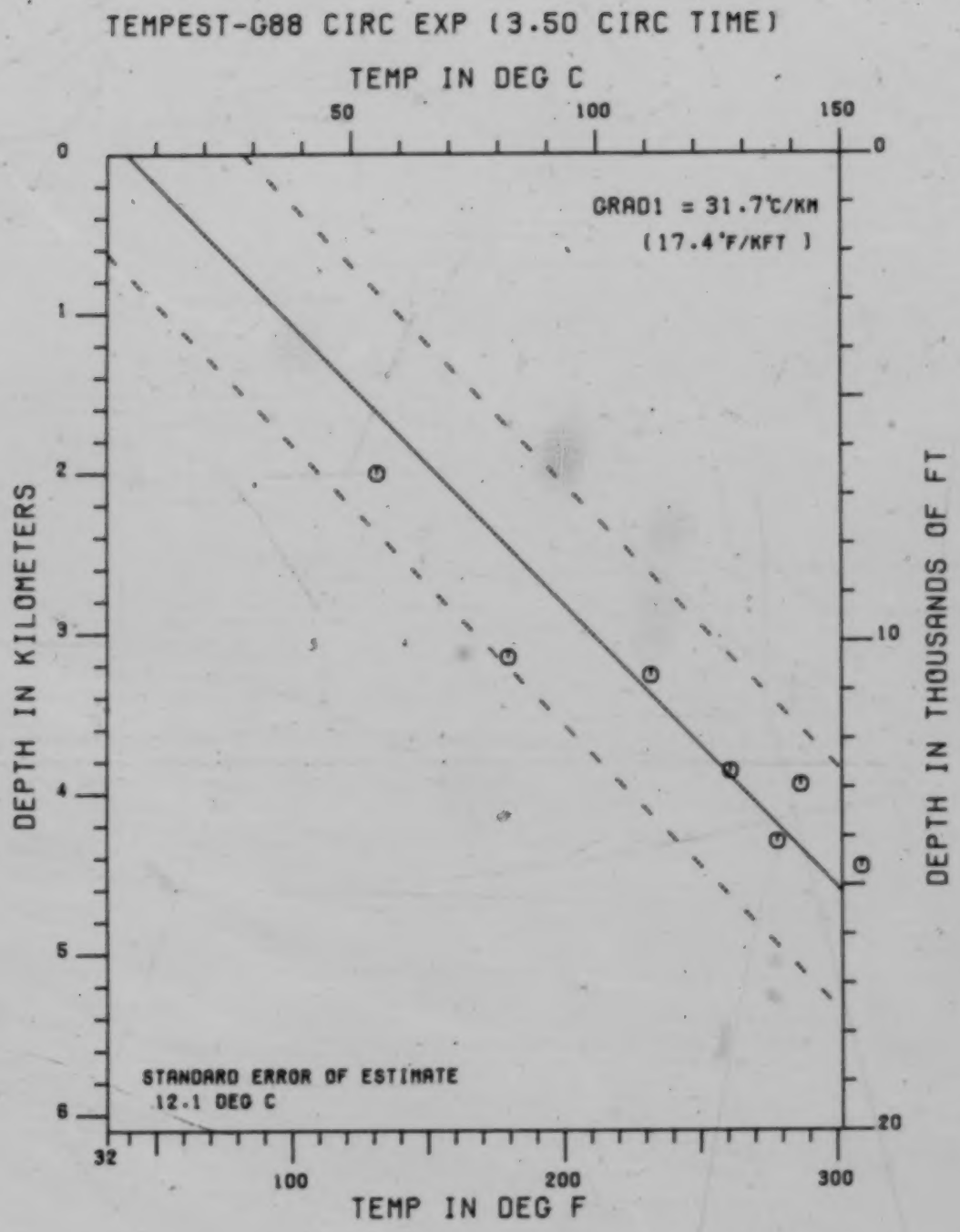
TEMPEST-G88 CIRC EXP (3.50 CIRC TIME)
TEMP IN DEG C
50
100
150
0
GRAD1 = 31.7°C/KM
(17.4°F/KFT)
1
2
3
4
5
6
DEPTH IN KILOMETERS
DEPTH IN THOUSANDS OF FT
10
20
STANDARD ERROR OF ESTIMATE
12.1 DEG C
32
100
200
300
TEMP IN DEG F

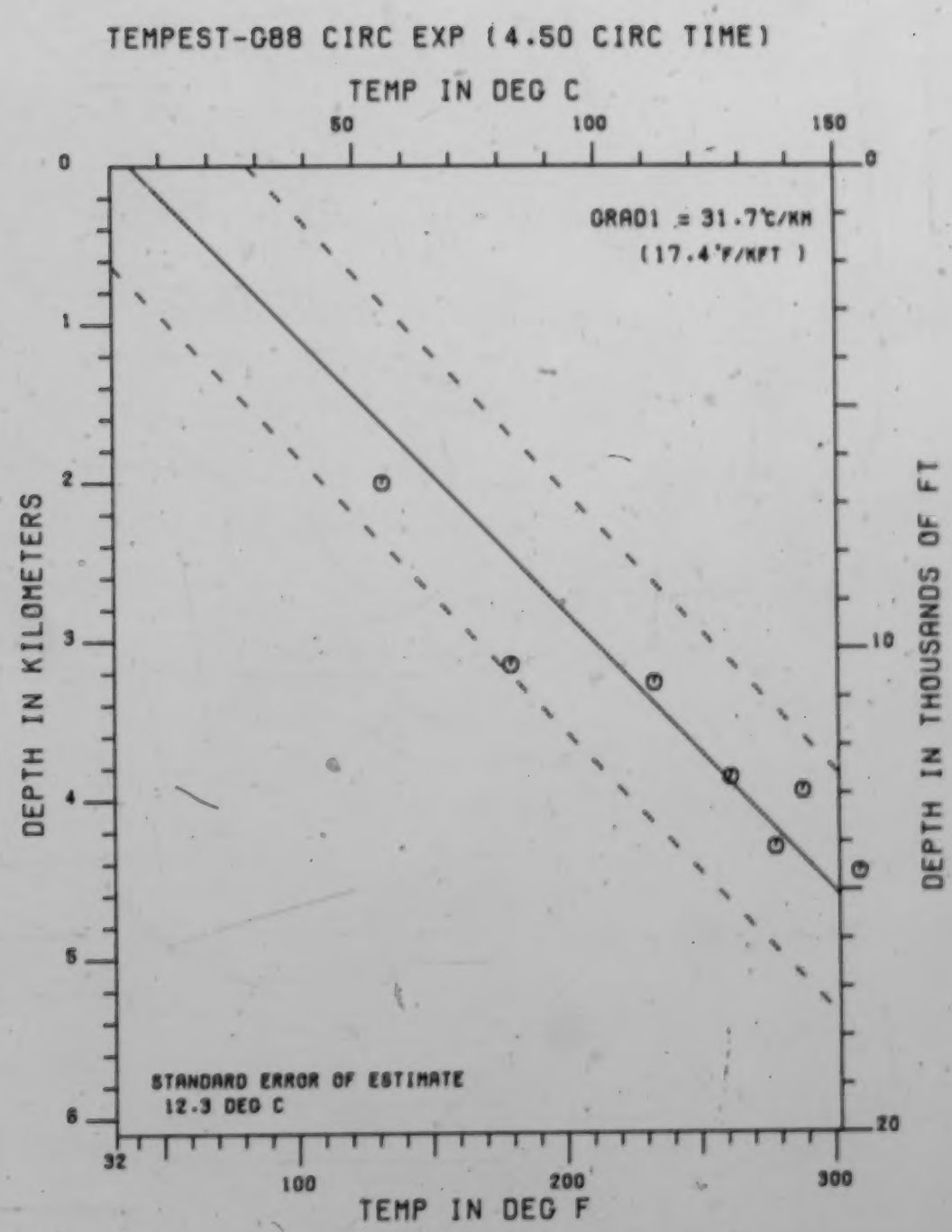
TEMPEST-G88 CIRC EXP (4.50 CIRC TIME)
TEMP IN DEG C
50
100
150
0
GRAD1 = 31.7°C/KM
(17.4°F/KFT)
1
2
3
4
5
6
DEPTH IN KILOMETERS
10
20
DEPTH IN THOUSANDS OF FT
STANDARD ERROR OF ESTIMATE
12.3 DEG C
32
100
200
300
TEMP IN DEG F

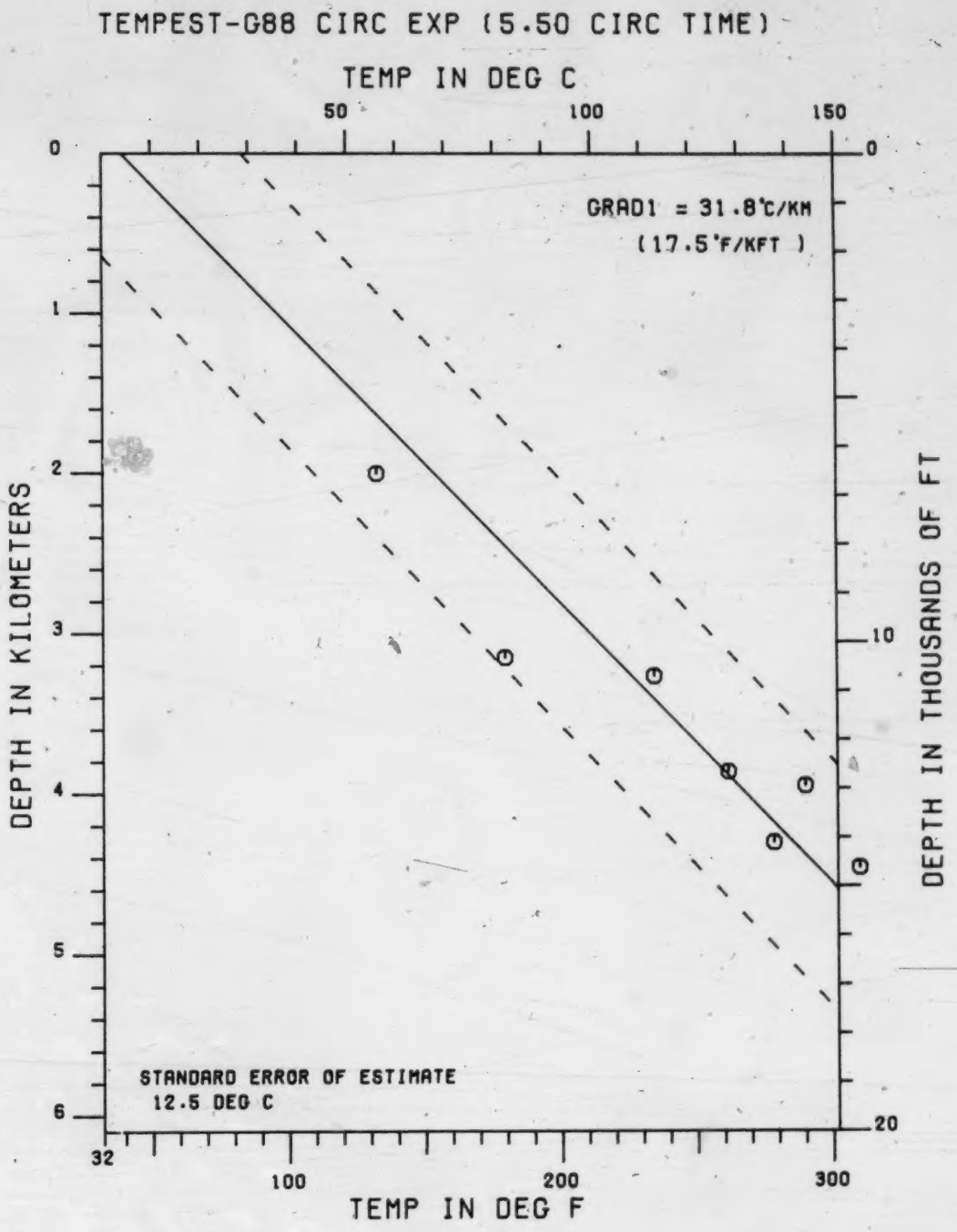
TEMPEST-G88 CIRC EXP (5.50 CIRC TIME)
TEMP IN DEG C
50
100
150
0
GRAD1 = 31.8°C/KM
(17.5°F/KFT)
1
2
3
4
5
6
DEPTH IN KILOMETERS
10
20
DEPTH IN THOUSANDS OF FT
STANDARD ERROR OF ESTIMATE
12.5 DEG C
32
100
200
300
TEMP IN DEG F

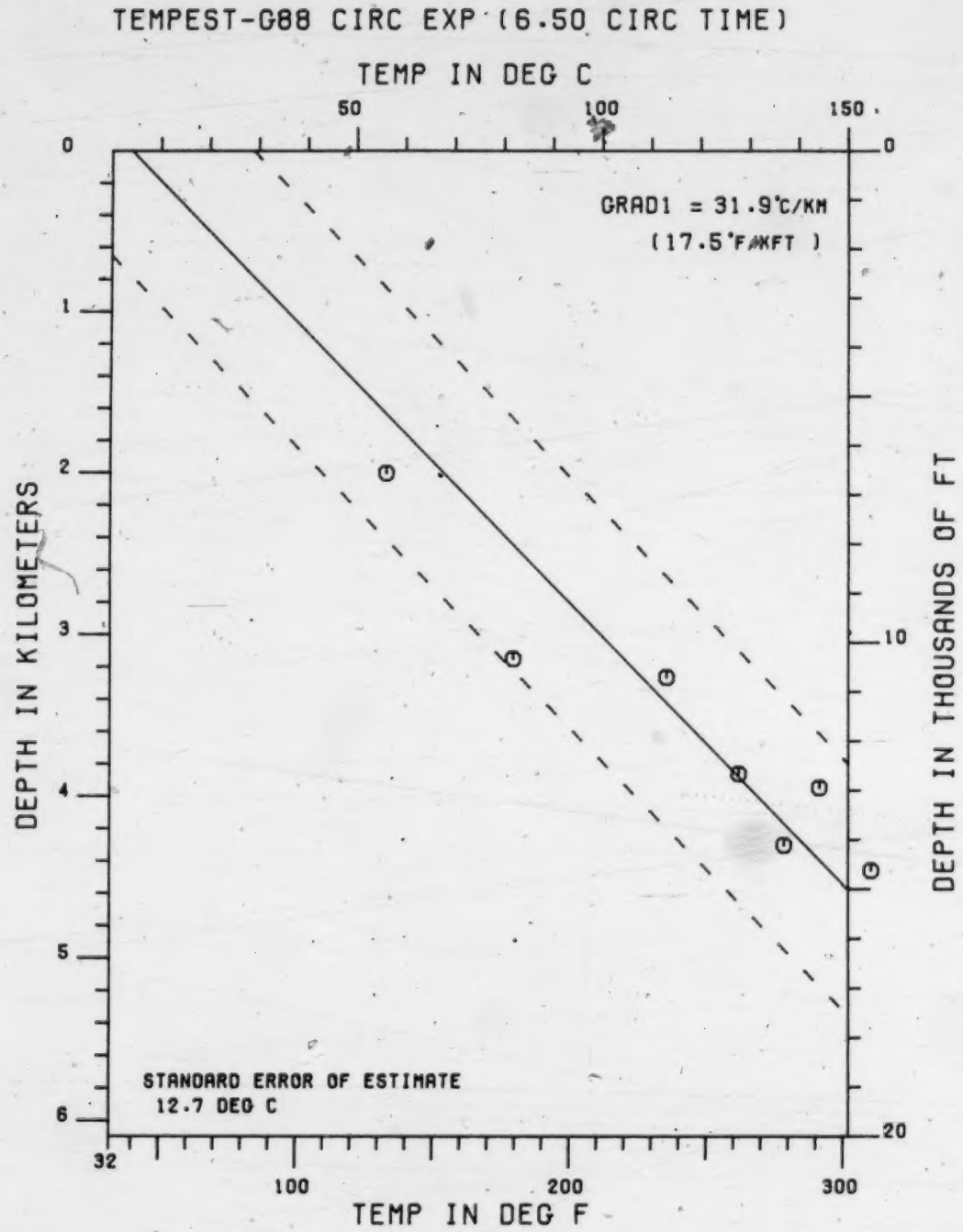
TEMPEST-G88 CIRC EXP (6.50 CIRC TIME)
TEMP IN DEG C
50
100
150
0
GRAD1 = 31.9°C/KM
(17.5°F/KFT)
DEPTH IN KILOMETERS
DEPTH IN THOUSANDS OF FT
1
2
3
4
5
6
10
20
STANDARD ERROR OF ESTIMATE
12.7 DEG C
32
100
200
300
TEMP IN DEG F

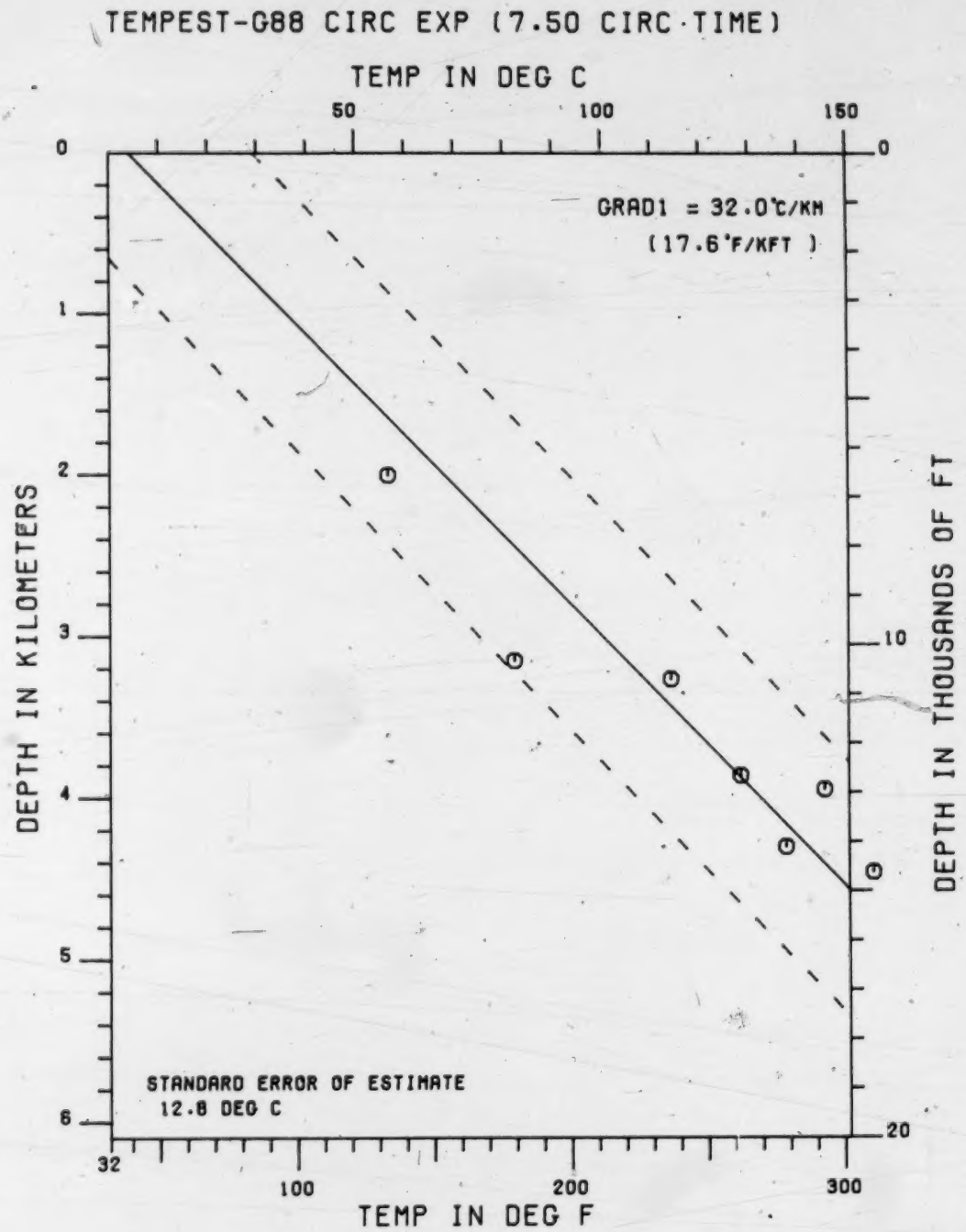
TEMPEST-G88 CIRC EXP (7.50 CIRC TIME)
TEMP IN DEG C
50
100
150
0
GRAD1 = 32.0°C/KM
(17.6°F/KFT)
1
2
3
4
5
6
DEPTH IN KILOMETERS
DEPTH IN THOUSANDS OF FT
10
20
STANDARD ERROR OF ESTIMATE
12.8 DEG C
32
100
200
300
TEMP IN DEG F

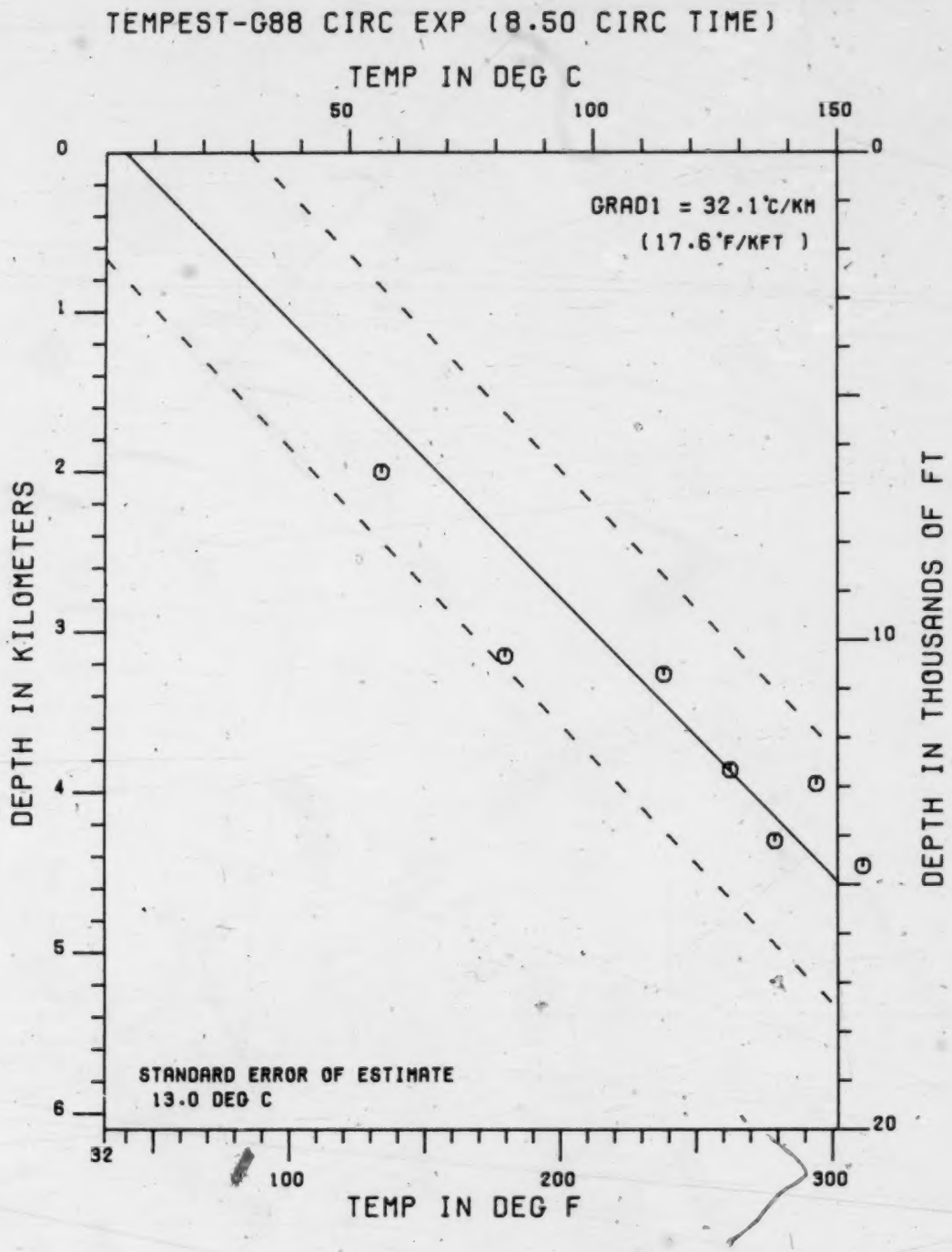
TEMPEST-G88 CIRC EXP (8.50 CIRC TIME)
TEMP IN DEG C
50
100
150
0
GRAD1 = 32.1°C/KM
(17.6°F/KFT)
1
2
3
4
5
6
DEPTH IN KILOMETERS
10
20
DEPTH IN THOUSANDS OF FT
STANDARD ERROR OF ESTIMATE
13.0 DEG C
32
100
200
300
TEMP IN DEG F

APPENDIX II

Corrected temperature versus depth plots and average corrected geothermal gradients for the wells used in this thesis.

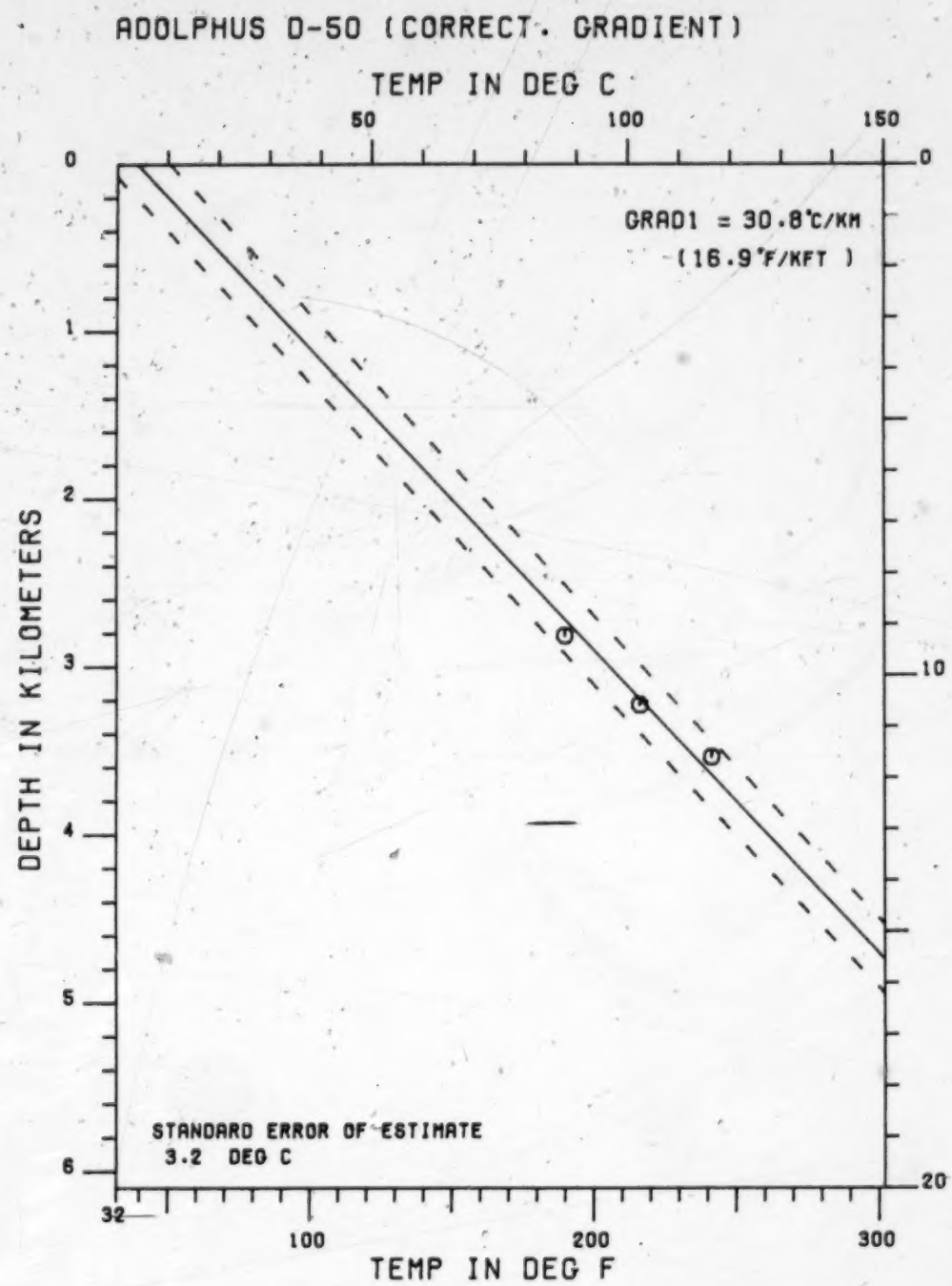
ADOLPHUS D-50 (CORRECT. GRADIENT)
TEMP IN DEG C
50
100
150
0
0
GRAD1 = 30.8°C/KM
(16.9°F/KFT)
1
2
3
4
5
6
DEPTH IN KILOMETERS
10
20
DEPTH IN THOUSANDS OF FT
STANDARD ERROR OF ESTIMATE
3.2 DEG C
32
100
200
300
TEMP IN DEG F

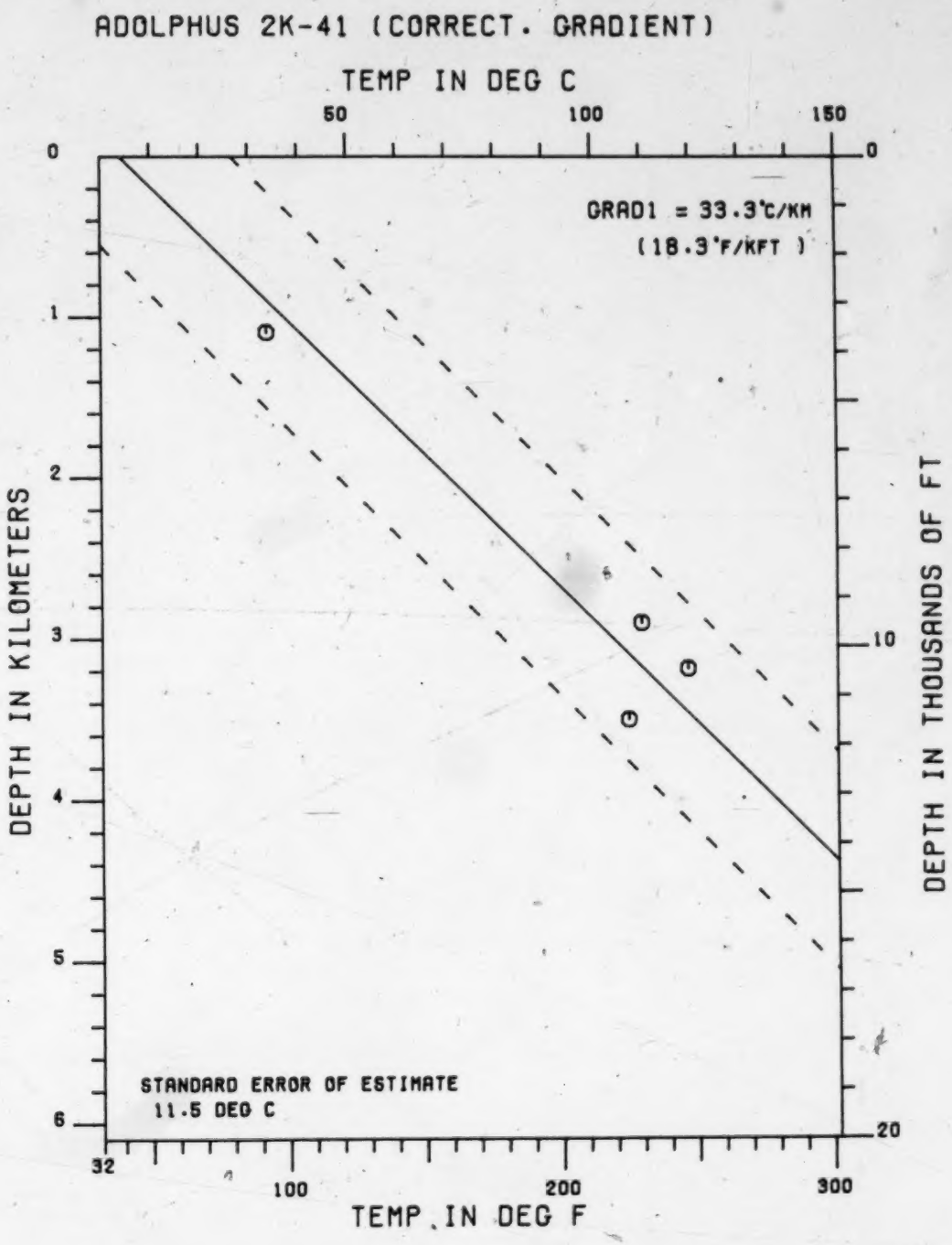
ADOLPHUS 2K-41 (CORRECT. GRADIENT)
TEMP IN DEG C
50
100
150
0
GRAD1 = 33.3°C/KM
(18.3°F/KFT)
1
2
3
4
5
6
DEPTH IN KILOMETERS
10
20
DEPTH IN THOUSANDS OF FT
STANDARD ERROR OF ESTIMATE
11.5 DEG C
32
100
200
300
TEMP IN DEG F

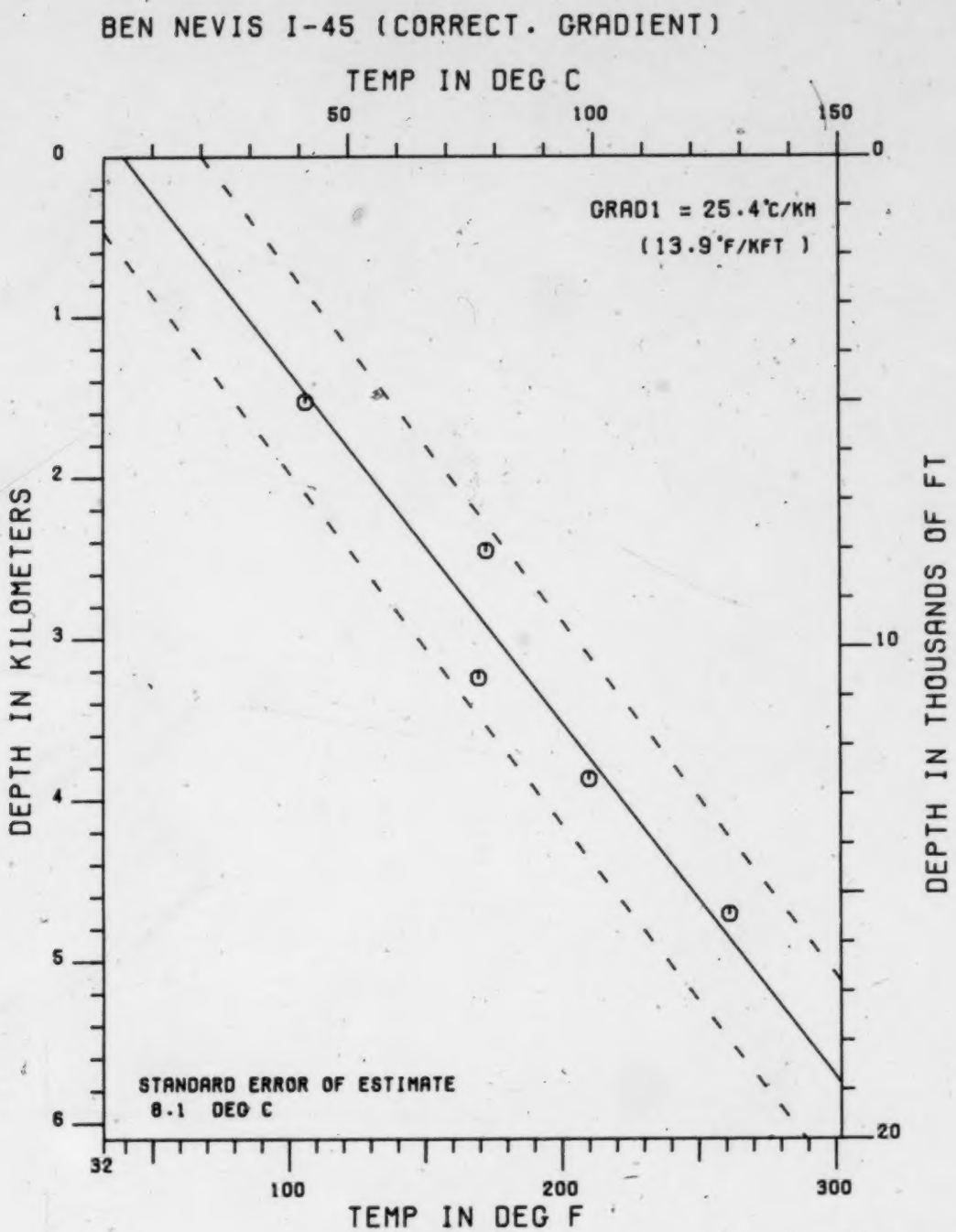
BEN NEVIS I-45 (CORRECT. GRADIENT)
TEMP IN DEG C
50
100
150
0
GRAD1 = 25.4°C/KM
(13.9°F/KFT)
1
2
3
4
5
6
DEPTH IN KILOMETERS
DEPTH IN THOUSANDS OF FT
10
20
STANDARD ERROR OF ESTIMATE
8.1 DEG C
32
100
200
300
TEMP IN DEG F

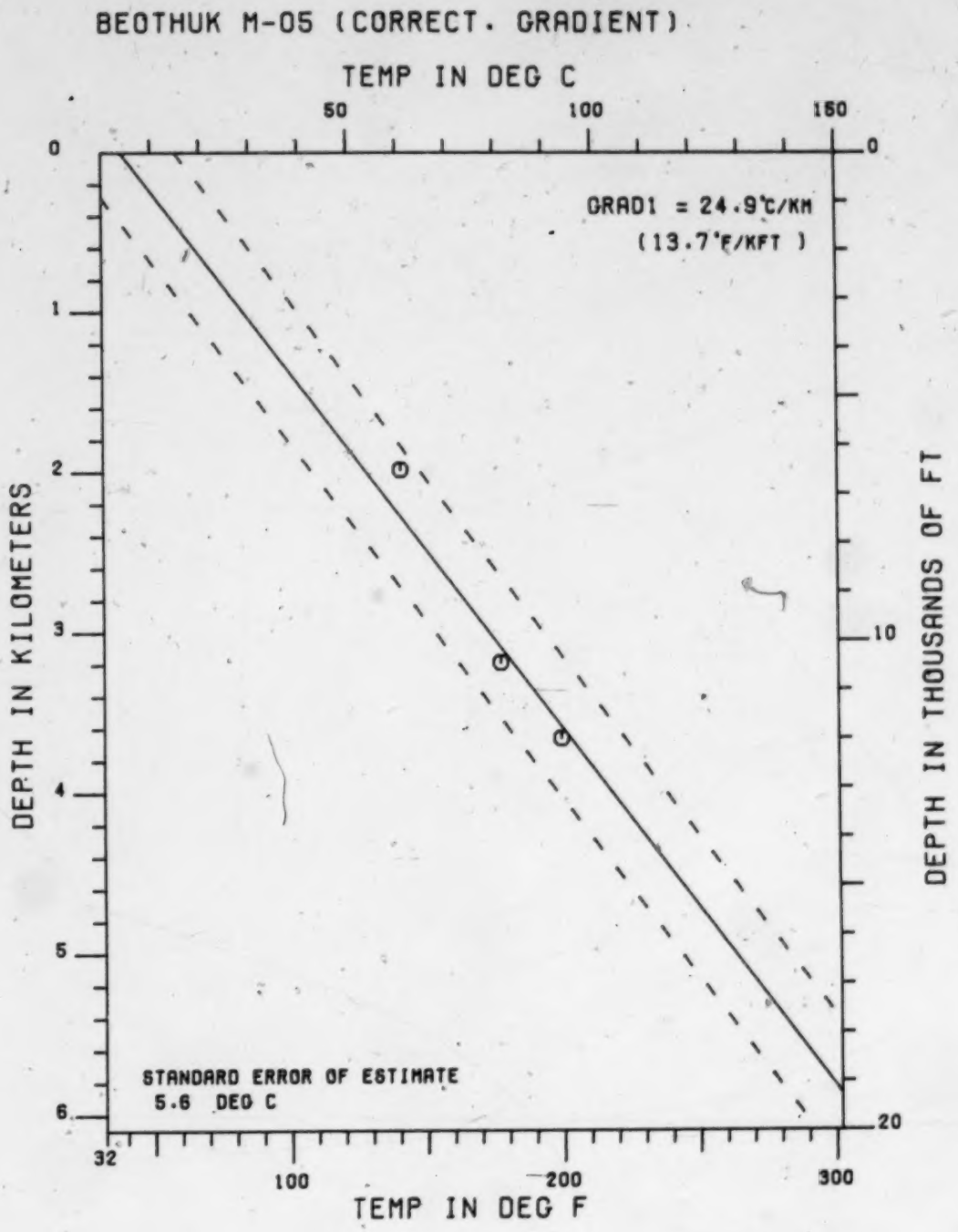
BEOTHUK M-05 (CORRECT. GRADIENT)
TEMP IN DEG C
50
100
150
0
GRAD1 = 24.9°C/KM
(13.7°F/KFT)
1
2
3
4
5
6
DEPTH IN KILOMETERS
10
20
DEPTH IN THOUSANDS OF FT
STANDARD ERROR OF ESTIMATE
5.6 DEG C
32
100
200
300
TEMP IN DEG F

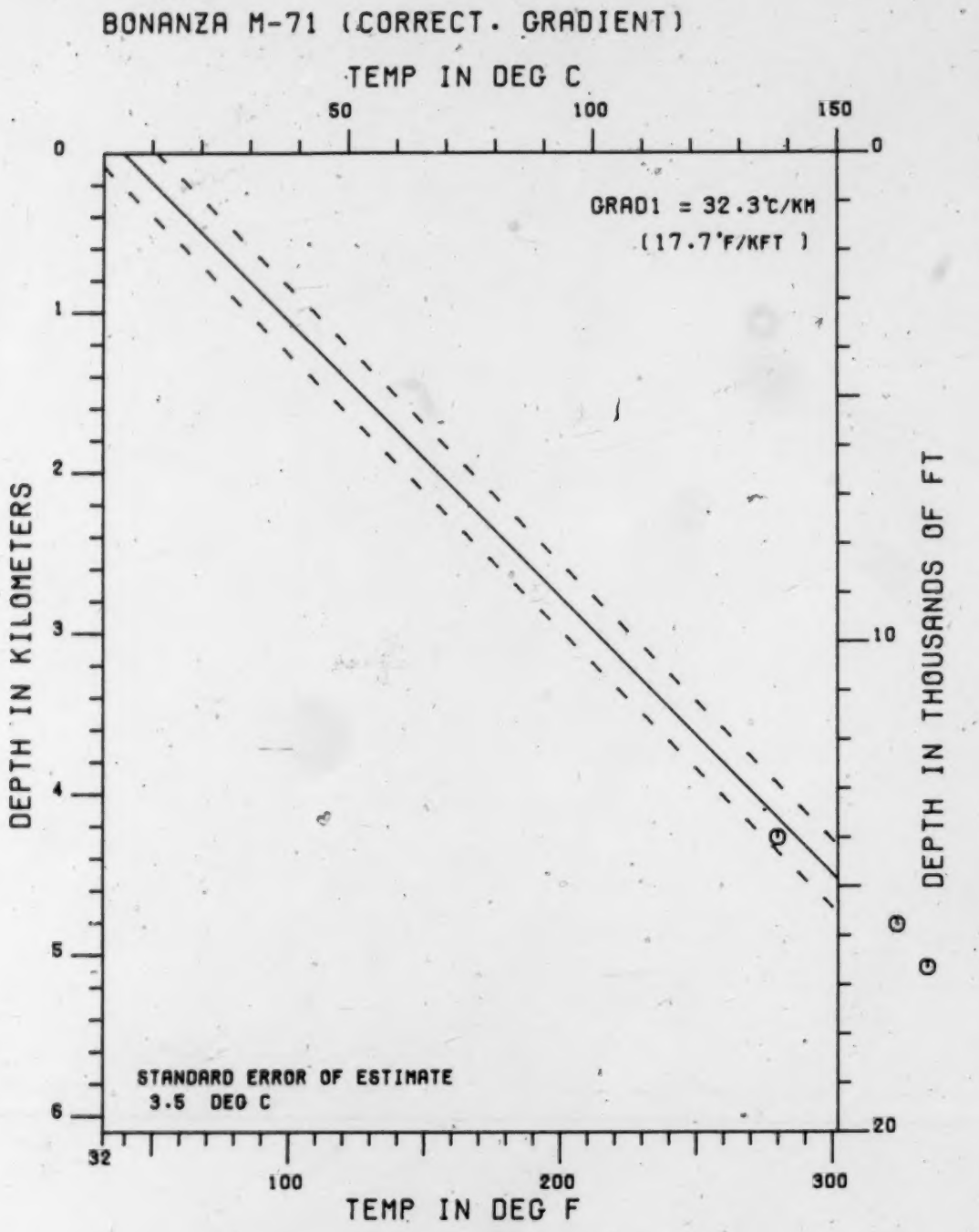
BONANZA M-71 (CORRECT. GRADIENT)
TEMP IN DEG C
50
100
150
0
GRAD1 = 32.3°C/KM
(17.7°F/KFT)
1
2
3
4
5
6
DEPTH IN KILOMETERS
STANDARD ERROR OF ESTIMATE
3.5 DEG C
32
100
200
300
TEMP IN DEG F
10
20
DEPTH IN THOUSANDS OF FT

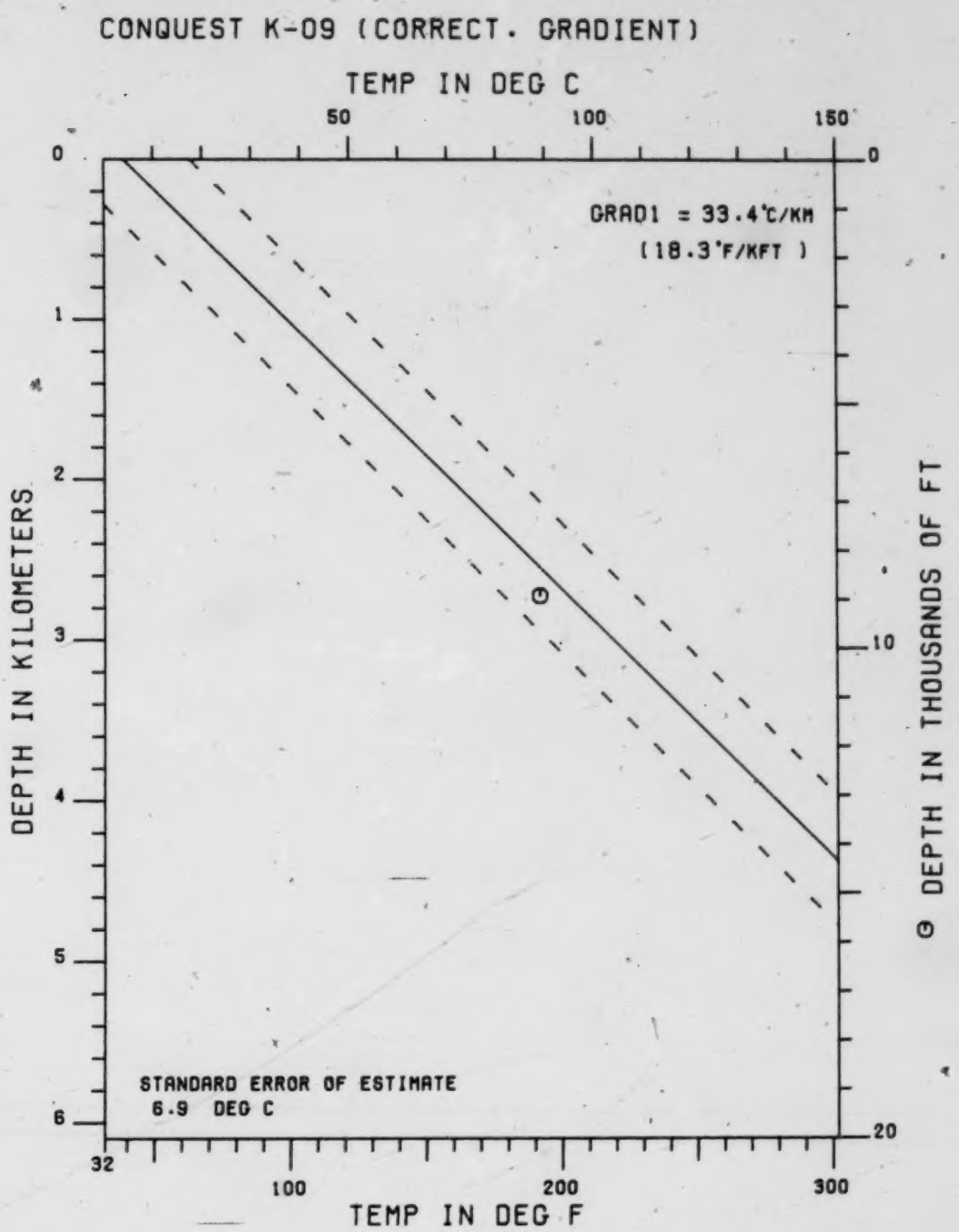
CONQUEST K-09 (CORRECT. GRADIENT)
TEMP IN DEG C
50
100
150
0
GRAD1 = 33.4°C/KM
(18.3°F/KFT)
1
2
3
4
5
6
DEPTH IN KILOMETERS
10
20
DEPTH IN THOUSANDS OF FT
STANDARD ERROR OF ESTIMATE
6.9 DEG C
32
100
200
300
TEMP IN DEG F

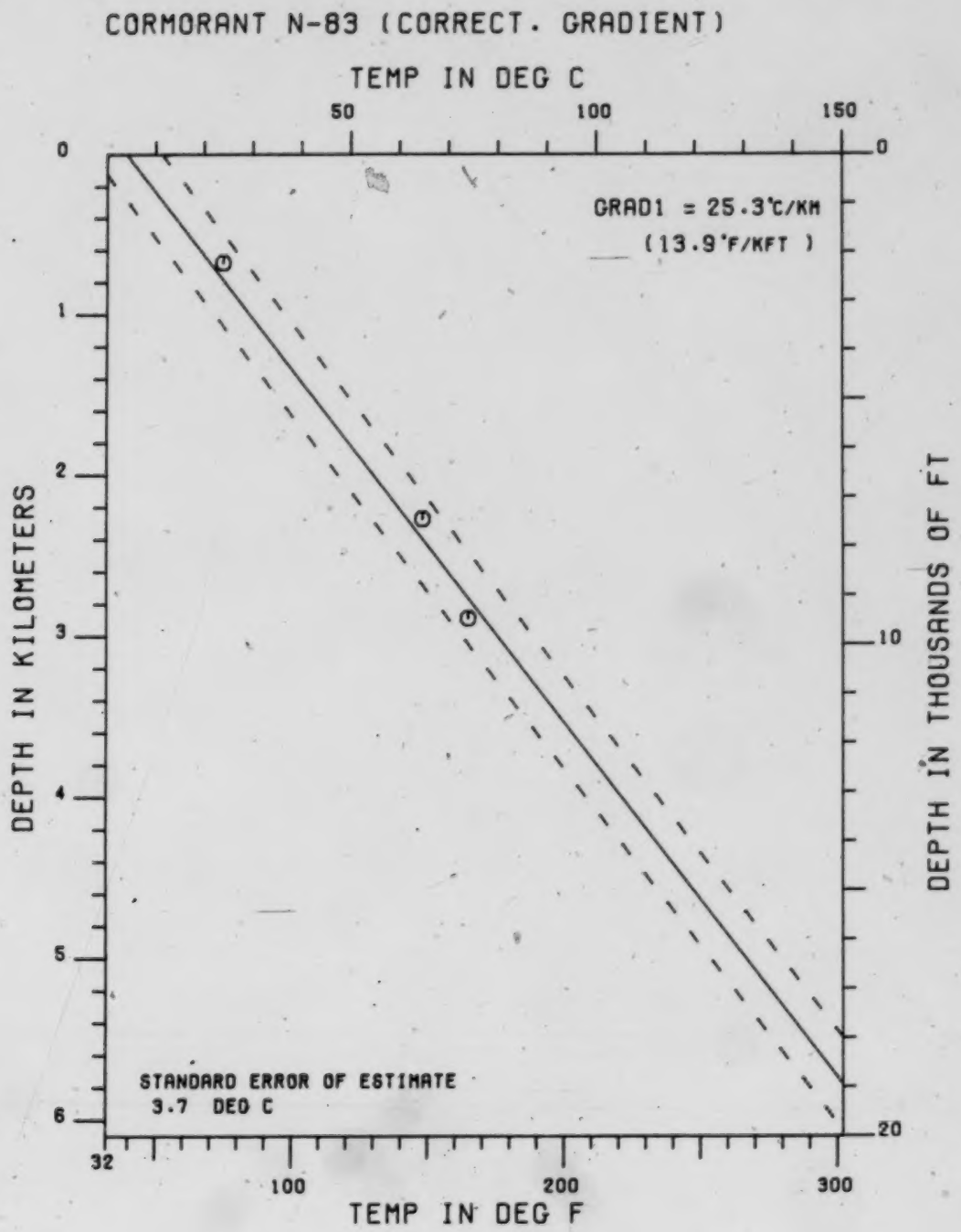
CORMORANT N-83 (CORRECT. GRADIENT)
TEMP IN DEG C
50
100
150
0
GRAD1 = 25.3°C/KM
(13.9°F/KFT)
1
2
3
4
5
6
DEPTH IN KILOMETERS
DEPTH IN THOUSANDS OF FT
10
20
STANDARD ERROR OF ESTIMATE
3.7 DEG C
32
100
200
300
TEMP IN DEG F

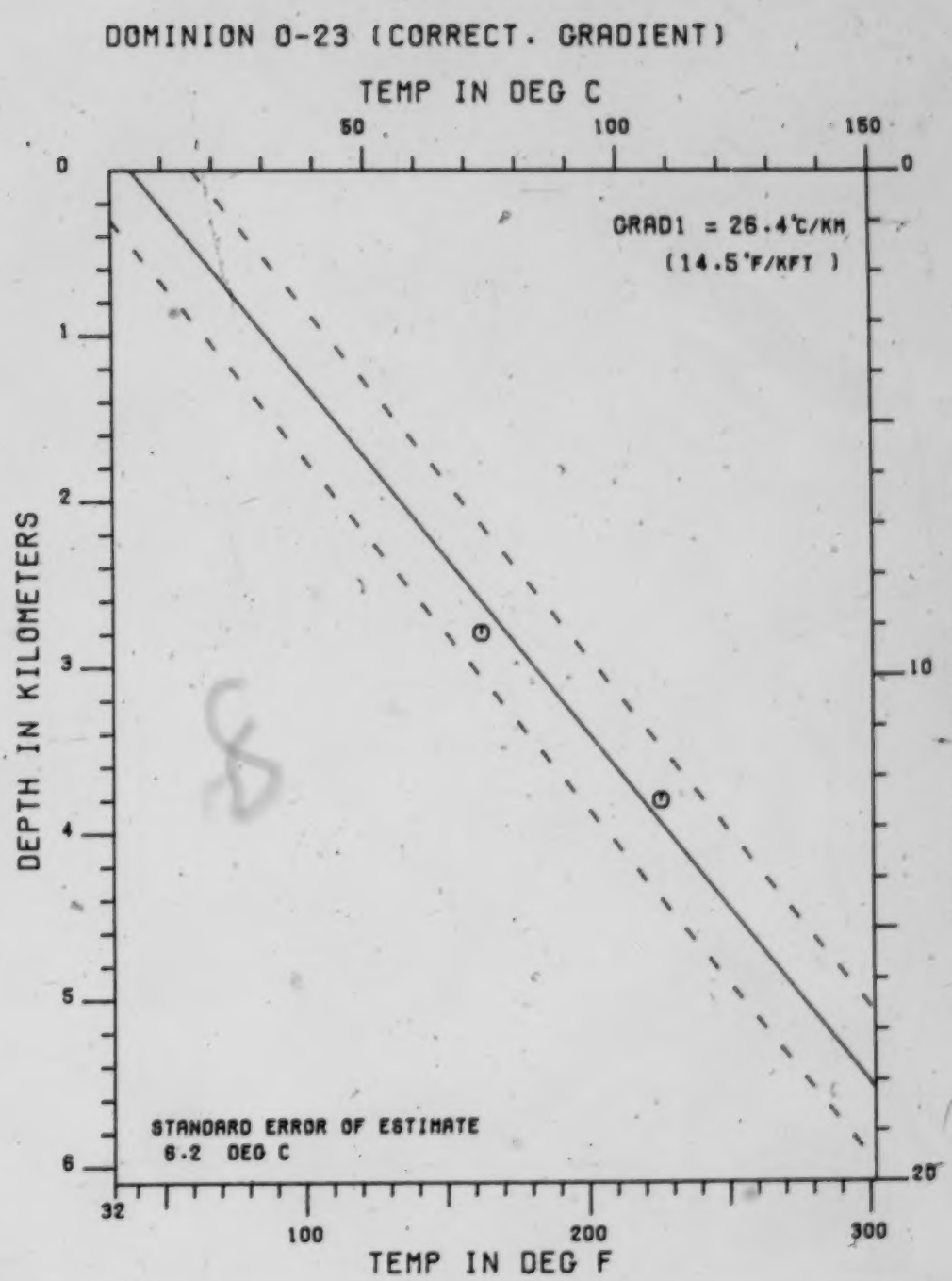
DOMINION O-23 (CORRECT. GRADIENT)
TEMP IN DEG C
50
100
150
0
GRAD1 = 26.4°C/KM
(14.5°F/KFT)
1
2
3
4
5
6
DEPTH IN KILOMETERS
DEPTH IN THOUSANDS OF FT
10
20
STANDARD ERROR OF ESTIMATE
6.2 DEG C
32
100
200
300
TEMP IN DEG F

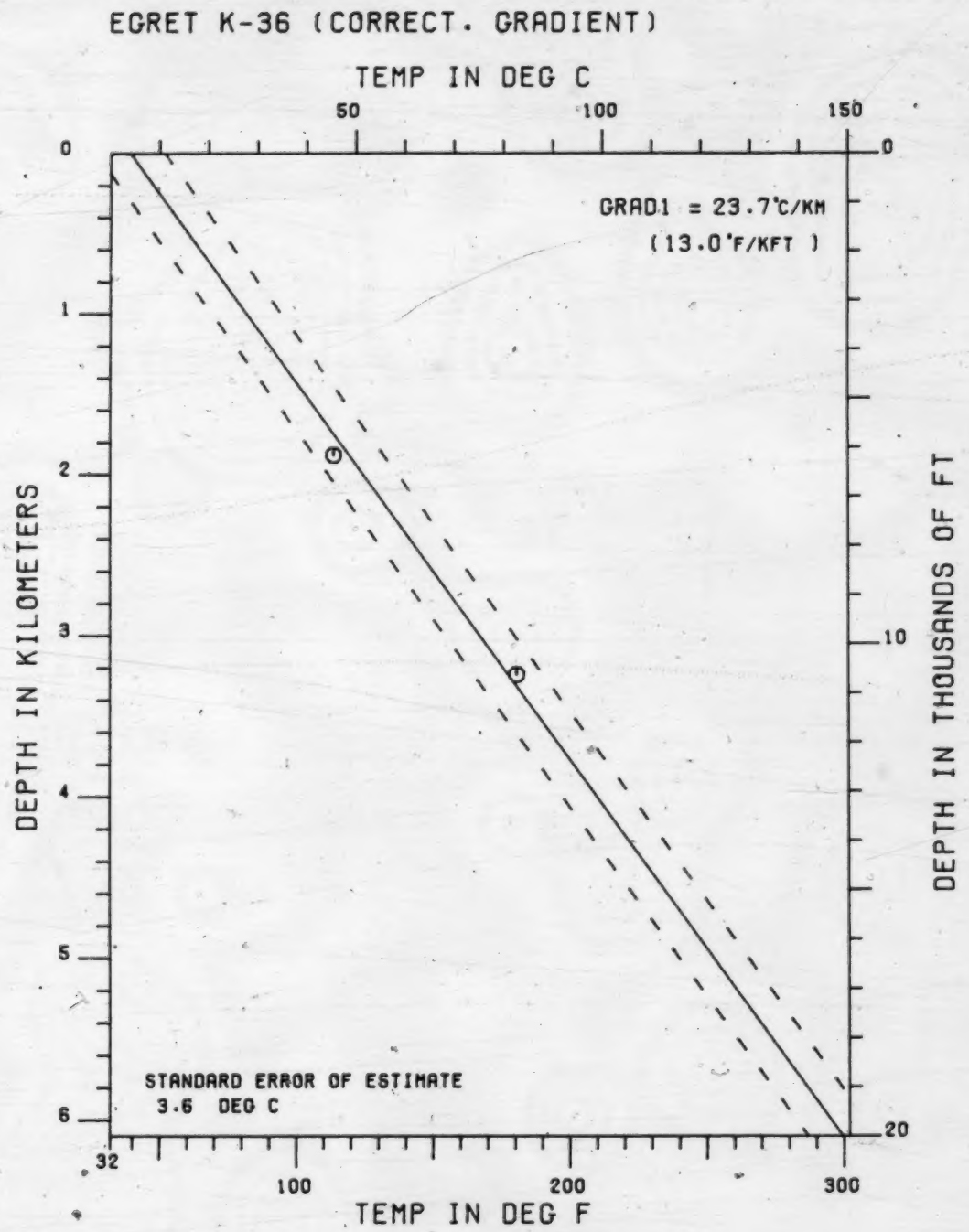
EGRET K-36 (CORRECT. GRADIENT)
TEMP IN DEG C
50
100
150
0
GRAD1 = 23.7°C/KM
(13.0°F/KFT)
1
2
3
4
5
6
DEPTH IN KILOMETERS
10
20
DEPTH IN THOUSANDS OF FT
STANDARD ERROR OF ESTIMATE
3.6 DEG C
32
100
200
300
TEMP IN DEG F

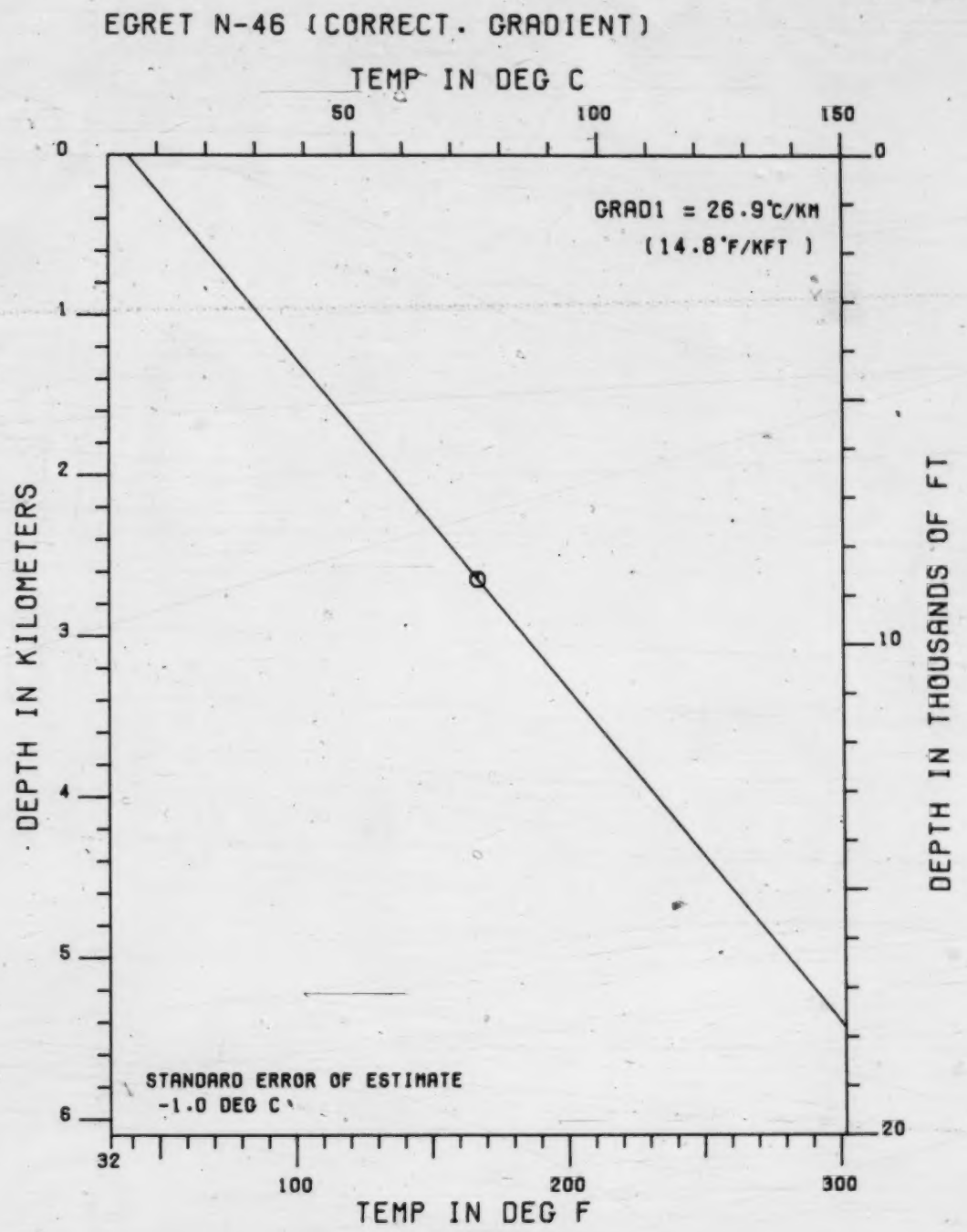
EGRET N-46 (CORRECT. GRADIENT)
TEMP IN DEG C
50
100
150
0
GRAD1 = 26.9°C/KM
(14.8°F/KFT)
1
2
3
4
5
6
DEPTH IN KILOMETERS
10
20
DEPTH IN THOUSANDS OF FT
STANDARD ERROR OF ESTIMATE
-1.0 DEG C
32
100
200
300
TEMP IN DEG F

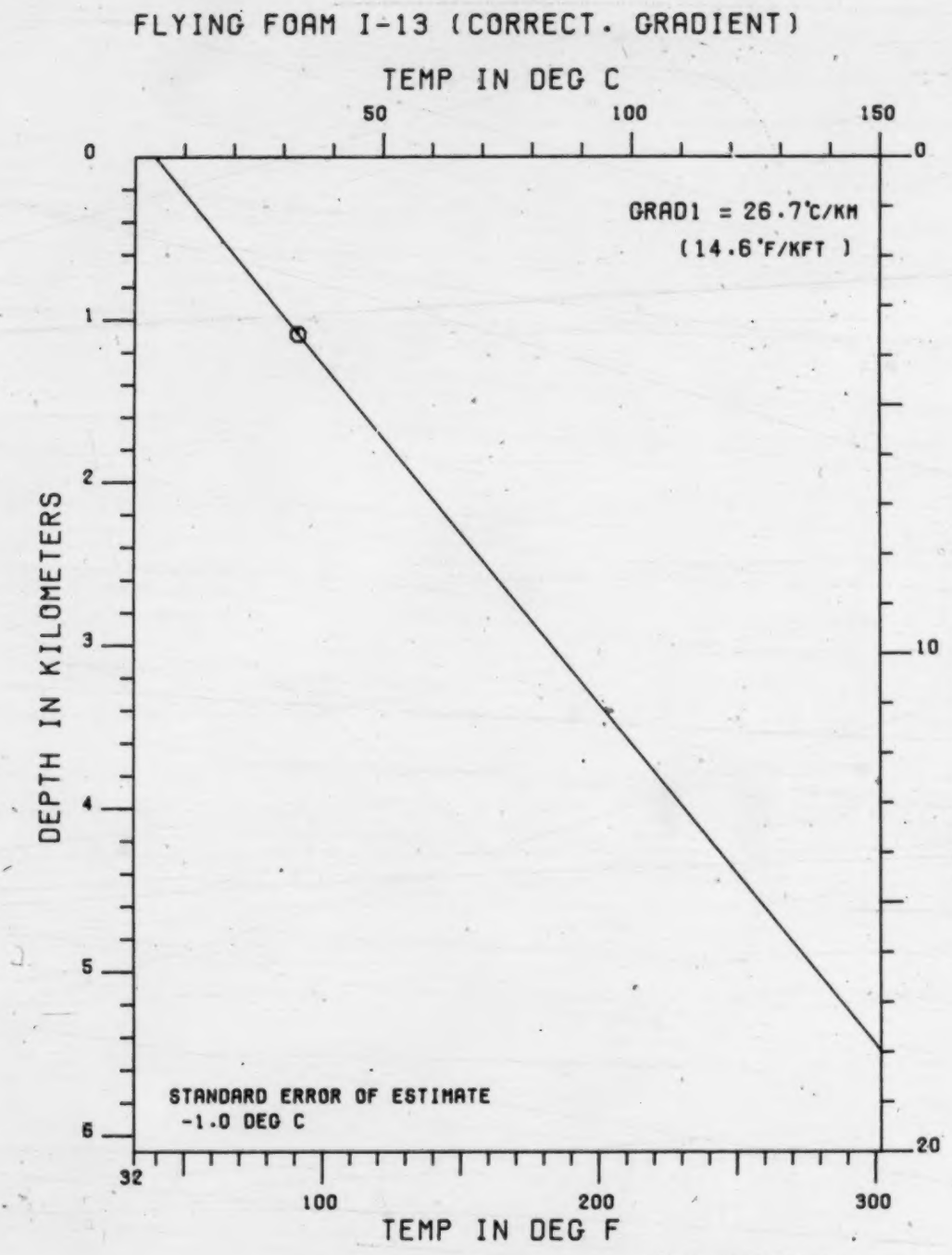
FLYING FOAM I-13 (CORRECT. GRADIENT)
TEMP IN DEG C
50
100
150
0
GRAD1 = 26.7°C/KM
(14.6°F/KFT)
1
2
3
4
5
6
DEPTH IN KILOMETERS
DEPTH IN THOUSANDS OF FT
10
20
STANDARD ERROR OF ESTIMATE
-1.0 DEG C
32
100
200
300
TEMP IN DEG F

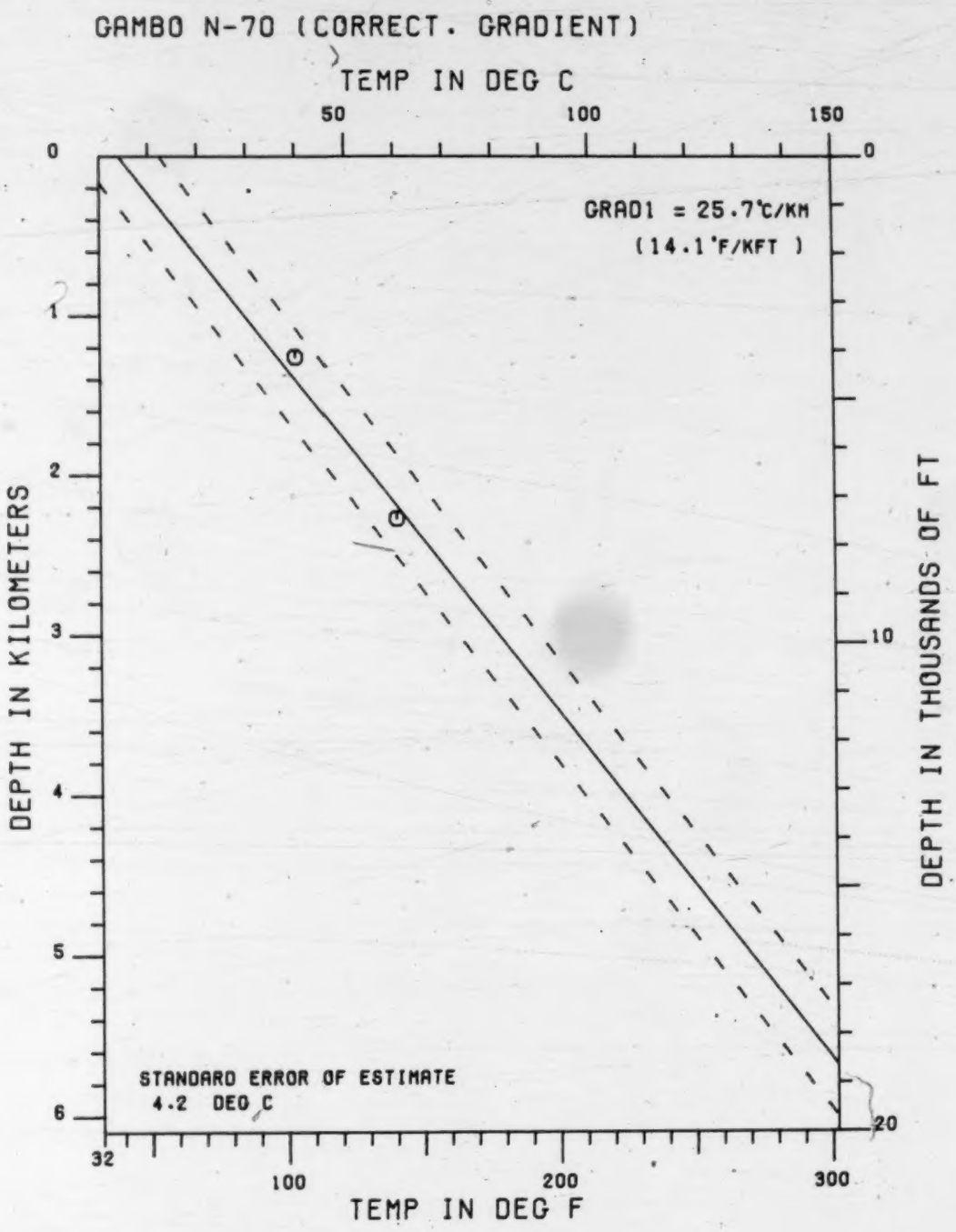
GAMBO N-70 (CORRECT. GRADIENT)
TEMP IN DEG C
50
100
150
0
GRAD1 = 25.7°C/KM
(14.1°F/KFT)
1
2
3
4
5
6
DEPTH IN KILOMETERS
10
20
DEPTH IN THOUSANDS OF FT
STANDARD ERROR OF ESTIMATE
4.2 DEG C
32
100
200
300
TEMP IN DEG F

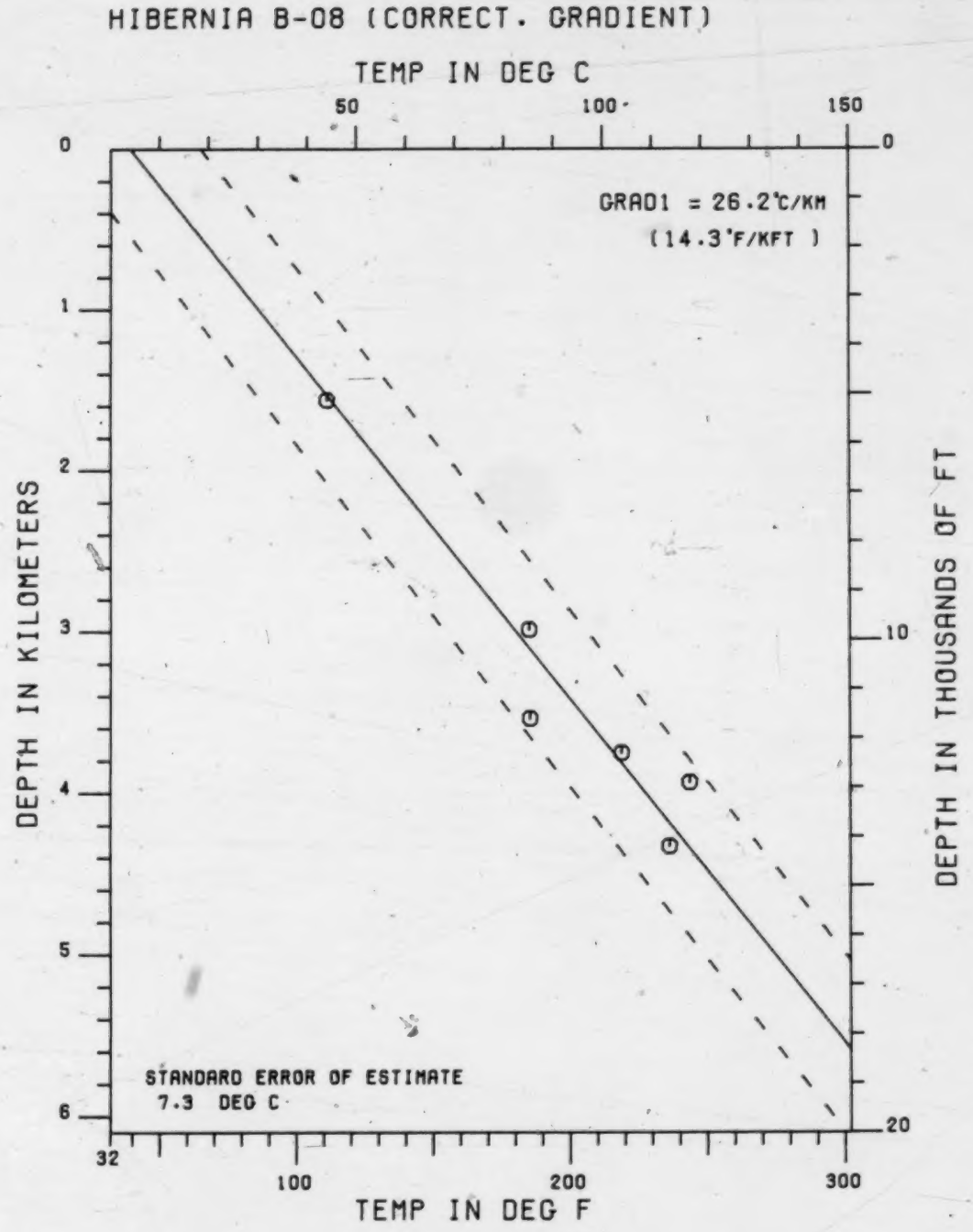
HIBERNIA B-08 (CORRECT. GRADIENT)
TEMP IN DEG C
50
100
150
0
GRAD1 = 26.2°C/KM
(14.3°F/KFT)
1
2
3
4
5
6
DEPTH IN KILOMETERS
DEPTH IN THOUSANDS OF FT
10
20
STANDARD ERROR OF ESTIMATE
7.3 DEG C
32
100
200
300
TEMP IN DEG F

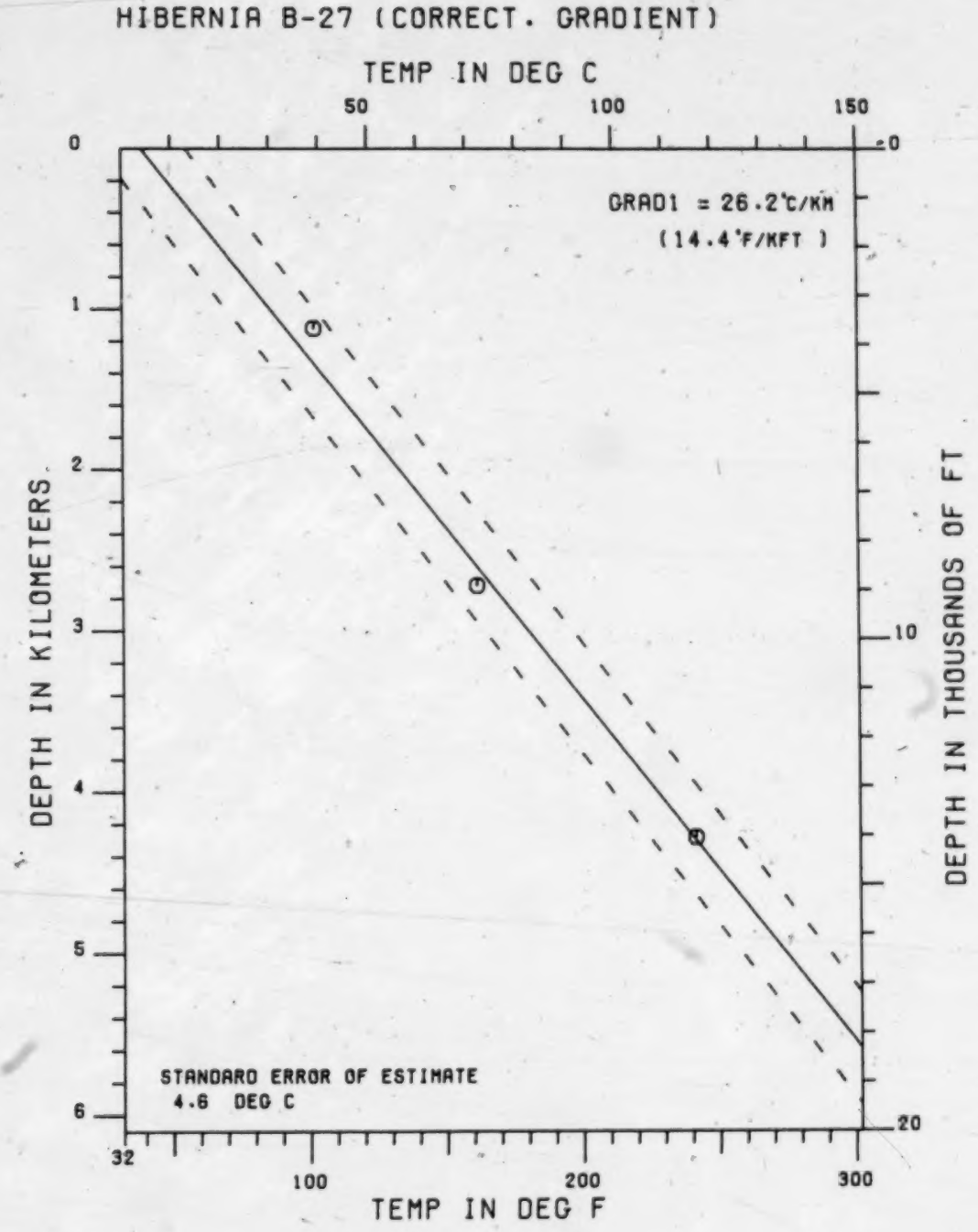
HIBERNIA B-27 (CORRECT. GRADIENT)
TEMP IN DEG C
50
100
150
0
GRAD1 = 26.2°C/KM
(14.4°F/KFT)
1
2
3
4
5
6
DEPTH IN KILOMETERS
DEPTH IN THOUSANDS OF FT
10
20
STANDARD ERROR OF ESTIMATE
4.6 DEG C
32
100
200
300
TEMP IN DEG F

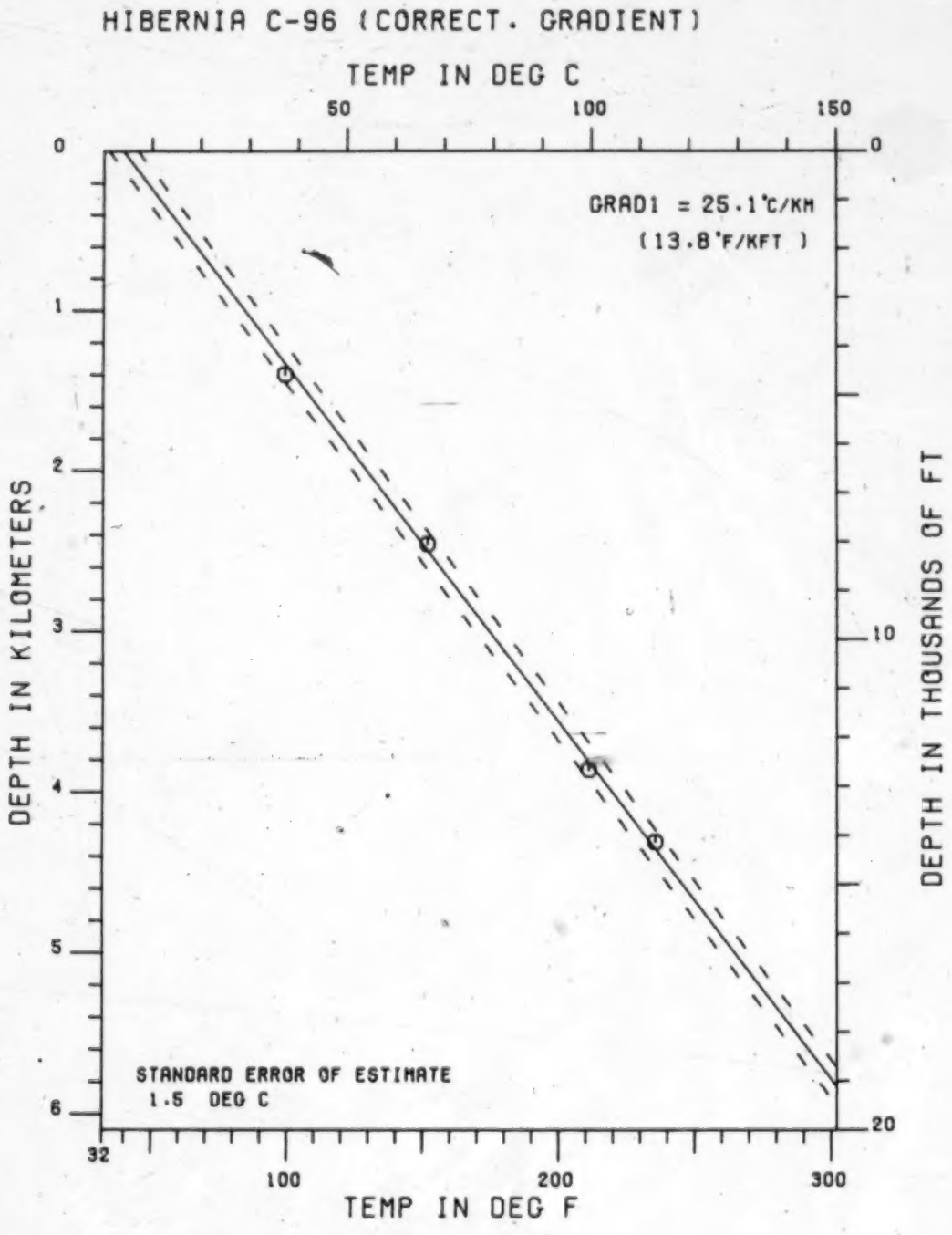
HIBERNIA C-96 (CORRECT. GRADIENT)
TEMP IN DEG C
50
100
150
0
GRAD1 = 25.1°C/KM
(13.8°F/KFT)
1
2
3
4
5
6
DEPTH IN KILOMETERS
10
20
DEPTH IN THOUSANDS OF FT
STANDARD ERROR OF ESTIMATE
1.5 DEG C
32
100
200
300
TEMP IN DEG F

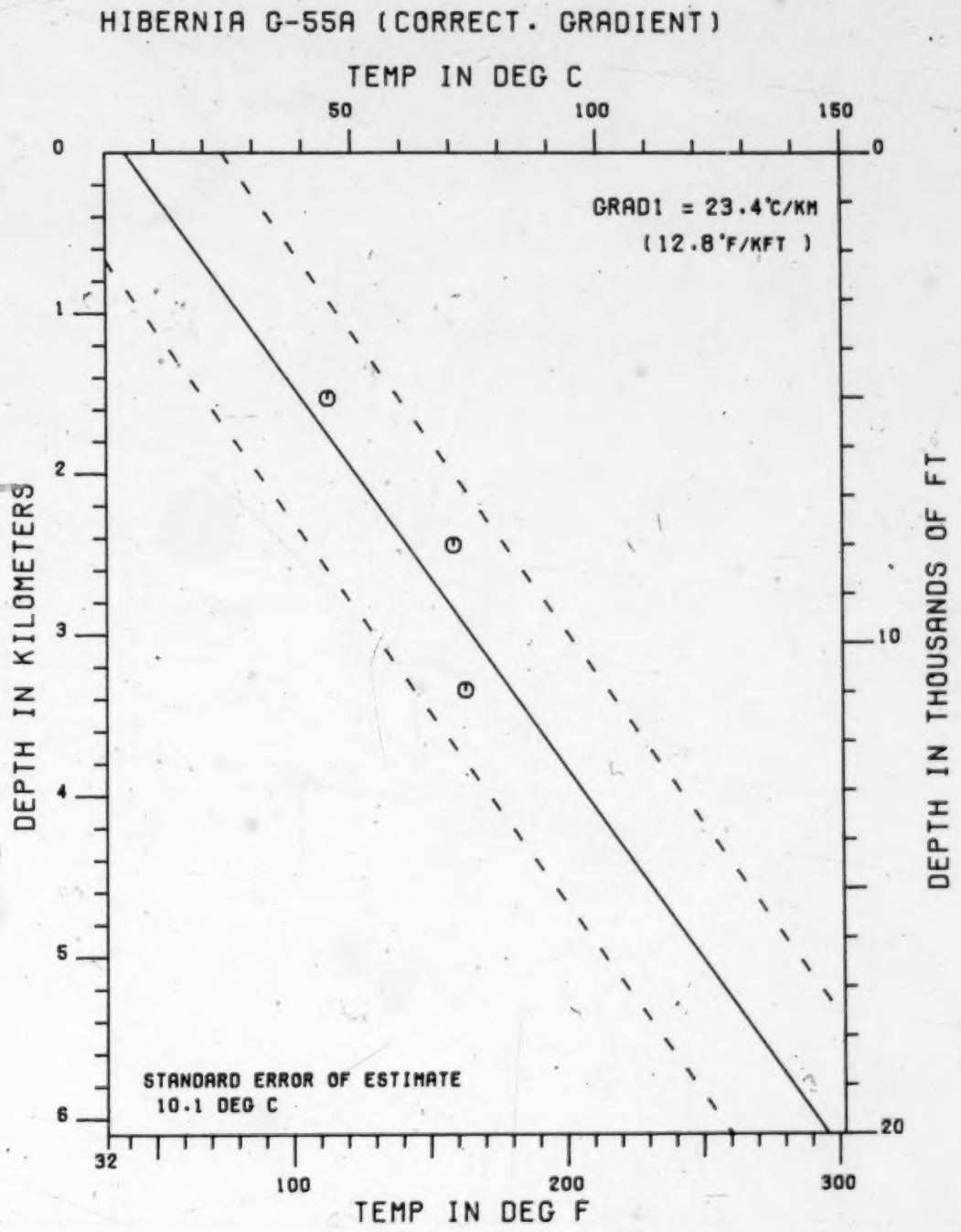
HIBERNIA G-55A (CORRECT. GRADIENT)
TEMP IN DEG C
50
100
150
0
GRAD1 = 23.4°C/KM
(12.8°F/KFT)
1
2
3
4
5
6
DEPTH IN KILOMETERS
DEPTH IN THOUSANDS OF FT
10
20
STANDARD ERROR OF ESTIMATE
10.1 DEG C
32
100
200
300
TEMP IN DEG F

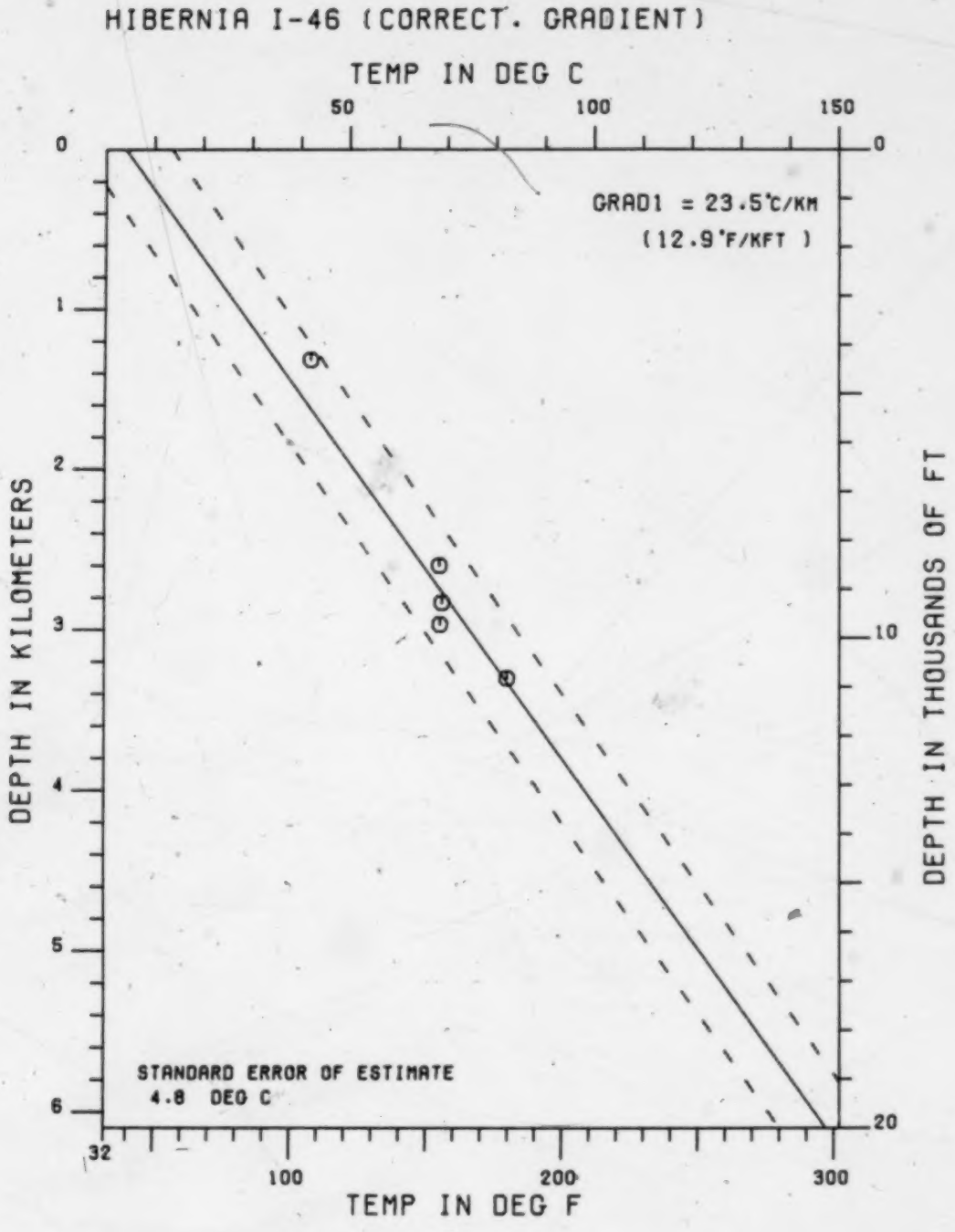
HIBERNIA I-46 (CORRECT. GRADIENT)
TEMP IN DEG C
50
100
150
0
GRAD1 = 23.5°C/KM
(12.9°F/KFT)
1
2
3
4
5
6
DEPTH IN KILOMETERS
DEPTH IN THOUSANDS OF FT
10
20
STANDARD ERROR OF ESTIMATE
4.8 DEG C
32
100
200
300
TEMP IN DEG F

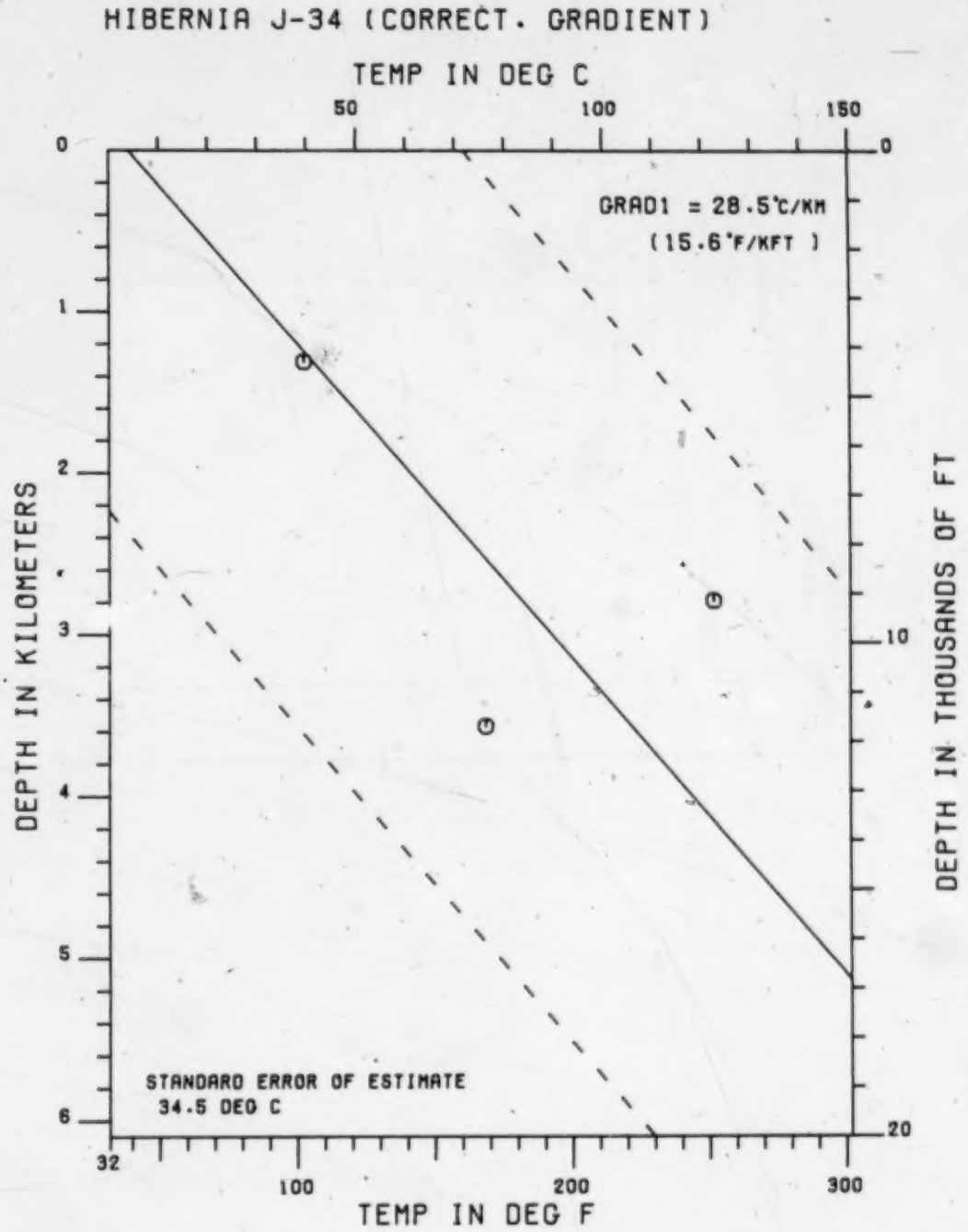
HIBERNIA J-34 (CORRECT. GRADIENT)
TEMP IN DEG C
50
100
150
0
GRAD1 = 28.5°C/KM
(15.6°F/KFT)
1
2
3
4
5
6
DEPTH IN KILOMETERS
10
20
DEPTH IN THOUSANDS OF FT
STANDARD ERROR OF ESTIMATE
34.5 DEG C
32
100
200
300
TEMP IN DEG F

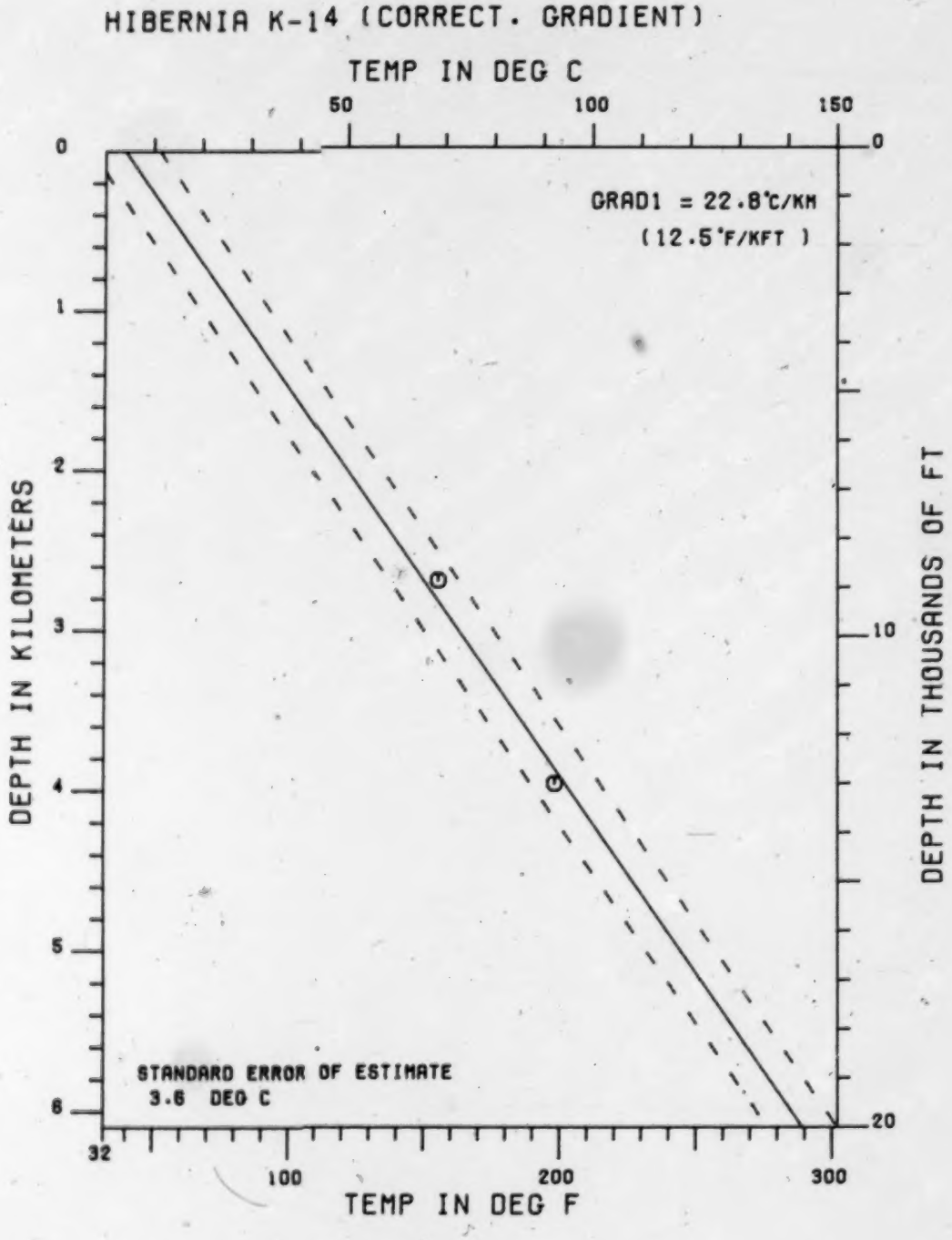
HIBERNIA K-14 (CORRECT. GRADIENT)
TEMP IN DEG C
50
100
150
0
GRAD1 = 22.8°C/KM
(12.5°F/KFT)
1
2
3
4
5
6
DEPTH IN KILOMETERS
DEPTH IN THOUSANDS OF FT
10
20
STANDARD ERROR OF ESTIMATE
3.6 DEG C
32
100
200
300
TEMP IN DEG F

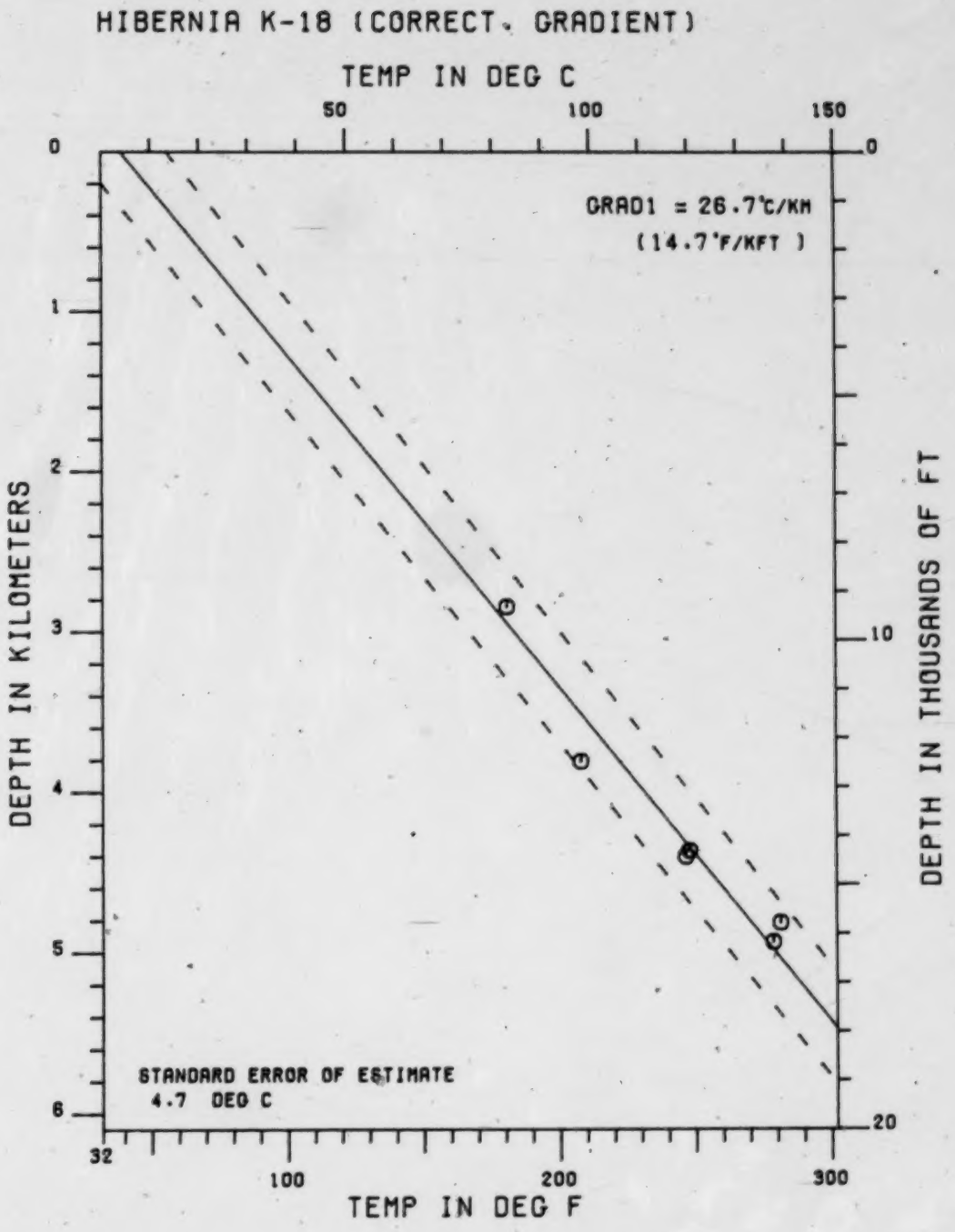
HIBERNIA K-18 (CORRECT. GRADIENT)
TEMP IN DEG C
50
100
150
0
GRAD1 = 26.7°C/KM
(14.7°F/KFT)
1
2
3
4
5
6
DEPTH IN KILOMETERS
DEPTH IN THOUSANDS OF FT
10
20
STANDARD ERROR OF ESTIMATE
4.7 DEG C
32
100
200
300
TEMP IN DEG F

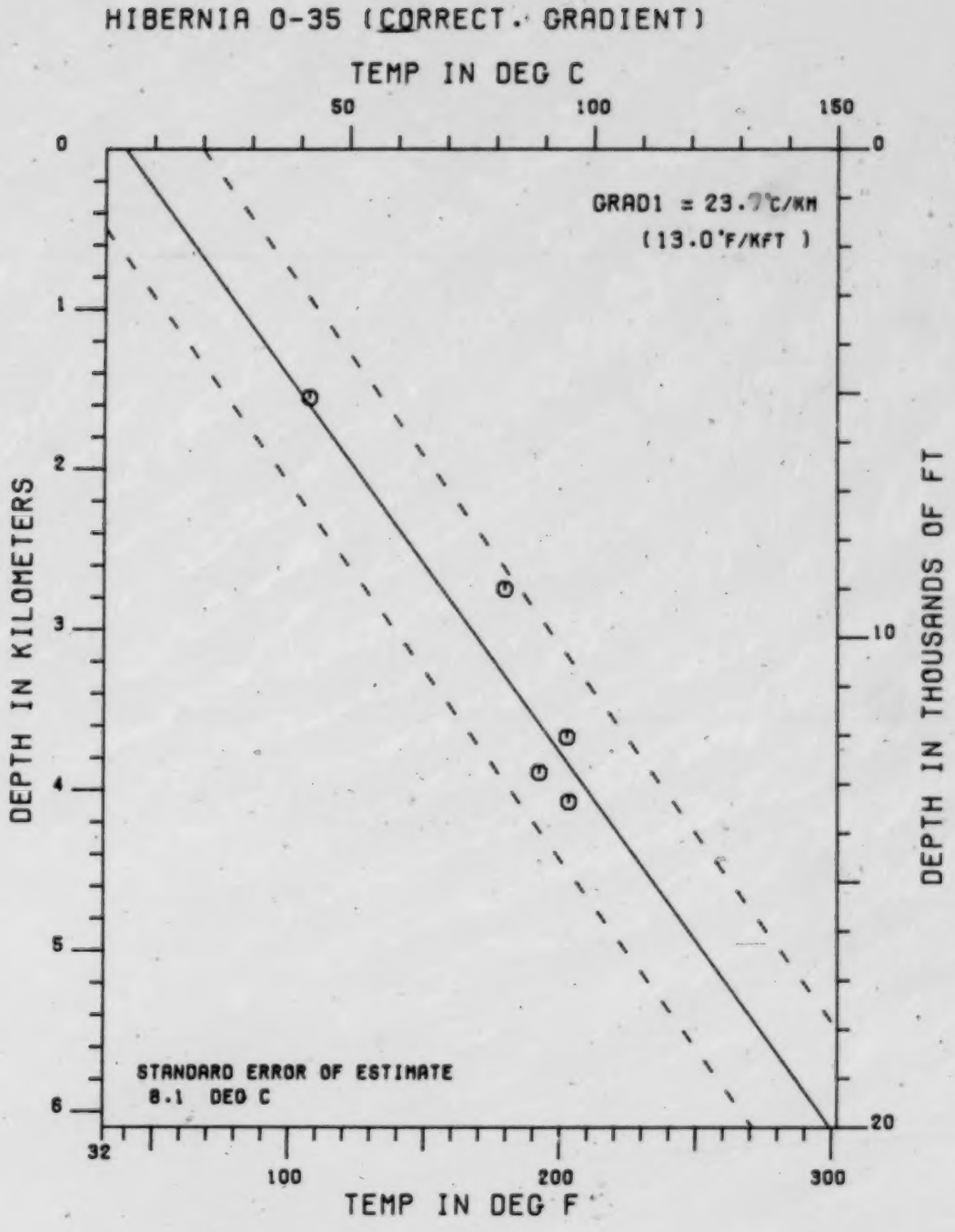
HIBERNIA O-35 (CORRECT. GRADIENT)
TEMP IN DEG C
50
100
150
0
GRAD1 = 23.7°C/KM
(13.0°F/KFT)
1
2
3
4
5
6
DEPTH IN KILOMETERS
10
20
DEPTH IN THOUSANDS OF FT
STANDARD ERROR OF ESTIMATE
8.1 DEG C
32
100
200
300
TEMP IN DEG F

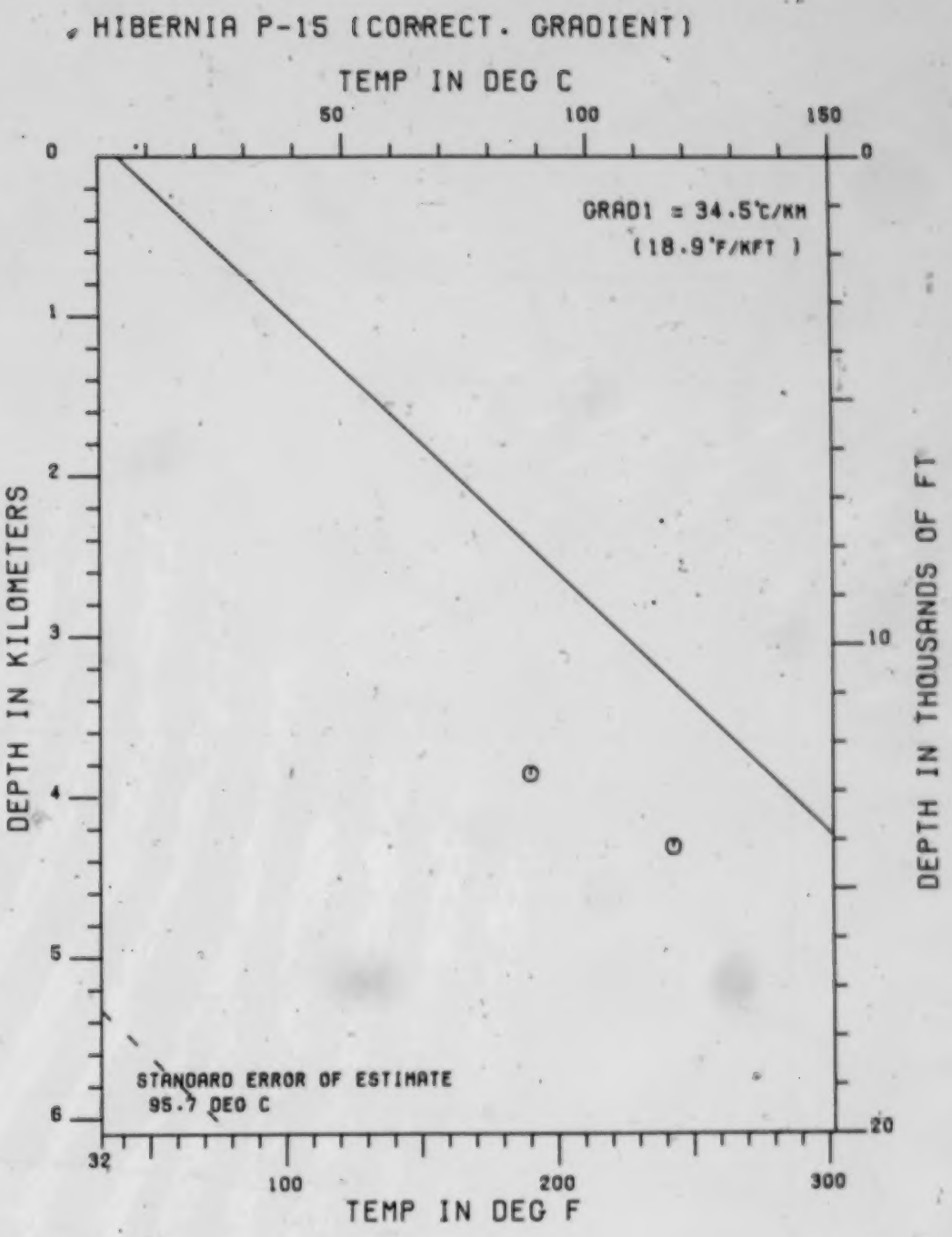
HIBERNIA P-15 (CORRECT. GRADIENT)
TEMP IN DEG C
50
100
150
0
GRAD1 = 34.5°C/KM
(18.9°F/KFT)
1
2
3
4
5
6
DEPTH IN KILOMETERS
10
20
DEPTH IN THOUSANDS OF FT
STANDARD ERROR OF ESTIMATE
95.7 DEG C
32
100
200
300
TEMP IN DEG F

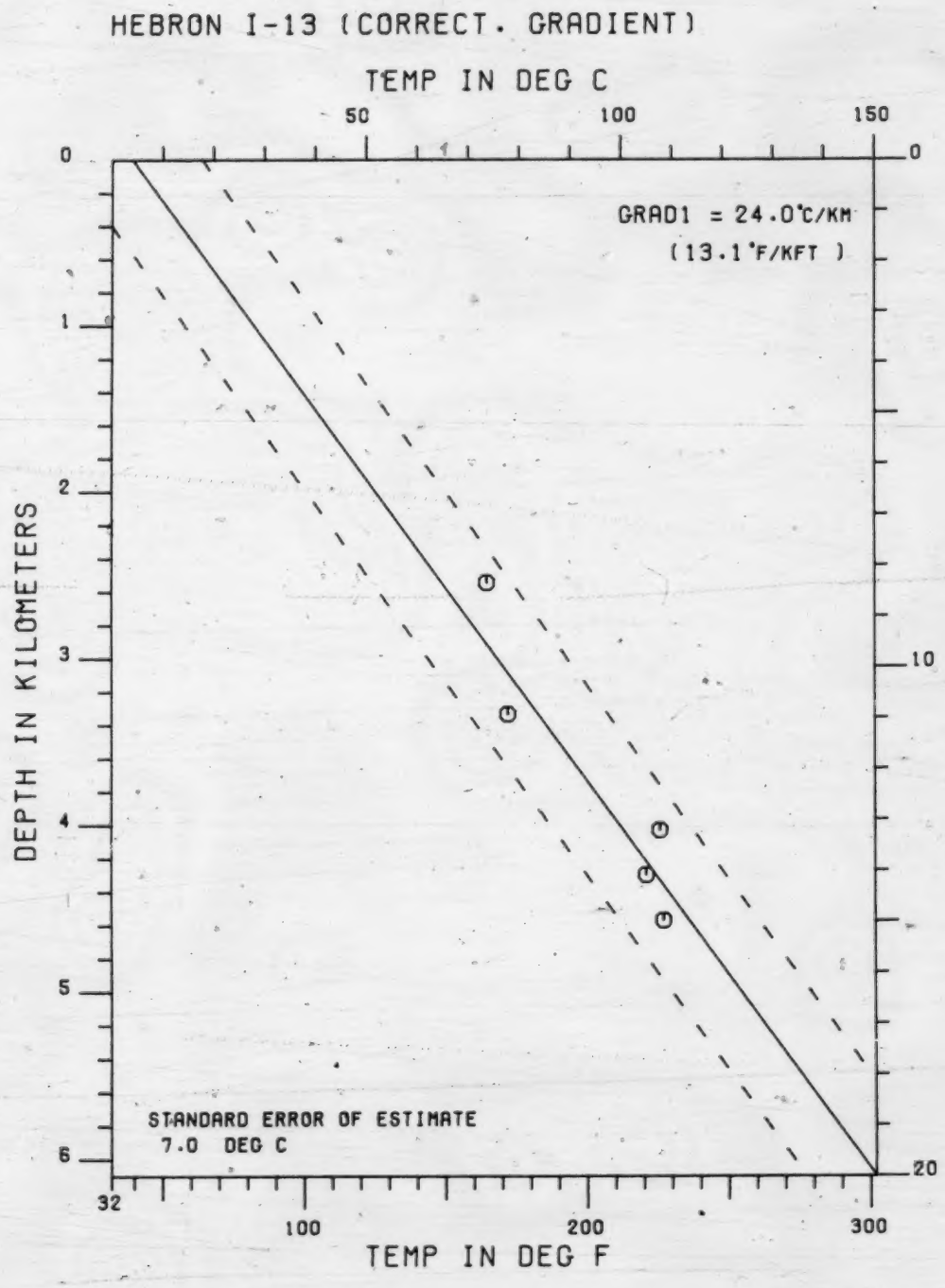
HEBRON I-13 (CORRECT. GRADIENT)
TEMP IN DEG C
50
100
150
0
GRAD1 = 24.0°C/KM
(13.1°F/KFT)
1
2
3
4
5
6
DEPTH IN KILOMETERS
10
20
DEPTH IN THOUSANDS OF FT
STANDARD ERROR OF ESTIMATE
7.0 DEG C
32
100
200
300
TEMP IN DEG F

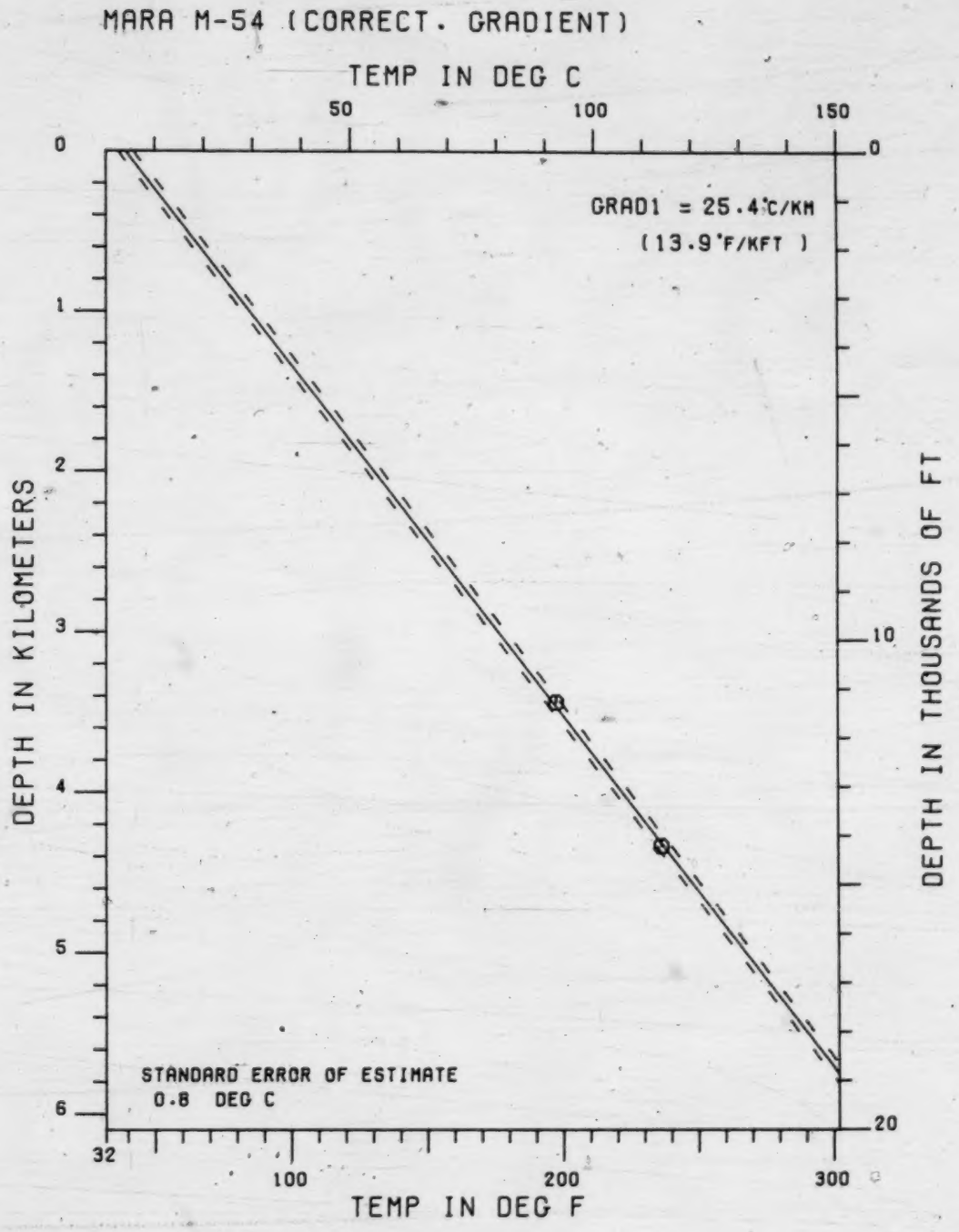
MARA M-54 (CORRECT. GRADIENT)
TEMP IN DEG C
50
100
150
0
GRAD1 = 25.4°C/KM
(13.9°F/KFT)
1
2
3
4
5
6
DEPTH IN KILOMETERS
10
20
DEPTH IN THOUSANDS OF FT
STANDARD ERROR OF ESTIMATE
0.8 DEG C
32
100
200
300
TEMP IN DEG F

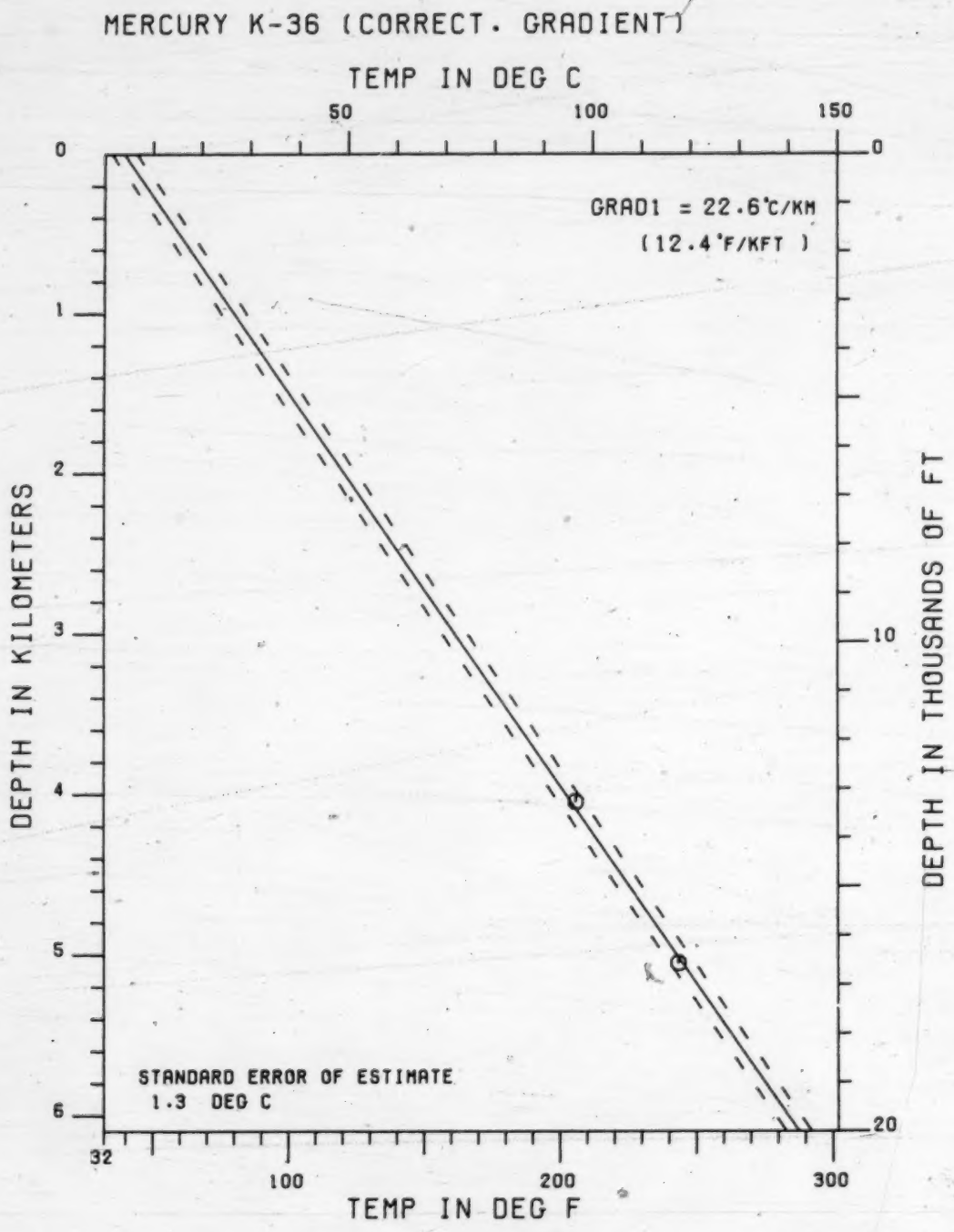
MERCURY K-36 (CORRECT. GRADIENT)
TEMP IN DEG C
50
100
150
0
GRAD1 = 22.6°C/KM
(12.4°F/KFT)
1
2
3
4
5
6
DEPTH IN KILOMETERS
10
20
DEPTH IN THOUSANDS OF FT
STANDARD ERROR OF ESTIMATE
1.3 DEG C
32
100
200
300
TEMP IN DEG F

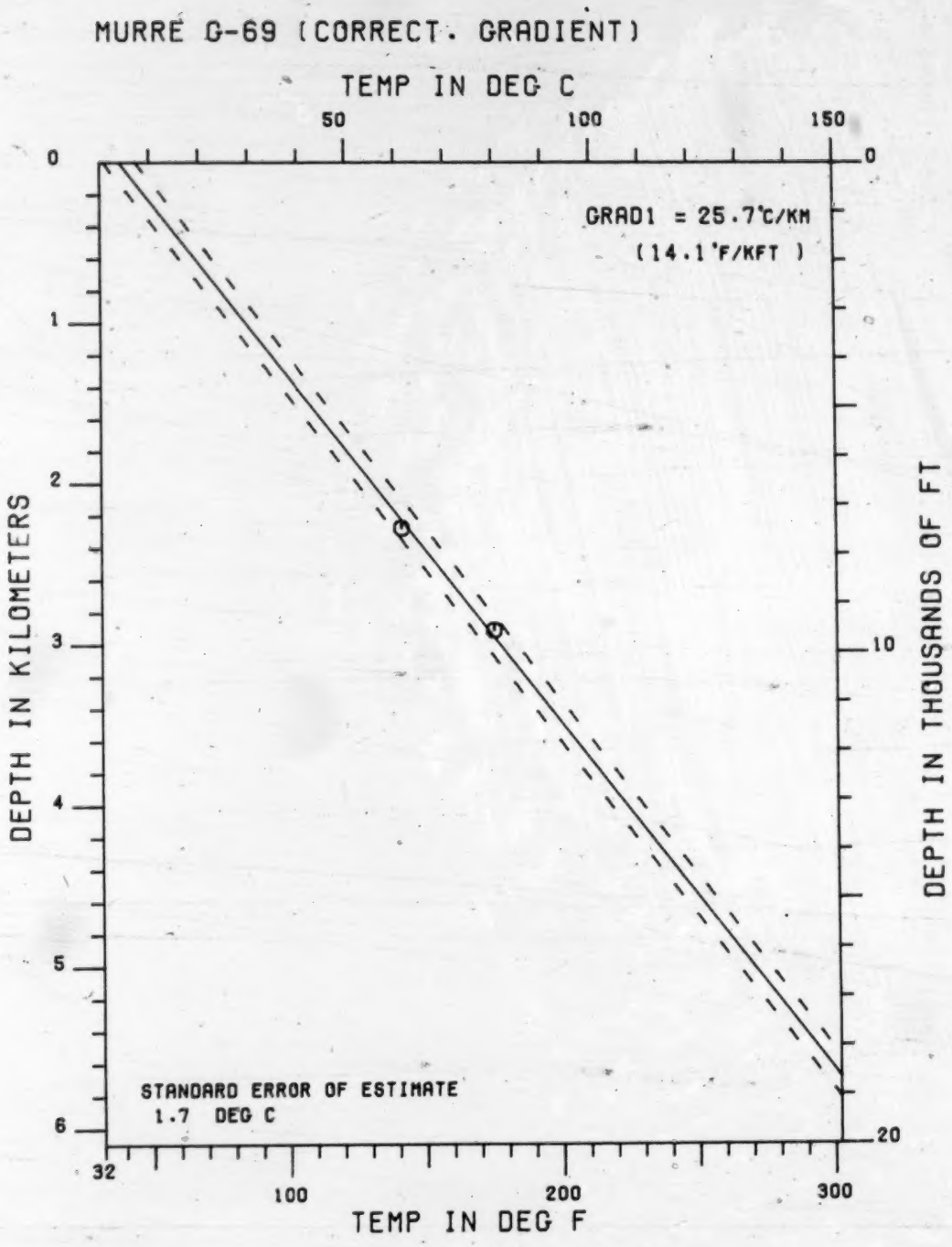
MURRE G-69 (CORRECT. GRADIENT)
TEMP IN DEG C
50
100
150
0
GRAD1 = 25.7°C/KM
(14.1°F/KFT)
1
2
3
4
5
6
DEPTH IN KILOMETERS
10
20
DEPTH IN THOUSANDS OF FT
STANDARD ERROR OF ESTIMATE
1.7 DEG C
32
100
200
300
TEMP IN DEG F

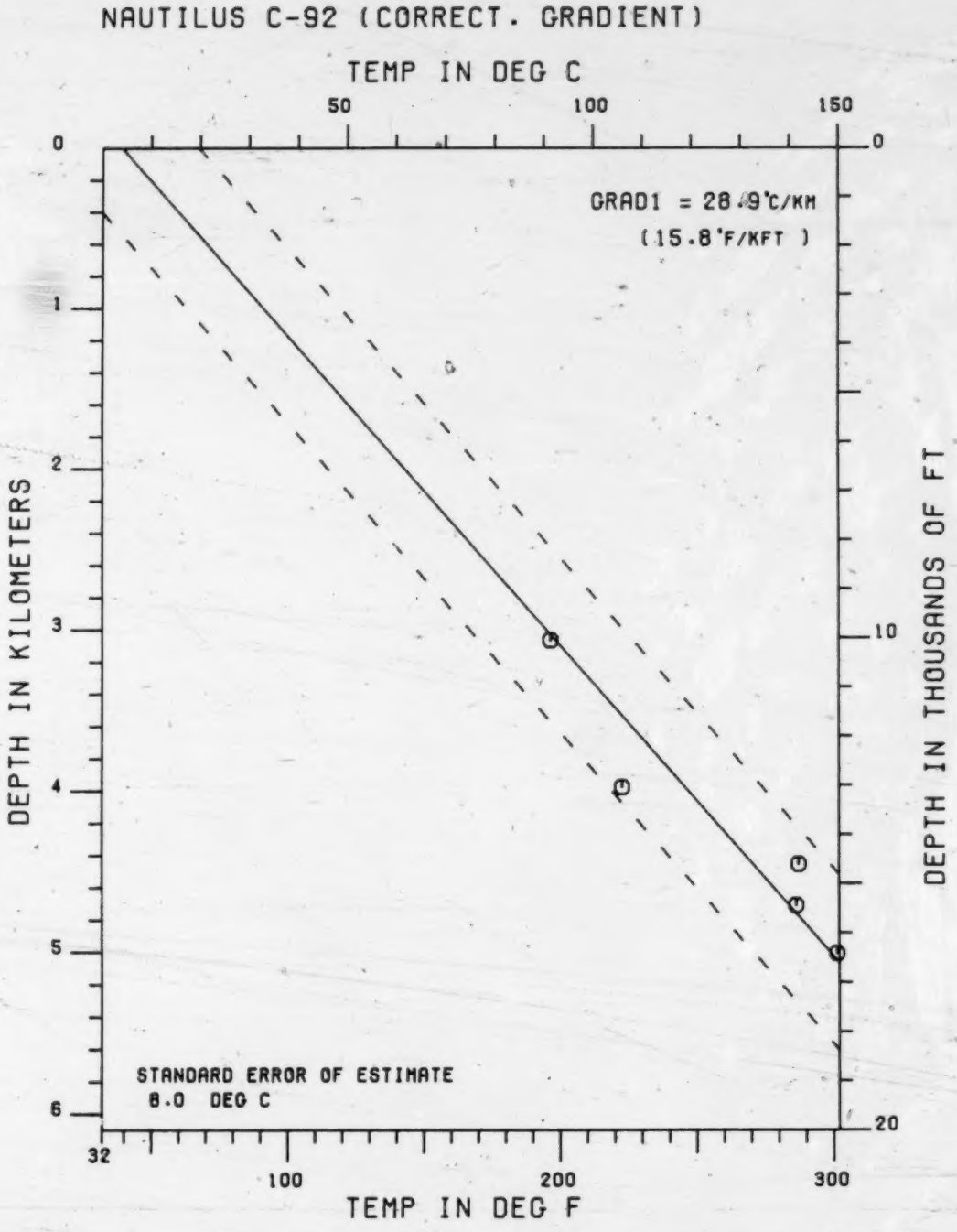
NAUTILUS C-92 (CORRECT. GRADIENT)
TEMP IN DEG C
50
100
150
0
GRAD1 = 28.9°C/KM
(15.8°F/KFT)
1
2
3
4
5
6
DEPTH IN KILOMETERS
10
20
DEPTH IN THOUSANDS OF FT
STANDARD ERROR OF ESTIMATE
8.0 DEG C
32
100
200
300
TEMP IN DEG F

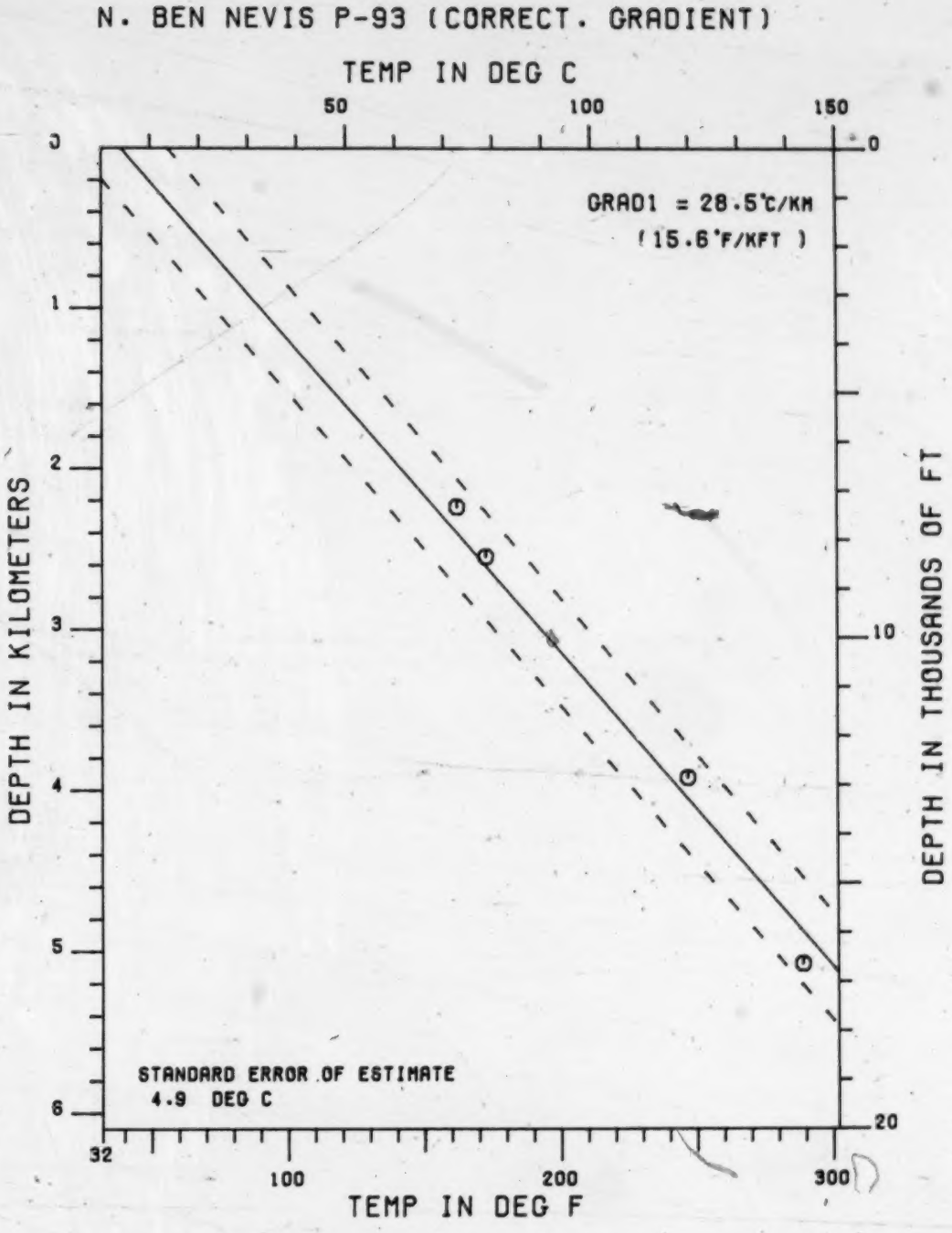
N. BEN NEVIS P-93 (CORRECT. GRADIENT)
TEMP IN DEG C
50
100
150
0
GRAD1 = 28.5°C/KM
(15.6°F/KFT)
1
2
3
4
5
6
DEPTH IN KILOMETERS
10
20
DEPTH IN THOUSANDS OF FT
STANDARD ERROR OF ESTIMATE
4.9 DEG C
32
100
200
300
TEMP IN DEG F

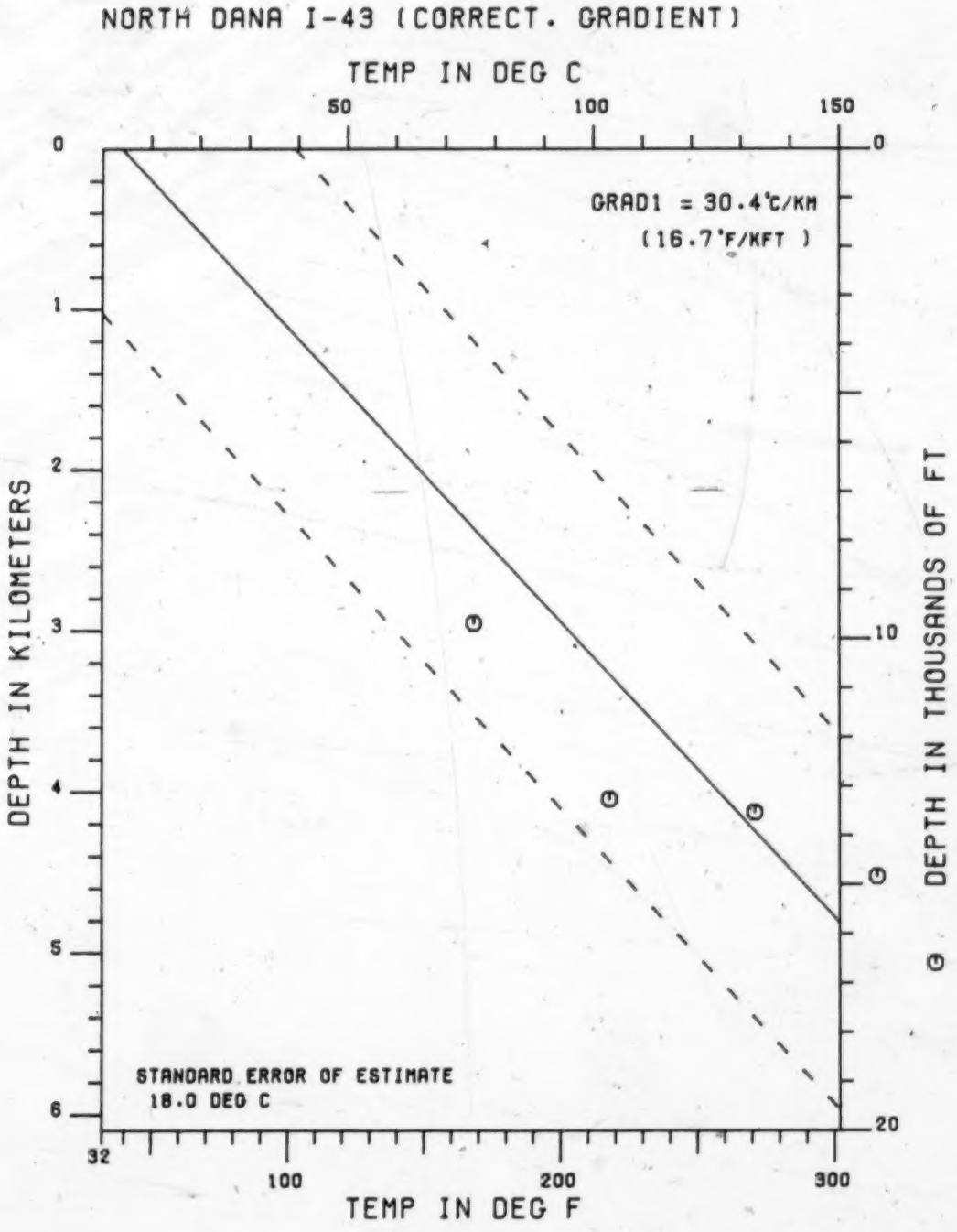
NORTH DANA I-43 (CORRECT. GRADIENT)
TEMP IN DEG C
50
100
150
0
GRAD1 = 30.4°C/KM
(16.7°F/KFT)
1
2
3
4
5
6
DEPTH IN KILOMETERS
STANDARD ERROR OF ESTIMATE
18.0 DEG C
32
100
200
300
TEMP IN DEG F
10
20
DEPTH IN THOUSANDS OF FT

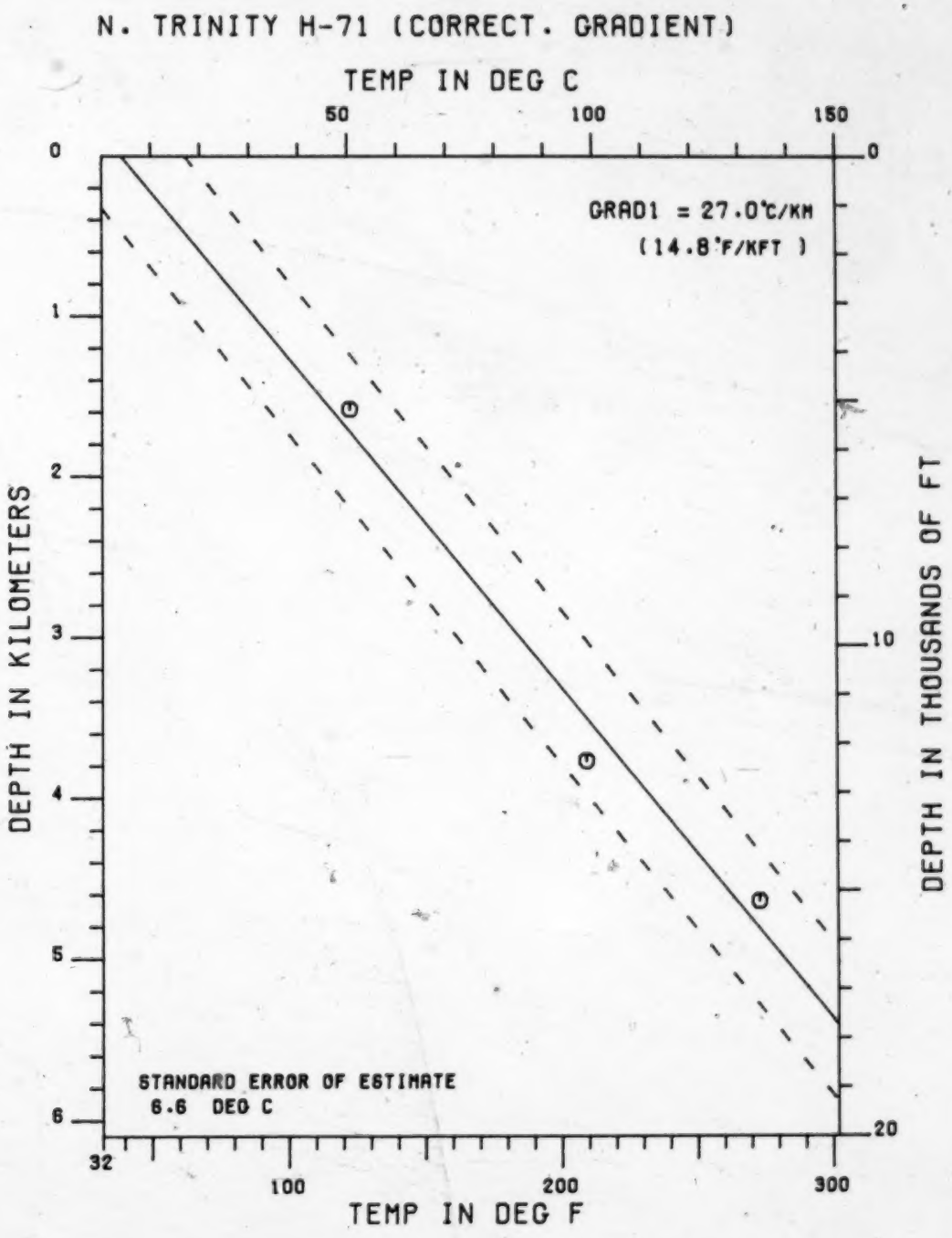
N. TRINITY H-71 (CORRECT. GRADIENT)
TEMP IN DEG C
50
100
150
0
GRAD1 = 27.0°C/KM
(14.8°F/KFT)
1
2
3
4
5
6
DEPTH IN KILOMETERS
DEPTH IN THOUSANDS OF FT
10
20
STANDARD ERROR OF ESTIMATE
6.6 DEG C
32
100
200
300
TEMP IN DEG F

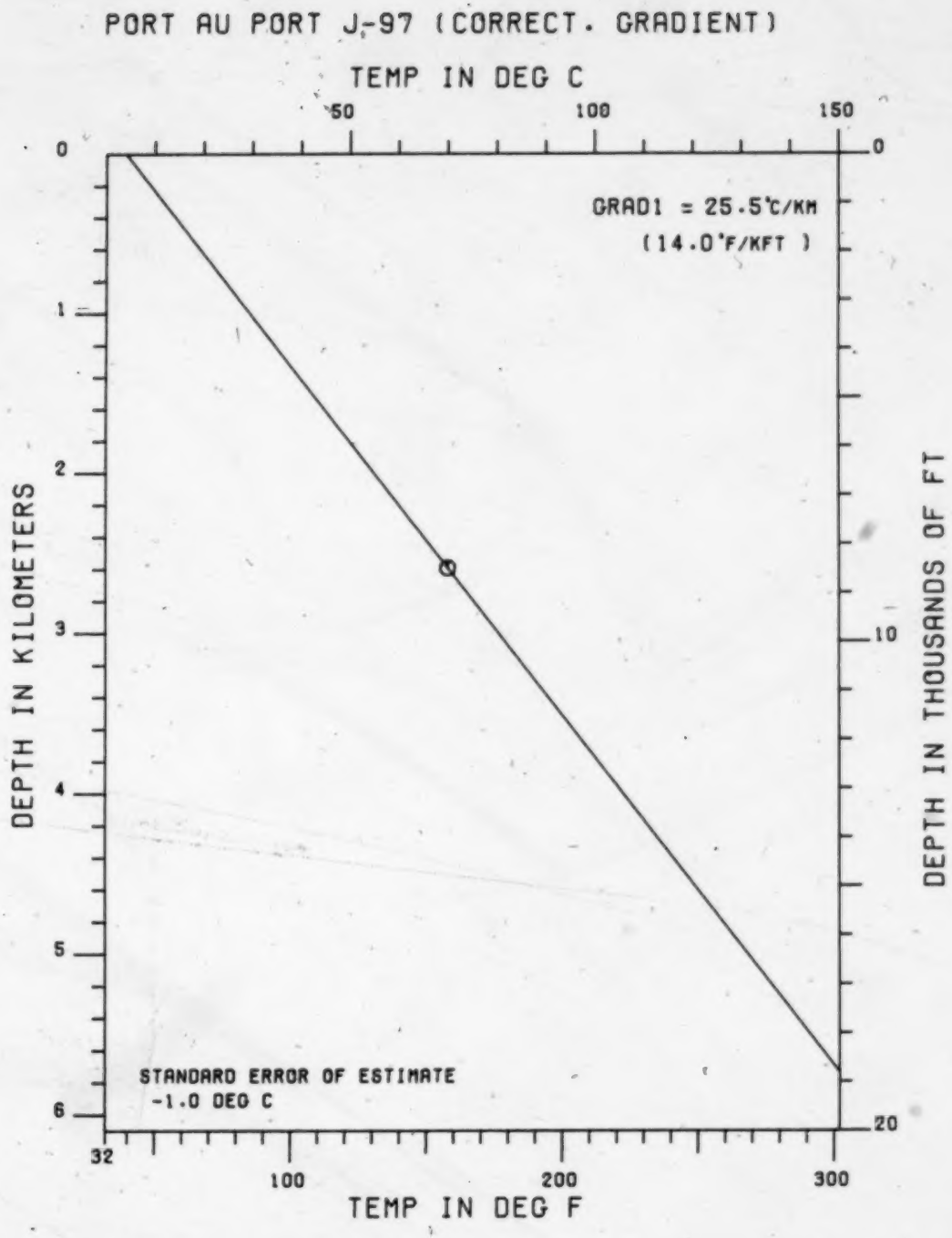
PORT AU PORT J-97 (CORRECT. GRADIENT)
TEMP IN DEG C
50
100
150
0
GRAD1 = 25.5°C/KM
(14.0°F/KFT)
1
2
3
4
5
6
DEPTH IN KILOMETERS
DEPTH IN THOUSANDS OF FT
10
20
STANDARD ERROR OF ESTIMATE
-1.0 DEG C
32
100
200
300
TEMP IN DEG F

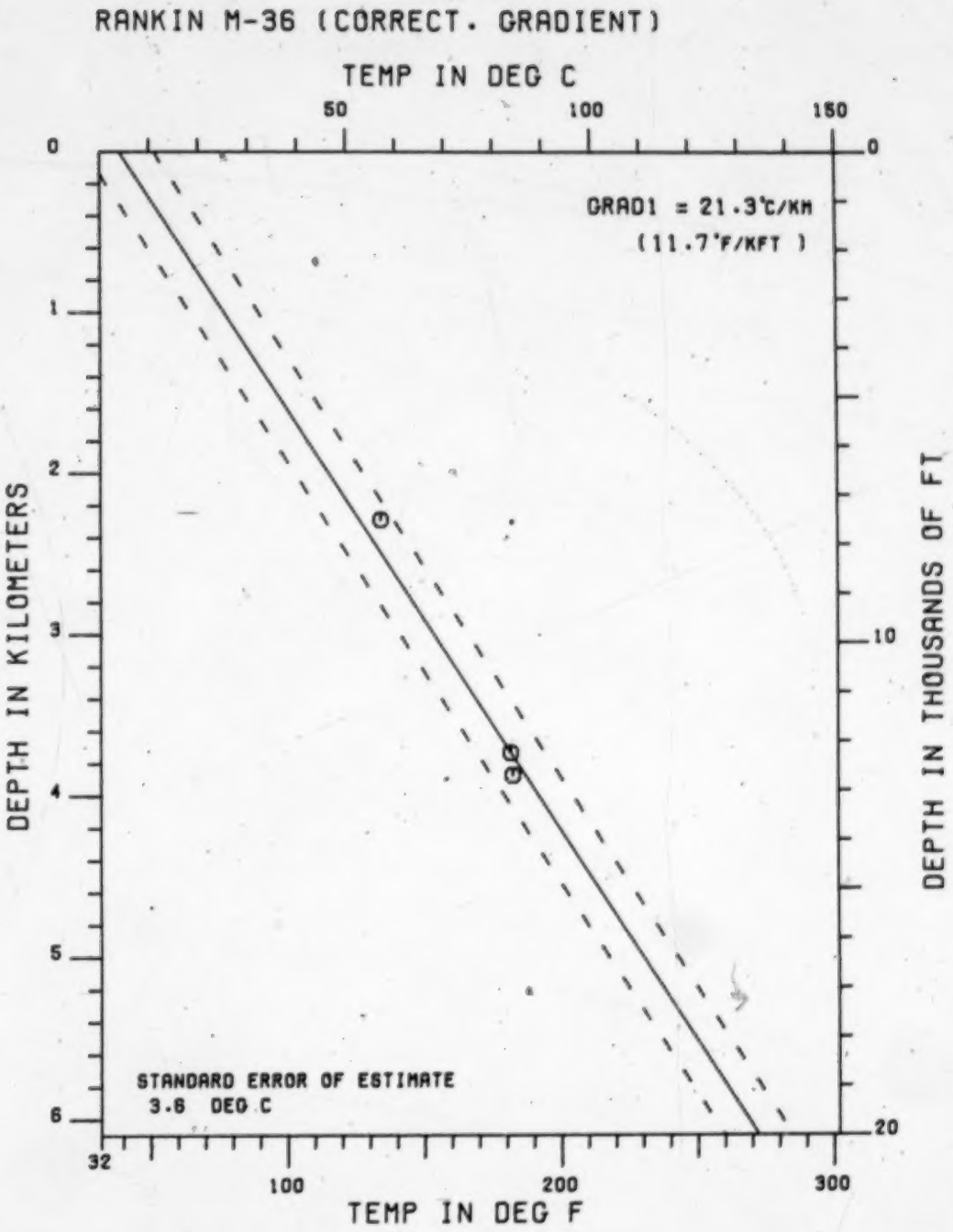
RANKIN M-36 (CORRECT. GRADIENT)
TEMP IN DEG C
50
100
150
0
GRAD1 = 21.3°C/KM
(11.7°F/KFT)
1
2
3
4
5
6
DEPTH IN KILOMETERS
DEPTH IN THOUSANDS OF FT
10
20
STANDARD ERROR OF ESTIMATE
3.6 DEG C
32
100
200
300
TEMP IN DEG F

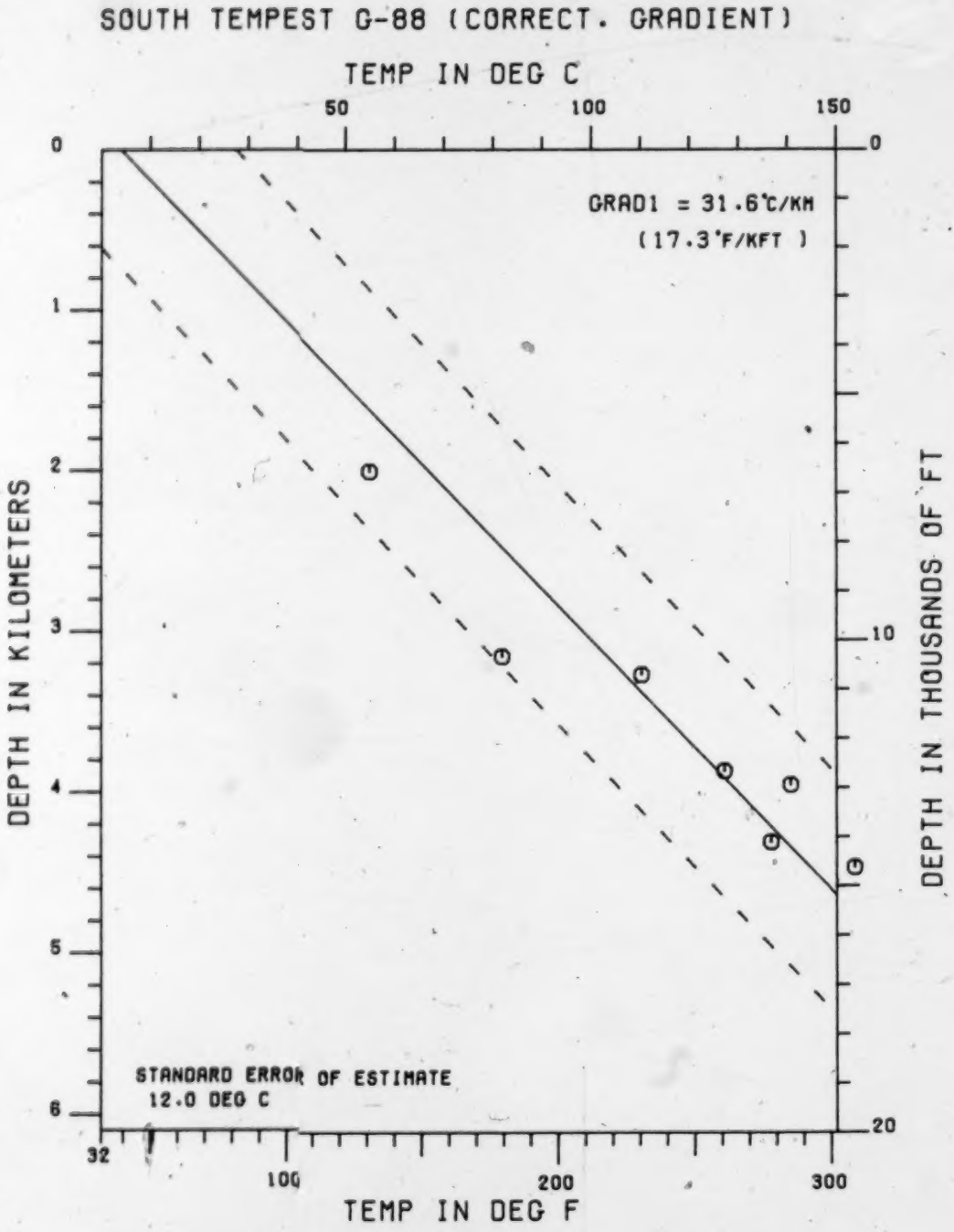
SOUTH TEMPEST G-88 (CORRECT. GRADIENT)
TEMP IN DEG C
50
100
150
0
GRAD1 = 31.6°C/KM
(17.3°F/KFT)
1
2
3
4
5
6
DEPTH IN KILOMETERS
DEPTH IN THOUSANDS OF FT
10
20
STANDARD ERROR OF ESTIMATE
12.0 DEG C
32
100
200
300
TEMP IN DEG F

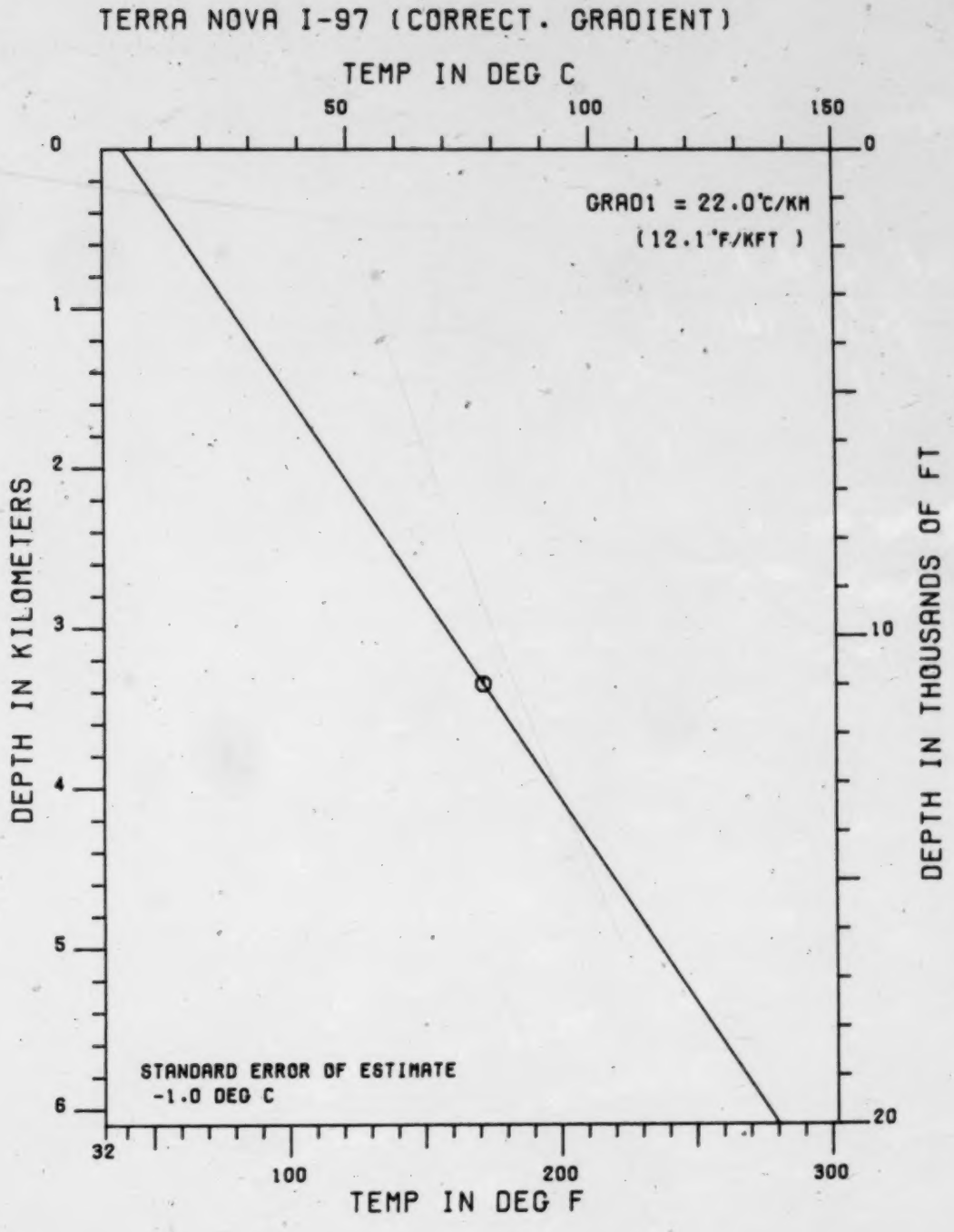
TERRA NOVA I-97 (CORRECT. GRADIENT)
TEMP IN DEG C
50
100
150
0
GRAD1 = 22.0°C/KM
(12.1°F/KFT)
1
2
3
4
5
6
DEPTH IN KILOMETERS
DEPTH IN THOUSANDS OF FT
10
20
STANDARD ERROR OF ESTIMATE
-1.0 DEG C
32
100
200
300
TEMP IN DEG F

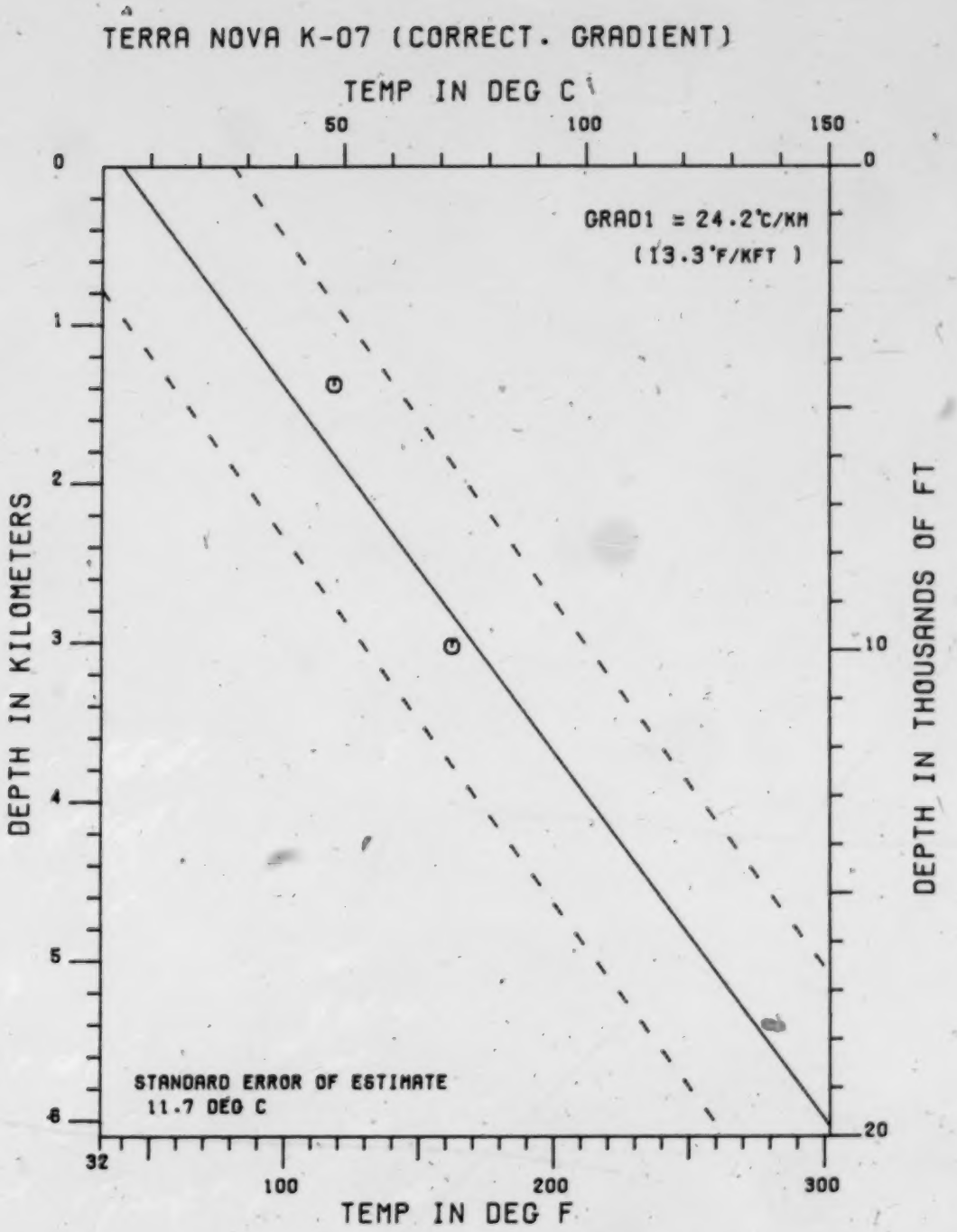
TERRA NOVA K-07 (CORRECT. GRADIENT)
TEMP IN DEG C
50
100
150
0
GRAD1 = 24.2°C/KM
(13.3°F/KFT)
1
2
3
4
5
6
DEPTH IN KILOMETERS
DEPTH IN THOUSANDS OF FT
10
20
STANDARD ERROR OF ESTIMATE
11.7 DEG C
32
100
200
300
TEMP IN DEG F

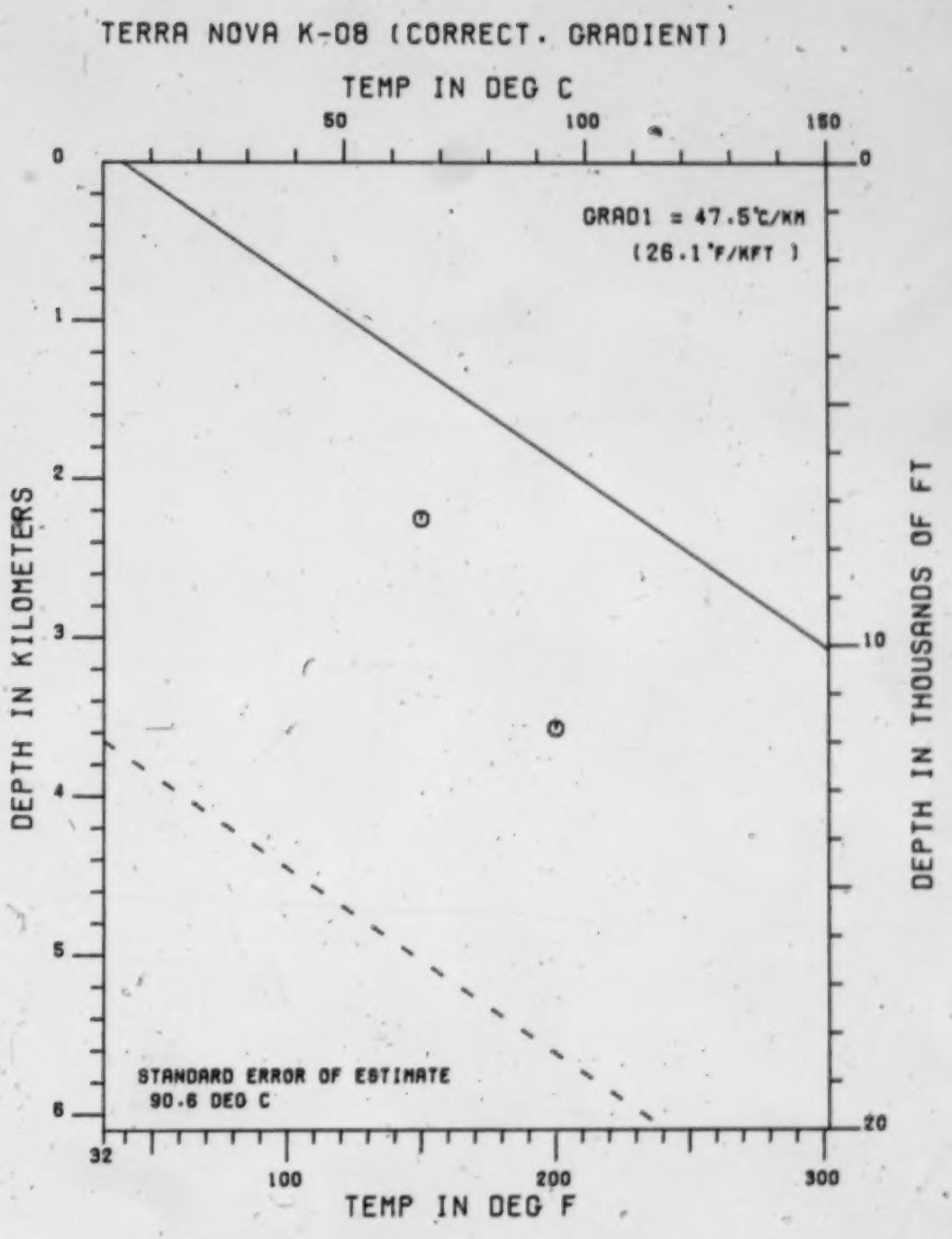
TERRA NOVA K-08 (CORRECT. GRADIENT)
TEMP IN DEG C
50
100
150
0
GRAD1 = 47.5°C/KM
(26.1°F/KFT)
1
2
3
4
5
6
DEPTH IN KILOMETERS
10
20
DEPTH IN THOUSANDS OF FT
STANDARD ERROR OF ESTIMATE
90.6 DEG C
32
100
200
300
TEMP IN DEG F

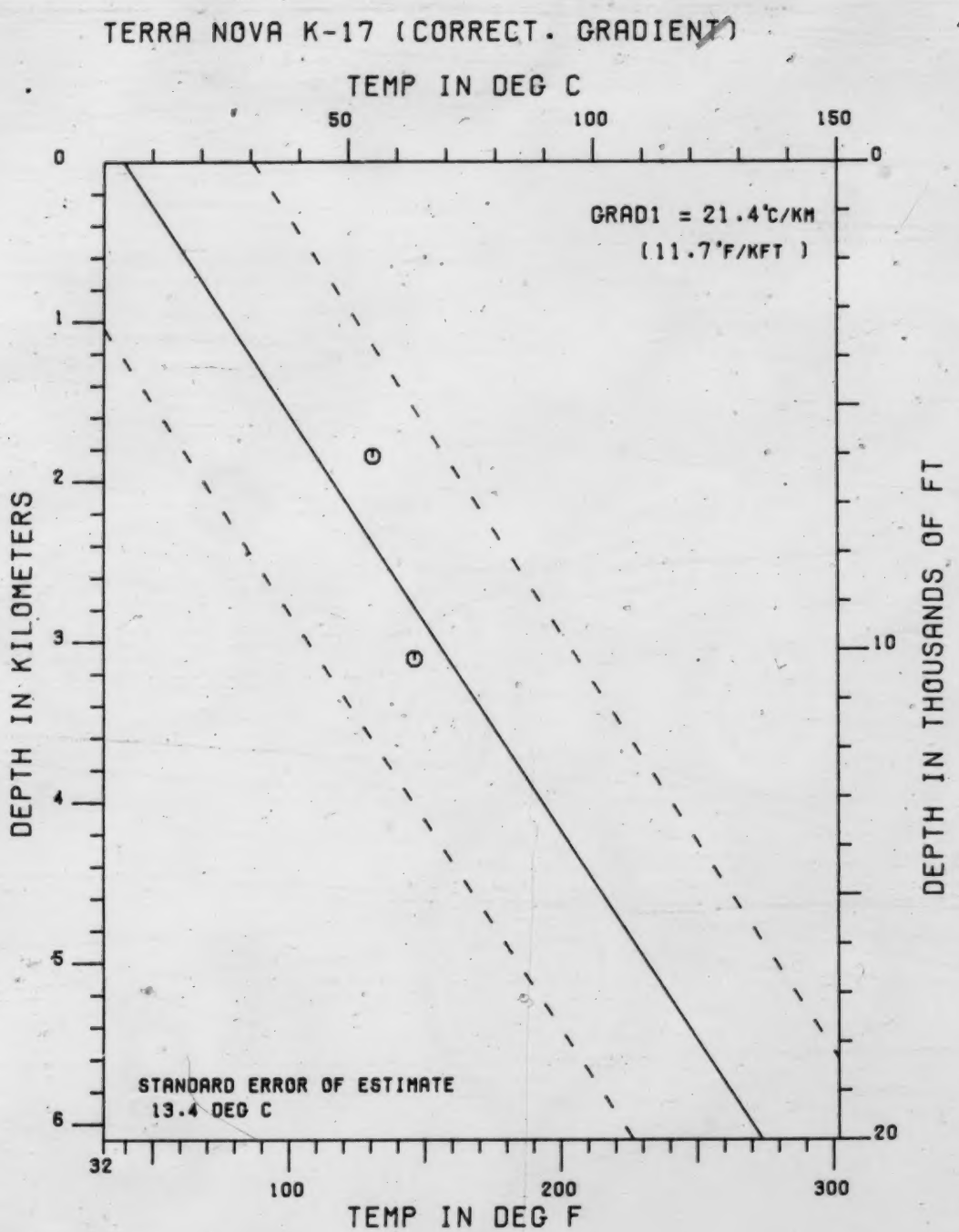
TERRA NOVA K-17 (CORRECT. GRADIENT)
TEMP IN DEG C
50
100
150
0
GRAD1 = 21.4°C/KM
(11.7°F/KFT)
1
2
3
4
5
6
DEPTH IN KILOMETERS
DEPTH IN THOUSANDS OF FT
10
20
STANDARD ERROR OF ESTIMATE
13.4 DEG C
32
100
200
300
TEMP IN DEG F

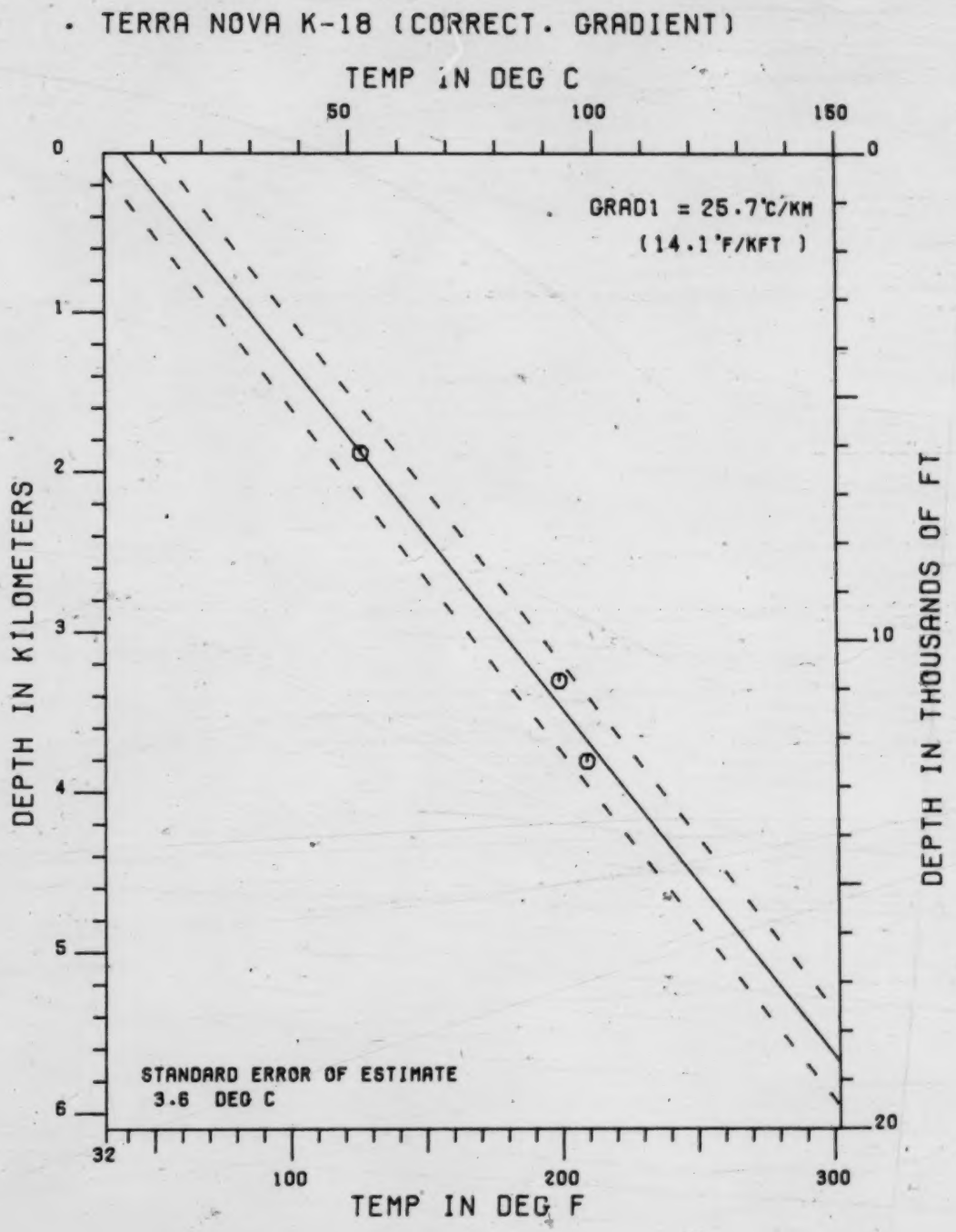
TERRA NOVA K-18 (CORRECT. GRADIENT)
TEMP IN DEG C
50
100
150
0
GRAD1 = 25.7°C/KM
(14.1°F/KFT)
1
2
3
4
5
6
DEPTH IN KILOMETERS
DEPTH IN THOUSANDS OF FT
10
20
STANDARD ERROR OF ESTIMATE
3.6 DEG C
32
100
200
300
TEMP IN DEG F

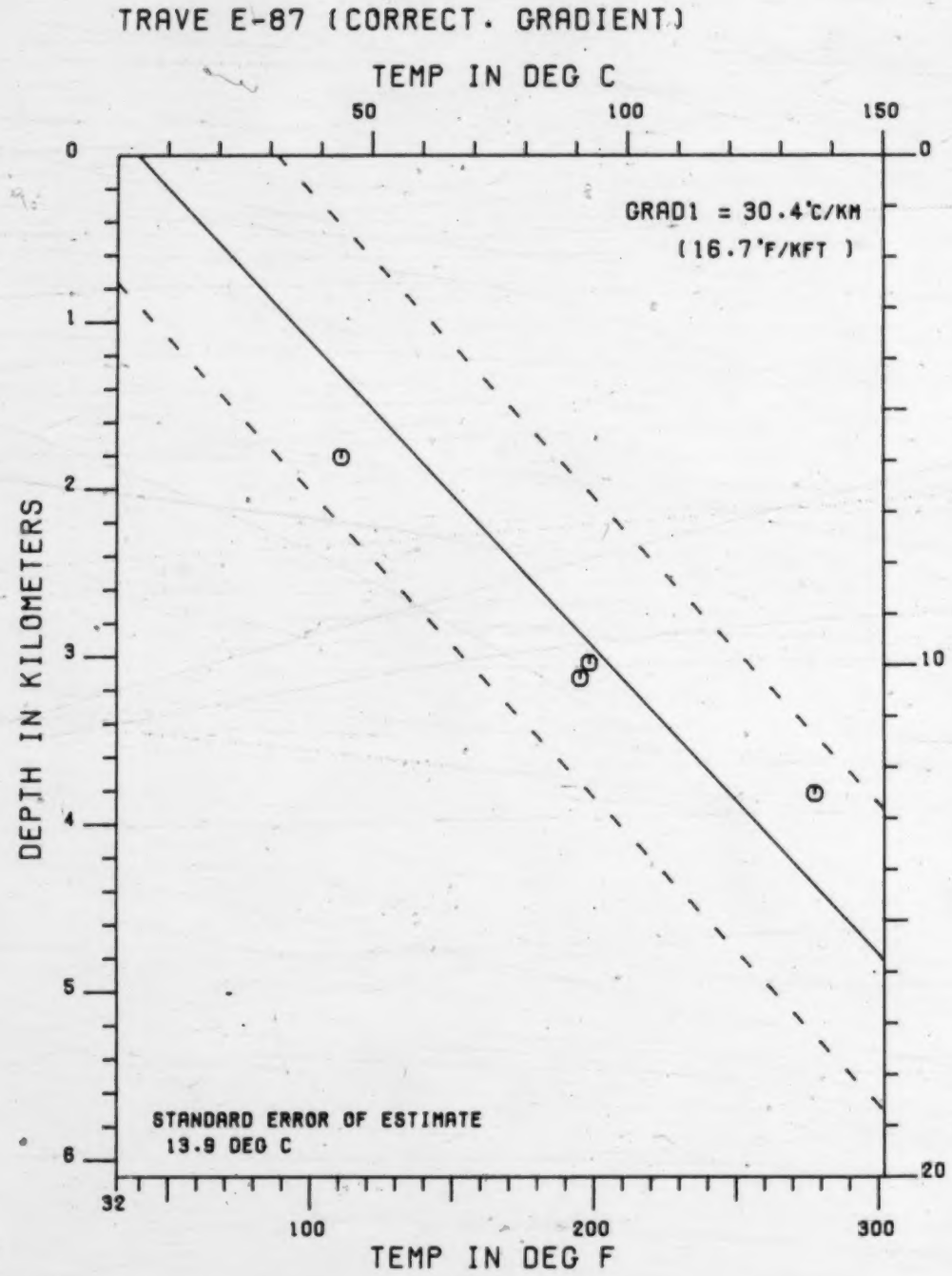
TRAVE E-87 (CORRECT. GRADIENT)
TEMP IN DEG C
50
100
150
0
GRAD1 = 30.4°C/KM
(16.7°F/KFT)
DEPTH IN KILOMETERS
DEPTH IN THOUSANDS OF FT
STANDARD ERROR OF ESTIMATE
13.9 DEG C
32
100
200
300
TEMP IN DEG F

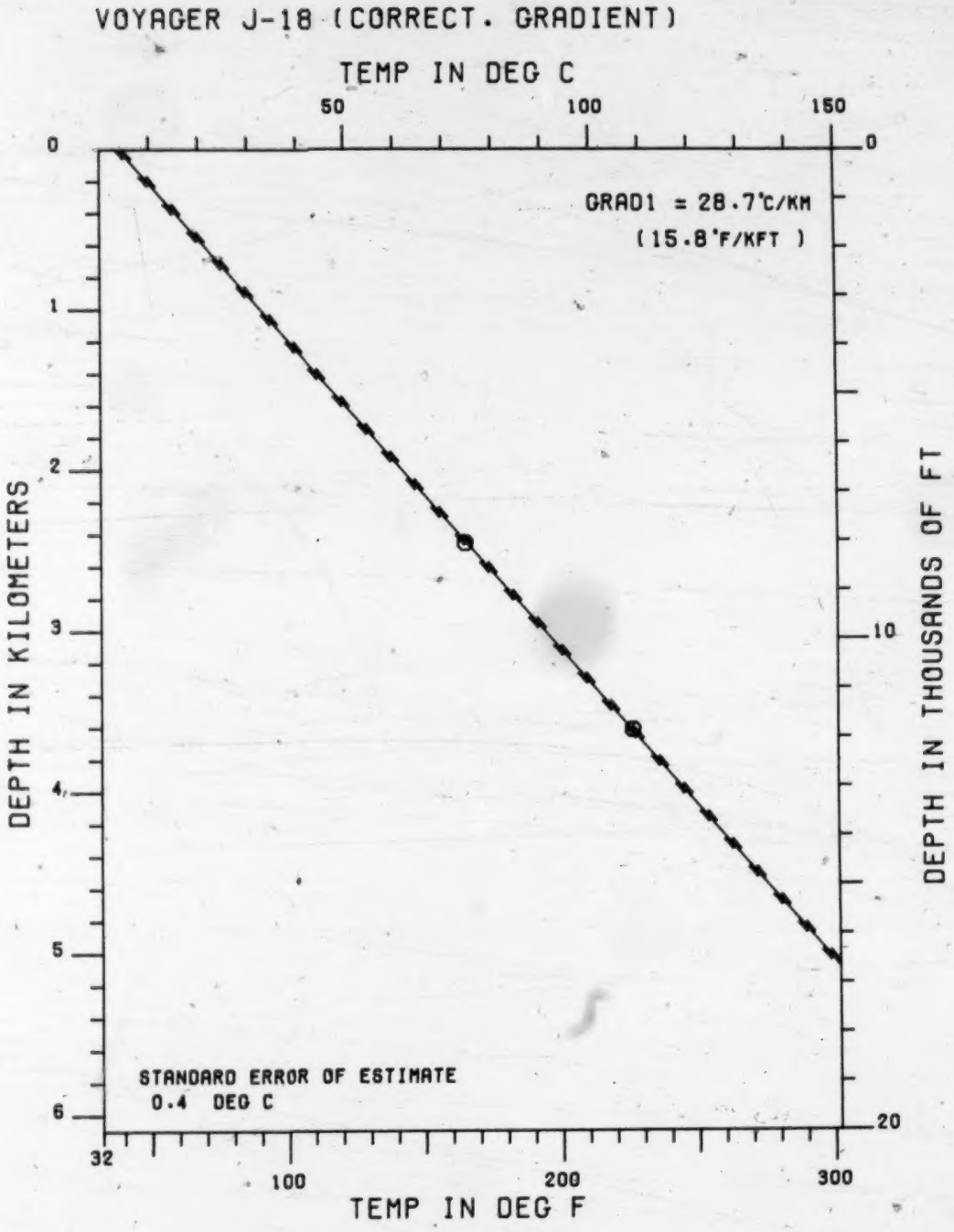
VOYAGER J-18 (CORRECT. GRADIENT)
TEMP IN DEG C
50
100
150
0
GRAD1 = 28.7°C/KM
(15.8°F/KFT)
1
2
3
4
5
6
DEPTH IN KILOMETERS
10
20
DEPTH IN THOUSANDS OF FT
STANDARD ERROR OF ESTIMATE
0.4 DEG C
32
100
200
300
TEMP IN DEG F

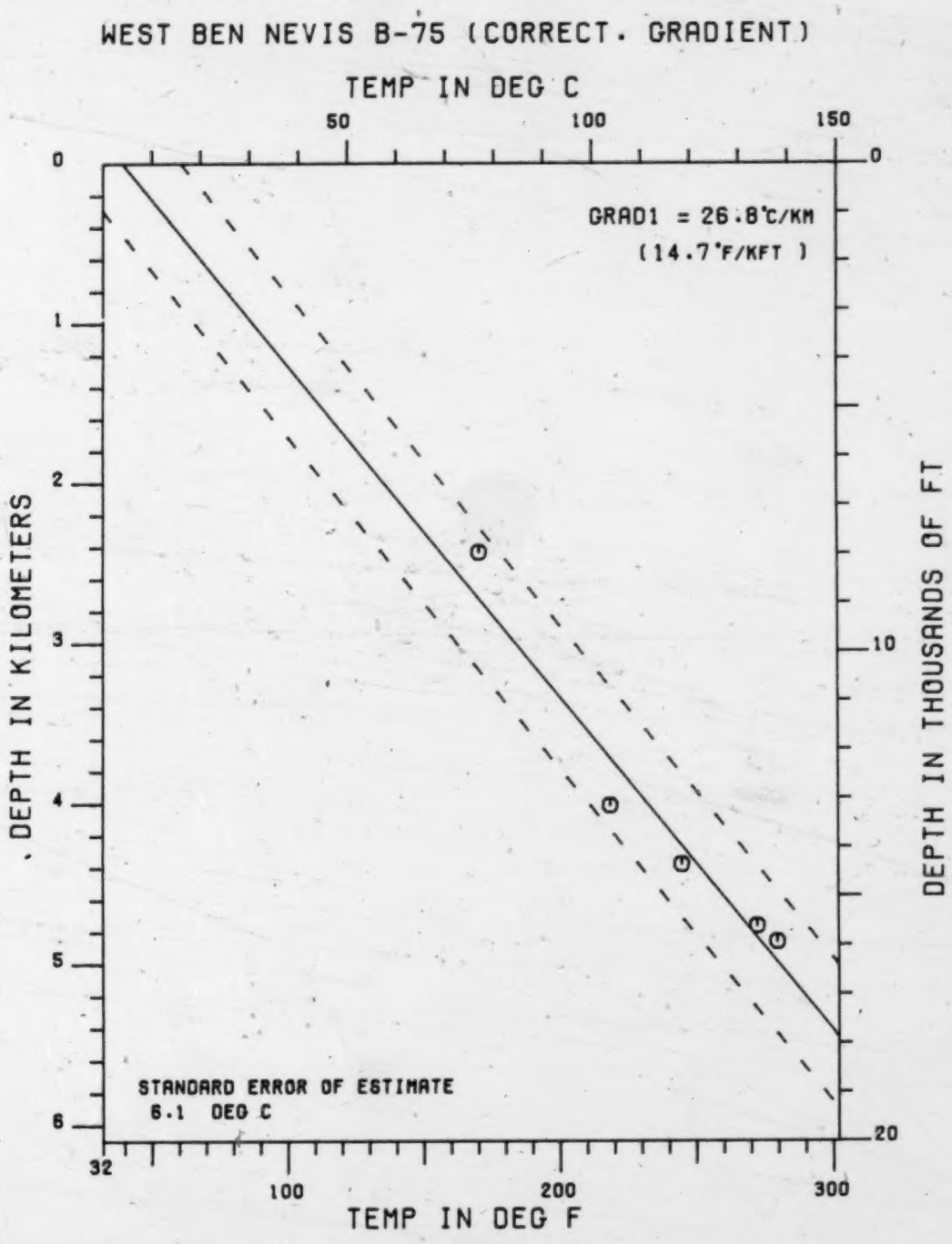
WEST BEN NEVIS B-75 (CORRECT. GRADIENT)
TEMP IN DEG C
50
100
150
0
GRAD1 = 26.8°C/KM
(14.7°F/KFT)
1
2
3
4
5
6
DEPTH IN KILOMETERS
DEPTH IN THOUSANDS OF FT
10
20
STANDARD ERROR OF ESTIMATE
6.1 DEG C
32
100
200
300
TEMP IN DEG F

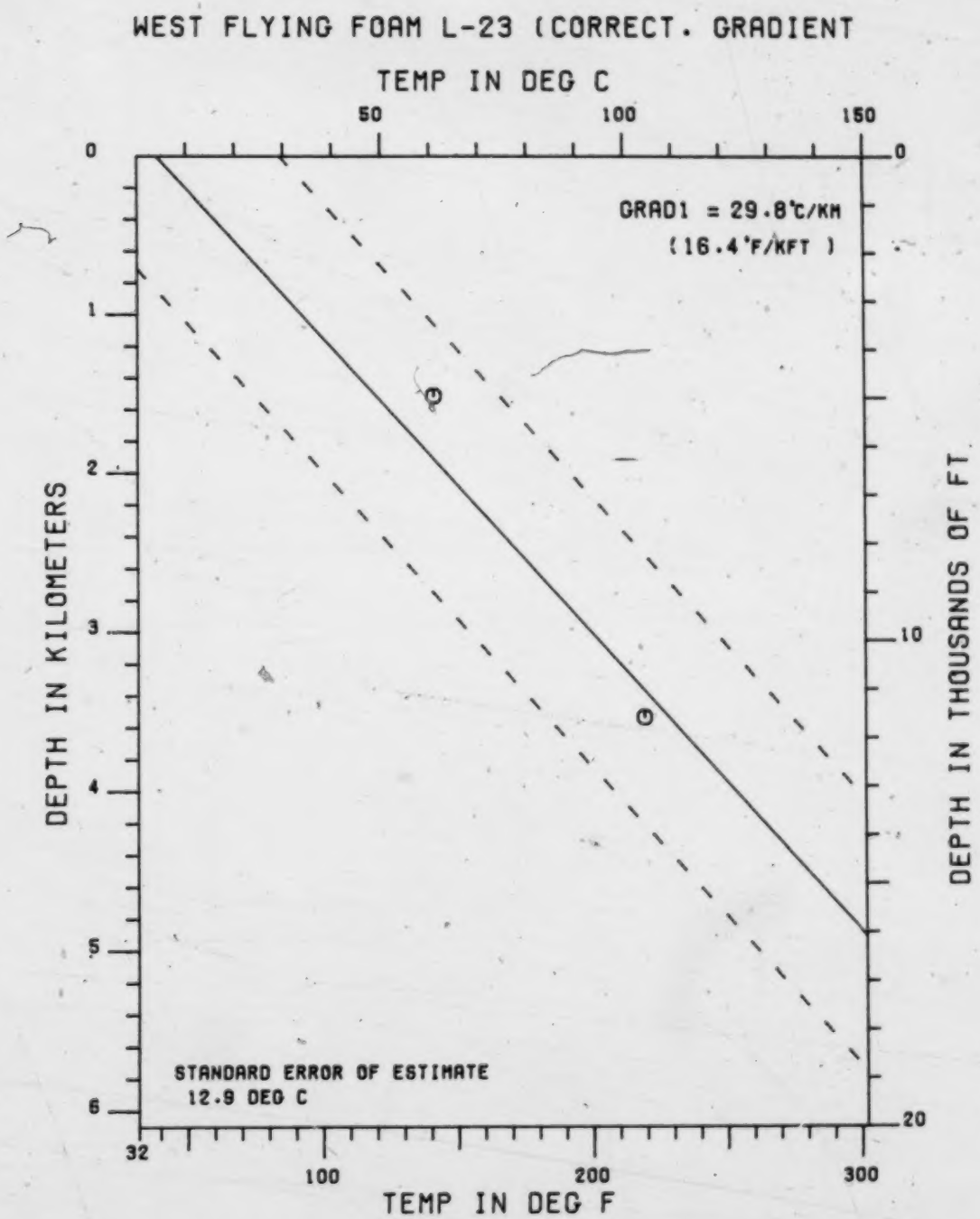
WEST FLYING FOAM L-23 (CORRECT. GRADIENT
TEMP IN DEG C
50
100
150
0
GRAD1 = 29.8°C/KM
(16.4°F/KFT)
1
2
3
4
5
6
DEPTH IN KILOMETERS
DEPTH IN THOUSANDS OF FT.
10
20
STANDARD ERROR OF ESTIMATE
12.9 DEG C
32
100
200
300
TEMP IN DEG F

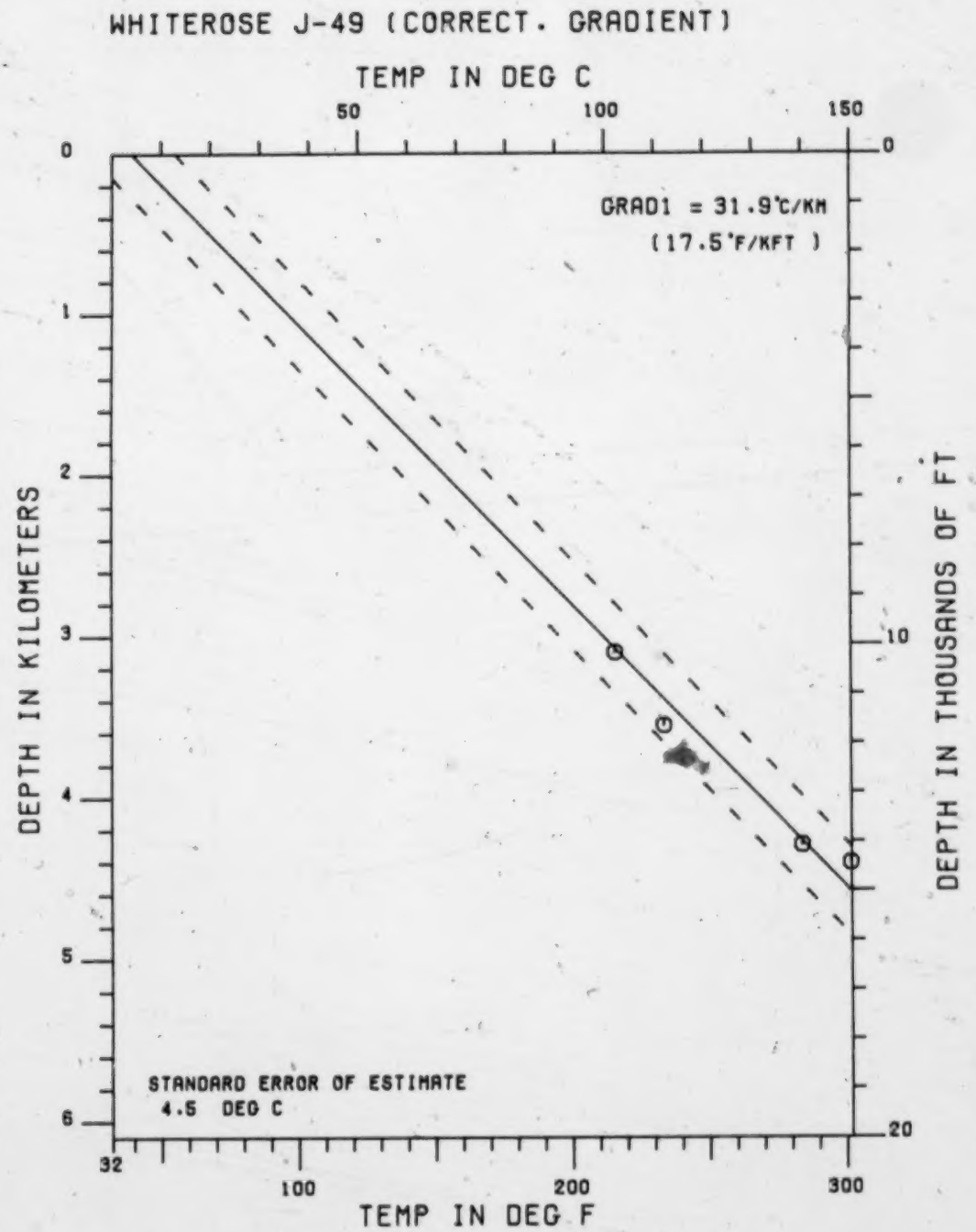
WHITEROSE J-49 (CORRECT. GRADIENT)
TEMP IN DEG C
50
100
150
0
GRAD1 = 31.9°C/KM
(17.5°F/KFT)
1
2
3
4
5
6
DEPTH IN KILOMETERS
10
20
DEPTH IN THOUSANDS OF FT
STANDARD ERROR OF ESTIMATE
4.5 DEG C
32
100
200
300
TEMP IN DEG F

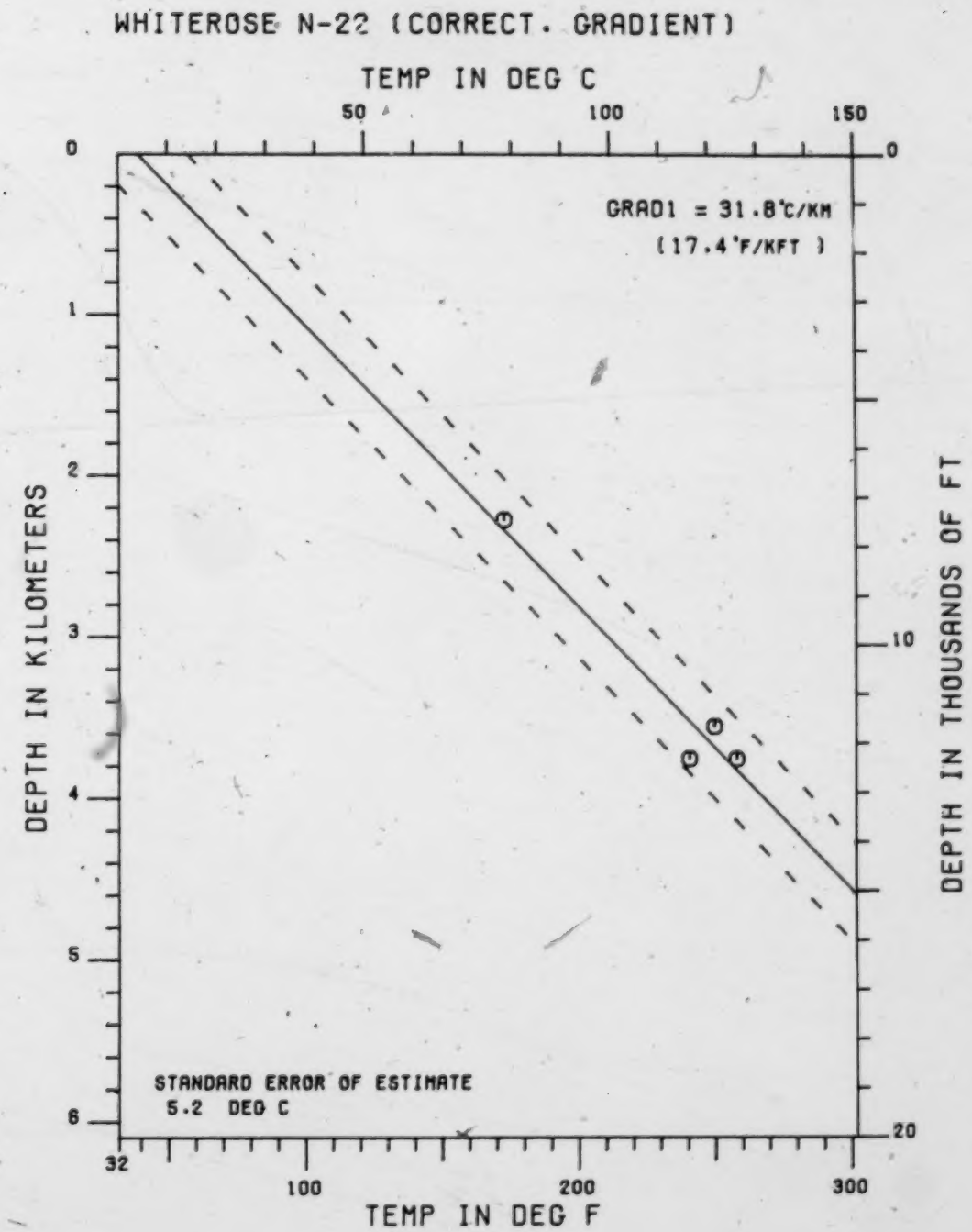
WHITEROSE N-22 (CORRECT. GRADIENT)
TEMP IN DEG C
50
100
150
0
GRAD1 = 31.8°C/KM
(17.4°F/KFT)
1
2
3
4
5
6
DEPTH IN KILOMETERS
DEPTH IN THOUSANDS OF FT
10
20
STANDARD ERROR OF ESTIMATE
5.2 DEG C
32
100
200
300
TEMP IN DEG F